UNIVERSITÀ DEGLI STUDI DI MILANO

PhD COURSE IN TRANSLATIONAL MEDICINE - 38th cycle

Dipartimento di Fisiopatologia Medico-Chirurgica e dei Trapianti

DOCTORAL DISSERTATION

Muscle-specific *MECP2* Misexpression Induces Skeletal and Visceral Muscle Defects Rescued by Butyrate Supplementation in *Drosophila*

Scientific-disciplinary sectors: MEDS-03/A, BIOS-10/A

PhD Student: Gaia Consonni

Student ID: R13986

ORCID iD: 0000-0003-3010-3265

Tutor: Prof.ssa Elisa Borghi

Cotutor: Prof. Thomas Vaccari

PhD Program Coordinator: Prof. Mario Clerici

Academic Year: 2024/2025

Ad majorem Dei gloriam

Table of Contents

Summary

Background

MeCP2 is a chromatin-associated protein whose dosage alterations cause two severe neurodevelopmental disorders: Rett syndrome (RTT), linked to loss-of-function mutations, and *MECP2* duplication syndrome (MDS), linked to overexpression. Although widely studied for their neurological symptoms, these disorders also display prominent non-exclusively neurological features, including gastrointestinal dysmotility and muscle hypotonia - suggesting that MeCP2 dysfunction may also impact peripheral tissues. Since *MECP2* is expressed in muscle, yet its role outside the nervous system remains poorly defined, this work explores the tissue-autonomous effects of *MECP2* misexpression in muscle.

Aims

This project aims to establish a *Drosophila* model to investigate the impact of *MECP2* misexpression in muscle tissue and its role in muscle development, assess whether the resulting phenotypes are autonomous or secondary to neuronal dysfunction, and test the therapeutic potential of short-chain fatty acids (SCFAs) - specifically butyrate - as chromatin-targeting interventions.

Results

Because *Drosophila* lacks an endogenous *MECP2* gene, we used transgenic lines overexpressing either wild-type or mutant human *MECP2*. Using the Gal4/UAS system, tissue-specific expression revealed that muscle-targeted *MECP2* overexpression led to the strongest phenotypes, such as reduced viability, disorganized skeletal and visceral muscle, impaired locomotion, and delayed gut transit. In addition, mitochondrial abnormalities - increased organelle number and altered cristae structure - were observed by electron microscopy in muscle fibers. Visceral muscle defects were most pronounced when *MECP2* was expressed during gut development, suggesting interference with tissue maturation.

We also employed the model to functionally classify *MECP2* variants. Alleles were scored based on their ability to enhance or suppress wild-type *MECP2* phenotypes. R106W suppressed lethality and caused mild muscle disruption, consistent with loss of function. Δ166 enhanced lethality but caused minimal pathology, suggesting a benign effect. R294X produced strong muscle phenotypes and variable lethality across tissues, indicating partial function.

To determine whether these effects were secondary to neural dysfunction, we expressed *MECP2* in neurons but observed no impact on muscle structure or gut function. Similarly, *MECP2* expression in muscle did not disrupt synaptic architecture. These findings support a tissue-autonomous mechanism.

With a clear muscle-specific phenotype and considering their energetic and epigenetic functions, we next tested whether SCFAs supplementation could reverse these defects. High-dose propionate reduced survival. In contrast, acetate, sodium butyrate, and the butyrate-rich postbiotic Lalbaay® improved viability and development, with Lalbaay® showing the strongest effects.

Motor function was also enhanced, supporting the beneficial role of butyrate molecule. Indeed, supplementation with sodium butyrate, an HDAC inhibitor with energetic role, specifically restored muscle structure and gut motility. Valproic acid, a pan-HDAC inhibitor without metabolic properties, produced similar improvements, suggesting an epigenetic mechanism of action.

Finally, we began dissecting genetic interactions. Since *Drosophila* lacks endogenous *MECP2*, it provides a clean background to identify functional modifiers. Recent work implicated PHF14 - a MeCP2 interactor mutated in a Rett-like syndrome - as a candidate modifier. Given its conservation in flies, we initiated a mutagenesis screen via transposon excision. To date, 22 candidate mutant lines have been isolated and are being validated, paving the way for future genetic interaction studies.

Conclusions

This thesis demonstrates that *MECP2* misexpression in *Drosophila* muscle leads to autonomous morphological and functional defects, which can be partially reversed by SCFAs such as butyrate and Lalbaay®, likely via chromatin remodeling and possibly metabolic support. Disease-associated MeCP2 variants reproduce the pathogenicity reported in patients, showing distinct tissue-specific behaviours and underscoring the validity of this model for functional interpretation. These findings highlight the systemic nature of *MECP2* disorders and advocate for therapeutic strategies that extend beyond the nervous system to include peripheral tissues such as muscle.

1. Introduction

1.1 MeCP2-related Diseases

1.1.1 DNA Methylation and Chromatin Regulation

Methyl-CpG-binding protein 2 (MeCP2) is classically defined by its ability to bind methylated cytosines in CpG contexts and to regulate chromatin structure by recruiting co-repressor complexes and influencing nucleosome positioning (Nan et al., 1997).

Chromatin structure is dynamically regulated by DNA methylation and histone modifications, which together determine the accessibility of genomic regions and gene expression programs (Y. Chen et al., 2024). DNA methylation is central to transcriptional repression, genomic imprinting, and neuronal development (Peña, 2025), while histone modifications and chromatin remodeling orchestrate gene expression patterns essential for cell differentiation and function (Geiman & Robertson, 2002).

These epigenetic mechanisms allow neurons and other cell types to adjust transcriptional output in response to developmental and environmental cues, and their dysregulation is associated with altered chromatin architecture, transcriptional defects, and disease (Armstrong et al., 2023; Fasolino & Zhou, 2017; Li et al., 2024).

In muscle development, DNA methylation and chromatin regulation also play crucial roles. Myogenic transcription factors such as MyoD and MEF2 recruit chromatin-modifying enzymes, including histone acetyltransferases (HATs) and deacetylases (HDACs), to coordinate muscle-specific gene expression and differentiation (McKinsey et al., 2001).

Overall, DNA methylation and chromatin regulation are central to controlling gene expression programs in both neurons and muscles, with MeCP2 functioning as a versatile mediator linking epigenetic marks to chromatin organization and cellular function. Emerging evidence further broadens this view, showing that MeCP2 can also recognize non-CpG regions and specific unmethylated DNA sequences and promote chromatin condensation independently of DNA methylation, a mechanism recently linked to transcriptional activation (Chua & Liu, 2024; Connelly et al., 2021; Galvão & Thomas, 2005; Hansen et al., 2010; Y. Liu et al., 2025). These

findings highlight the multifaceted nature of MeCP2, making its function even more complex (Figure I).

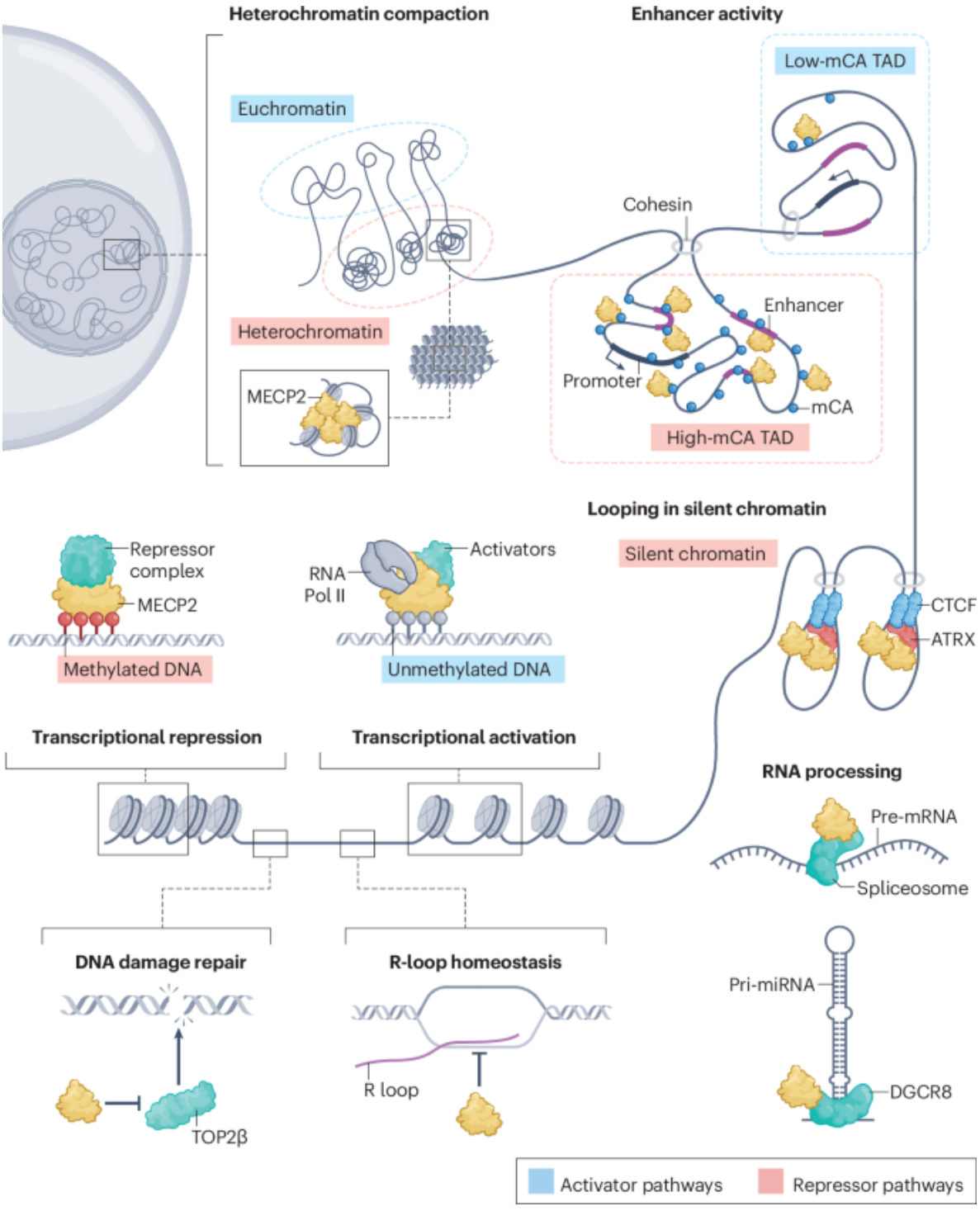

Figure I. MeCP2 regulates chromatin architecture and gene expression through DNA methylation –dependent and -independent mechanisms, including chromatin compaction, enhancer repression, chromatin looping, transcriptional modulation, genome stability, and RNA processing (Y. Liu et al., 2025).

1.1.2 MeCP2: Structure, Function, and Dosage sensitivity

MeCP2 is a modular protein encoded by a gene on the X chromosome and expressed as two major splice variants, E1 and E2, which differ at their N-termini (Figure II). Through this modular organization, MeCP2 bridges DNA methylation to chromatin regulation: the functional domains include an N-terminal region, a methyl-CpG-binding domain (MBD) that recognizes methylated CpG dinucleotides, and a transcriptional repression domain (TRD) that mediates interaction with corepressor complexes (Heckman et al., 2014; Lyst et al., 2013). The TRD contains a nuclear-receptor–corepressor interaction domain (NID) near its C-terminus, and mutations in this region, such as R306C, disrupt binding to corepressor complexes such as NCoR/SMRT and Sin3A/HDAC (Heckman et al., 2014; Ip et al., 2018).

Beyond these canonical functions, MeCP2 regulates chromatin structure and gene expression through multiple mechanisms. It promotes heterochromatin compaction via phase separation of intrinsically disordered regions, represses enhancer activity at mCA-rich topologically associating domains (TADs), and cooperates with chromatin remodelers such as ATRX and architectural proteins like CTCF to establish chromatin loops at imprinted loci (Figure I). MeCP2 also interacts with additional factors, including the DEAD-box helicase DDX1 and the PHD-finger protein PHF14, which participates in histone recognition and transcriptional regulation. Disruption of MeCP2–PHF14 complexes has been linked to Rett-like phenotypes, highlighting the role of these interactions in the heterogeneity of *MECP2*-related disorders (Dominguez et al., 2024; J. Zhou et al., 2022).

Depending on cellular context, MeCP2 can act as either a transcriptional repressor or activator. For example, occupancy at promoter CpG islands can enhance RNA polymerase II-driven transcription, functioning as a positive cofactor at many neuronal genes. In addition, MeCP2 contributes to genomic stability and RNA metabolism, including splicing and miRNA processing, further illustrating its versatile and complex role in chromatin organization and gene regulation (Y. Liu et al., 2024, 2025).

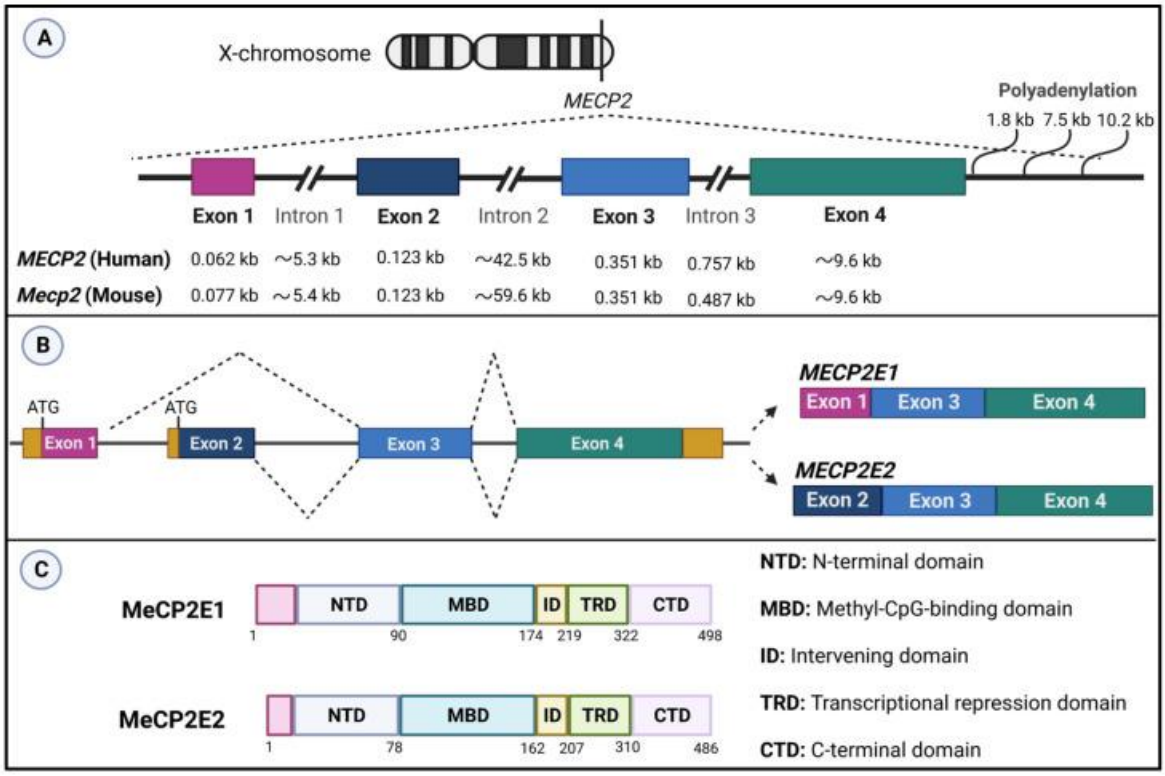

Figure II. Schematic diagram of (A) *MECP2/Mecp2* gene, (B) *MECP2E1* and *MECP2E2* transcripts, (C) MeCP2E1 and MeCP2E2 isoforms. MeCP2: methyl-CpG binding protein 2. The dark yellow boxes in B show 5' and 3' untranslated regions (UTR) *(Vuu et al., 2023).*

1.1.3 *MECP2*-Related Disorders

MECP2 is an exemplary dosage-sensitive gene: loss-of-function mutations cause Rett syndrome (RTT), whereas duplications or triplications result in *MECP2* duplication syndrome (MDS) (Figure III; Bajikar et al., 2023; Heckman et al., 2014). Both conditions lead to severe neurodevelopmental disease, highlighting that either deficiency or excess of MeCP2 disrupts chromatin homeostasis. Studies in mice have shown that alterations in either direction affect chromatin state, including histone acetylation patterns and gene expression, indicating convergence on disturbed epigenetic regulation (Ip et al., 2018; Y. Liu et al., 2024).

RTT is an X-linked dominant disorder caused by heterozygous *MECP2* mutations, affecting roughly 1 in 10,000 females. These mutations are almost always *de novo*, typically arising in the paternal germline. Classic RTT patients develop normally until 6–18 months, then experience regression of language and motor skills, stereotyped hand movements, and autonomic and

seizure disorders. RTT is usually lethal in hemizygous males; surviving males typically present with somatic mosaicism or sex chromosome anomalies (Bajikar et al., 2023; Moog et al., 2003). The severity of RTT depends on the type of *MECP2* alteration: missense mutations in the MBD often produce severe RTT, whereas certain TRD mutations result in milder courses (Heckman et al., 2014).

Figure III. Children affected by *MECP2*-related disorders. *Left*: Hannah, diagnosed with Rett syndrome at 21 months, exhibits motor and gastrointestinal impairments and requires a wheelchair and feeding support, yet retains a cheerful disposition. *Right*: Jackson, diagnosed with *MECP2* Duplication Syndrome at 3 years, shows hypotonia, developmental delays in motor, cognitive, and speech domains, and is prone to recurrent infections and seizures. These cases illustrate the diverse phenotypic spectrum of MeCP2 dysfunction and its impact on neuromuscular and gastrointestinal development. Sources: Texas Children's Hospital (Hannah's Story, 2023); Phoenix Children's Hospital (Jackson's Story, 2021).

The prevalence of MDS is estimated to be around 1 in 100,000 live male births (Akaba & Takahashi, 2025). MDS most commonly affects boys with duplication of the Xq28 region containing *MECP2*. Maternal carriers are generally asymptomatic due to extreme skewing of X-chromosome inactivation. Affected males show severe hypotonia, intellectual disability, absent or limited speech, recurrent seizures, and immune dysfunction (Bajikar et al., 2023; Van Esch et al., 2005).

Despite being caused by *MECP2* overexpression, MDS shares phenotypic features with RTT, including cognitive and motor impairments. Both disorders illustrate that cellular function is highly sensitive to MeCP2 dosage. Both loss and gain of MeCP2 perturb chromatin and transcriptional regulation, leading to overlapping clinical features.

1.1.4 Neurological Manifestations

The neurological-associated phenotype of MeCP2 disorders constitutes the main hallmarks. In RTT, classic onset includes developmental regression of speech and purposeful hand use, replaced by distinctive hand-wringing or hand-clapping stereotypes (Einspieler & Marschik, 2019). Most patients also develop gait abnormalities, muscle tone irregularities, and seizures; for example, in one large survey ~81% of RTT patients had epilepsy. Sleep disturbances, breathing irregularities, and autonomic instability are also common (Smirnov et al., 2021). MDS similarly causes profound intellectual disability, hypotonia, limited or absent speech, and frequent epilepsy; many duplication patients also display hand stereotypes and spasticity (Ta et al., 2022). Thus, both disorders share key neurological features, even though their genetic causes are opposite.

Neuropathological studies and animal models reveal that MeCP2 deficiency primarily impairs postnatal brain development rather than causing frank neurodegeneration (Smrt et al., 2007). Postmortem studies of RTT patients reveal a ~15–30% reduction in brain weight compared to controls, which is reflected in functional imaging and MRI as decreased gray matter volume (Chahrour & Zoghbi, 2007). Cortical neurons display reduced dendritic arborization and spine density, consistent with a synaptic phenotype: *Mecp2*-null mice have impaired excitatory synaptic transmission, whereas *Mecp2* overexpression increases excitatory synapse markers (Boggio et al., 2010). These findings indicate that MeCP2-related encephalopathy reflects arrested neuronal maturation and plasticity rather than irreversible neuron loss, as rescue experiments in mice demonstrate that reactivating Mecp2 even in adulthood can reverse symptoms (Robinson et al., 2012).

On the other hand, the primary neurological traits of MDS include infantile hypotonia, severe to profound intellectual disability, autism or autistic features, and poor speech development. Patients commonly experience epilepsy, progressive spasticity, and in some cases, developmental regression (Ramocki et al., 2010). Additional neurological features include severe motor and cognitive impairment, delayed or absent speech development, seizures, and ataxia. The syndrome is associated with shortened lifespan and recurrent respiratory infections (D'Mello, 2021). Female carriers, despite normal intelligence, may display neuropsychiatric phenotypes (Ramocki et al., 2010).

1.1.5 Non-Neurological phenotypes

Clinically, RTT patients commonly exhibit early-onset hypotonia (low muscle tone) and later develop severe scoliosis and osteoporosis (Hagberg et al., 1983; Neul et al., 2010). Furthermore, poor muscle tone and strength are prominent in patients. Scoliosis is also prevalent (>60%) in older RTT girls, likely reflecting both neuromuscular weakness and central dysregulation of bone growth (Guidera et al., 1991; Percy et al., 2010; Zysman et al., 2006).

The PLOS study by Conti et al. (2015) confirmed that *Mecp2*-null mice have markedly disorganized skeletal muscle architecture with fiber hypotrophy and fibrosis (Conti et al., 2015). However, in this paper conditional deletion of *Mecp2* only in muscle produced no intrinsic muscle defects, suggesting that hypotonia in Rett is mainly non–cell-autonomous.

Nevertheless, Ross et al., (2016) showed that *MECP2* is also expressed in peripheral tissues at lower levels (~10% of neuronal levels), and peripheral MeCP2 deficiency contributes to non-neurological phenotypes despite a normal brain. These include hypoactivity, muscle fatigue and exercise intolerance, and bone/skeletal abnormalities. This indicates that some features of RTT - for example reduced stamina and hypotonia - might arise from MeCP2 loss in peripheral tissues rather than central defects (Ross et al., 2016).

Gastrointestinal (GI) dysfunction is another major extra-CNS problem in MeCP2 disorders. RTT patients frequently suffer from constipation, reflux, delayed gastric emptying, and dysphagia. A large survey reported that ~80% of individuals with RTT had chronic constipation and ~40% had gastroesophageal reflux. Swallowing difficulties and prolonged feeding times are also common. These GI problems can be severe and constant across the lifespan, imposing a substantial burden on patients and families (Motil et al., 2012). Specifically, loss of MeCP2 is associated with an altered gut microbiota and increased intestinal permeability, impacting the gut's ability to function properly (Marballi & MacDonald, 2021; Nakhal et al., 2024; Strati et al., 2016; Vicentini et al., 2021; Wahba et al., 2015, 2016).

Key non-neurological traits of MDS include infantile hypotonia, recurrent respiratory infections, and gastrointestinal problems. Additionally, affected individuals exhibit dysmorphic features, though these are not yet well-characterized (Ramocki et al., 2010; Ta et al., 2022).

Together, these findings highlight that MeCP2 dysfunction affects multiple peripheral systems, significantly impairing patients' quality of life.

Table I. Neurological and non-neurological symptoms in Rett syndrome (RTT) and *MECP2* duplication syndrome (MDS).

	Rett Syndrome (RTT)	***MECP2* Duplication Syndrome (MDS)**	**References**
Neurological symptoms	• Developmental regression (speech, purposeful hand use) • Stereotypic hand movements (hand-wringing/clapping) • Gait abnormalities, ataxia, spasticity • Hypotonia • Epilepsy (~81%) • Sleep disturbances, breathing irregularities, autonomic instability • Reduced dendritic arborization and spine density • Impaired synaptic transmission, arrested neuronal maturation	• Profound intellectual disability • Limited or absent speech • Hypotonia • Frequent epilepsy • Hand stereotypes • Spasticity • Cognitive and motor impairment	Ross et al., 2016; Motil et al., 2013; Boggio et al., 2010; Van Esch et al., 2005; Bajikar et al., 2023
Non-neurological symptoms	• Early hypotonia • Severe scoliosis (>60% of older patients) • Osteoporosis • Skeletal muscle fiber hypotrophy and fibrosis (Mecp2-null mice) • Exercise intolerance, reduced stamina • GI dysfunction: constipation (~80%),	• Immune dysfunction (frequent infections) • Hypotonia (also neurological) • Feeding/swallowing difficulties reported in some cases	Conti et al., 2015; Ross et al., 2016; G. Wahba et al., 2016; Strati et al., 2016; Wahba et al., 2015; Vicentini et al., 2021; Nakhal et al., 2024; Marballi & MacDonald, 2022; Esch et al., 2005; Bajikar et al., 2023

	reflux (~40%), delayed gastric emptying, dysphagia • Altered gut microbiota, increased intestinal permeability		

1.2 *Drosophila melanogaster* as a Genetic Model for Human Disease

1.2.1 General Introduction to the Fly as a Model System

Drosophila melanogaster is an extremely versatile model organism for genetics and biomedicine (Kitani-Morii et al., 2021; Ugur et al., 2016). Its main experimental advantages include:

- **Life cycle and reproduction**: the fly completes a full cycle in ~10 days at 25 °C (egg→3 larval stages→pupa→adult) and each female lays 20 to 100 eggs per day allowing rapid multigenerational studies with homogeneous populations (Gomez et al., 2024; Mirzoyan et al., 2019).
- **High gene homology**: about 60% of the *D. melanogaster* genome is homologous to the human genome and 75% of human disease-associated genes have orthologues in the fly. This broad genetic overlap allows effective modeling of many human diseases, including rare genetic disorders. It also facilitates testing pathogenic variants and identifying novel disease genes (Link & Bellen, 2020; Ugur et al., 2016).
- **Sophisticated genetic tools**: binary expression systems (Gal4/UAS, LexA/LexAop, QF/QUAS) with regulators such as Gal80^ts, together with RNAi, CRISPR/Cas9, and recombination (Flp/FRT) techniques, allow precise and spatially controlled genetic manipulations (Casas-Tintó, 2024).
- **Cost and experimental flexibility**: *Drosophila* is inexpensive to maintain and does not involve vertebrate ethical issues. These qualities make it a practical model for biomedical research, respecting the 3Rs principles (Vidal et al., 2024).

These qualities make *Drosophila* an ideal model to investigate complex molecular pathways, allowing both genetic manipulations and drug or dietary supplementation studies in biomedical contexts.

1.2.2 *Drosophila* as a Model for Neurodevelopmental and Neurodegenerative Syndromes

Drosophila melanogaster has proven to be an effective model for studying neurological diseases due to its conserved genetic pathways and sophisticated experimental tools (Chan & Bonini, 2000; Deal & Yamamoto, 2019). Fly models recapitulate key features of both neurodegenerative and heritable neurodevelopmental diseases (Gatto & Broadie, 2011; Nitta & Sugie, 2022).

Neurodevelopmental disorders, including Angelman syndrome, Rett syndrome, Neurofibromatosis Type 1, and Fragile X syndrome, have been investigated in *Drosophila* models using mutants of human orthologs or transgenic expression systems (Gatto & Broadie, 2011).

Interestingly, large-scale genetic screens in *Drosophila* have identified evolutionarily conserved genes essential for neural maintenance, revealing that neurodegeneration often involves mitochondrial dysfunction, lipid/iron metabolism defects, impaired protein trafficking, and autophagy (Deal & Yamamoto, 2019; Yamamoto et al., 2014).

1.2.3 Misexpression of Human Proteins in *Drosophila* to model neurological diseases

Heterologous expression of human disease-associated proteins in *Drosophila* allows the generation of reproducible and quantifiable phenotypes, providing a robust platform for mechanistic studies and therapeutic screening.

Proteins such as amyloid-β (Aβ), tau, α-synuclein (αSyn), huntingtin (HTT), and parkin have been expressed in specific tissues and developmental stages, modeling a variety of neurodegenerative conditions, including Alzheimer's, Parkinson's, ALS, Huntington's disease, and ataxia telangiectasia (Bakhoum & Jackson, 2011; Bolus et al., 2020).

Aβ expression recapitulates key pathological features of Alzheimer's disease and has been successfully used to identify anti-proteotoxic candidates and to screen pharmacological compounds (Elovsson et al., 2021). Similarly, αSyn transgenic flies reproduce hallmarks of Parkinson's disease and other synucleinopathies, facilitating comprehensive genetic analyses and large-scale drug testing (Nagai et al., 2011). Misexpression of tau, HTT, and parkin also produces measurable cellular and functional phenotypes, such as protein aggregation, synaptic

defects, mitochondrial dysfunction, and neurodegeneration, which can be quantified in different tissues, including the eye, neurons, and muscles (Fernius, Starkenberg, & Thor, 2017).

Specific examples of human neurodegenerative protein misexpression in *Drosophila* and their associated phenotypes are summarized in Table II.

These studies demonstrate the versatility of *Drosophila* as a system to link molecular pathology with functional outcomes. By providing reproducible, accessible, and tissue-specific readouts, misexpression models complement mutant analyses, bridging mechanistic insights with translational applications.

Table II. Overview of human neurological and neurodevelopmental disorders modeled in *Drosophila melanogaster*. For each disorder, the table summarizes the experimental approach, key phenotypes observed, and relevant references. Models include transgenic expression of human genes or manipulation of fly orthologs, enabling studies of molecular, cellular, and behavioural outcomes.

Disease / Disorder	***Drosophila* Model / Approach**	**Key Phenotypes / Features**	**References**
Parkinson's Disease (PD)	Genetic or toxin-based models; expression of human α-synuclein (WT and mutant)	Dopaminergic neuron loss, protein aggregation, locomotor deficits	Feany & Bender, 2000; Paricio & Muñoz-Soriano, 2011
Huntington's Disease (HD) / Polyglutamine disorders	Expression of expanded human HTT	Hallmark phenotypes, assessment of familial mutations, genetic modifiers, pharmacological interventions	Michno et al., 2005; Shulman & Feany, 2003
Alzheimer's Disease (AD) / Amyloidopathies	Expression of Aβ1–42	Progressive neurodegeneration, mitochondrial defects, synaptic alterations	Chouhan et al., 2016; Elovsson et al., 2025; Fernius et al., 2017
Tauopathies	Expression of human tau	Neurodegeneration, protein aggregation, synaptic defects	Chouhan et al., 2016; Fernius, Starkenberg, & Thor, 2017; Wittmann et al., 2001

ALS	Expression of human ALS-associated proteins (e.g., mutant SOD1)	Neurodegeneration, motor deficits	Bakhoum & Jackson, 2011; Bolus et al., 2020
Ataxia Telangiectasia	Expression of human disease-associated proteins	Neurodegeneration, cellular dysfunction	Bolus et al., 2020
Angelman Syndrome	Expression of human UBE3A ortholog / transgenic systems	Genetic and behavioural phenotypes related to neurodevelopment	Gatto & Broadie, 2011
Rett Syndrome	Expression of human *MECP2* transgenes	Neurodevelopmental and behavioural phenotypes	Gatto & Broadie, 2011
Neurofibromatosis Type 1	Expression / manipulation of NF1 ortholog	Neurodevelopmental and synaptic phenotypes	Gatto & Broadie, 2011
Fragile X Syndrome	Expression / manipulation of FMR1 ortholog	Synaptic and behavioural deficits	Gatto & Broadie, 2011

1.2.4 *Drosophila* as a Model to Study Rett Syndrome

Despite lacking an endogenous *MECP2* ortholog and exhibiting only sparse DNA methylation, *Drosophila melanogaster* has proven to be a valuable model for investigating aspects of RTT pathophysiology, particularly those related to *MECP2* gain-of-function. Two landmark studies (Cukier et al., 2008; Vonhoff et al., 2012) demonstrated that heterologous expression of human *MECP2* in fly neurons recapitulates specific structural and behavioural phenotypes reminiscent of RTT, thereby validating the fruit fly as a complementary system to mammalian models.

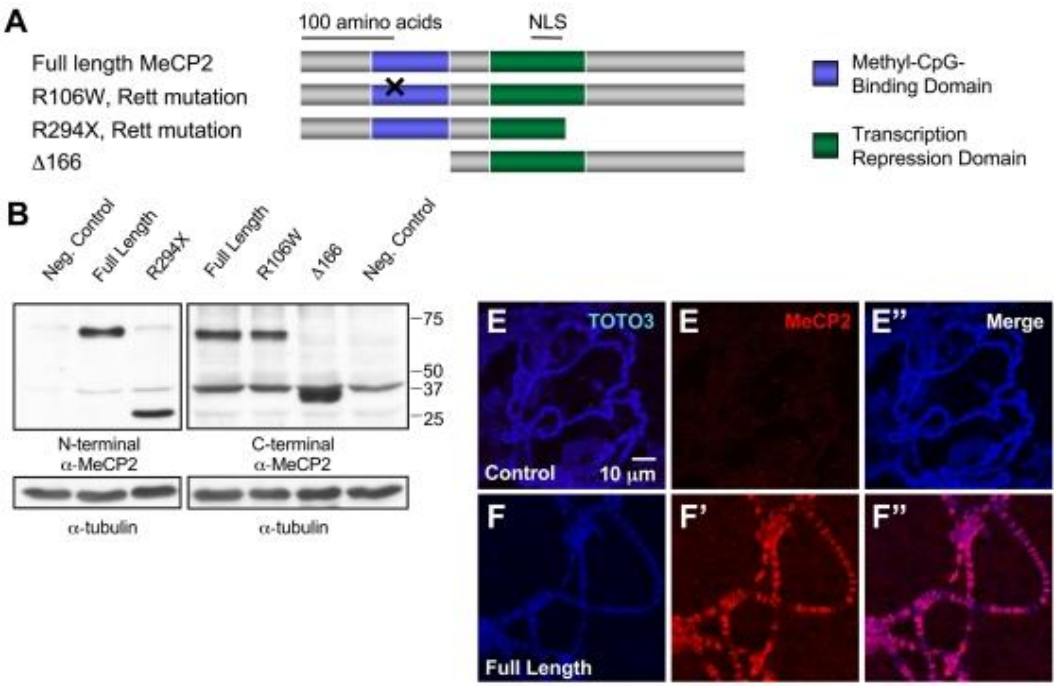

Figure IV. A. Schematic representation of four MeCP2 alleles cloned into pUAST to generate transgenic flies. The methyl-CpG-binding domain (MBD) is shown in blue and the transcription repression domain (TRD) in green; the nuclear localization signal (NLS) resides within the TRD. **B.** Western blot analysis of each allele expressed with *GMR*-Gal4 using two distinct MeCP2 antibodies to validate protein expression and epitope loss in deletion variants. **E–F"**. Immunofluorescence of polytene chromosomes from L3 larvae (25°C), showing MeCP2 binding absent in controls but present with transgenes (Adapted from Cukier et al., 2008).

Cukier et al. (2008) first generated *Drosophila* lines carrying wild-type and pathogenic MeCP2 alleles. They confirmed transgene expression by western blot and demonstrated that MeCP2 localizes to polytene chromosomes (Fig. IV).

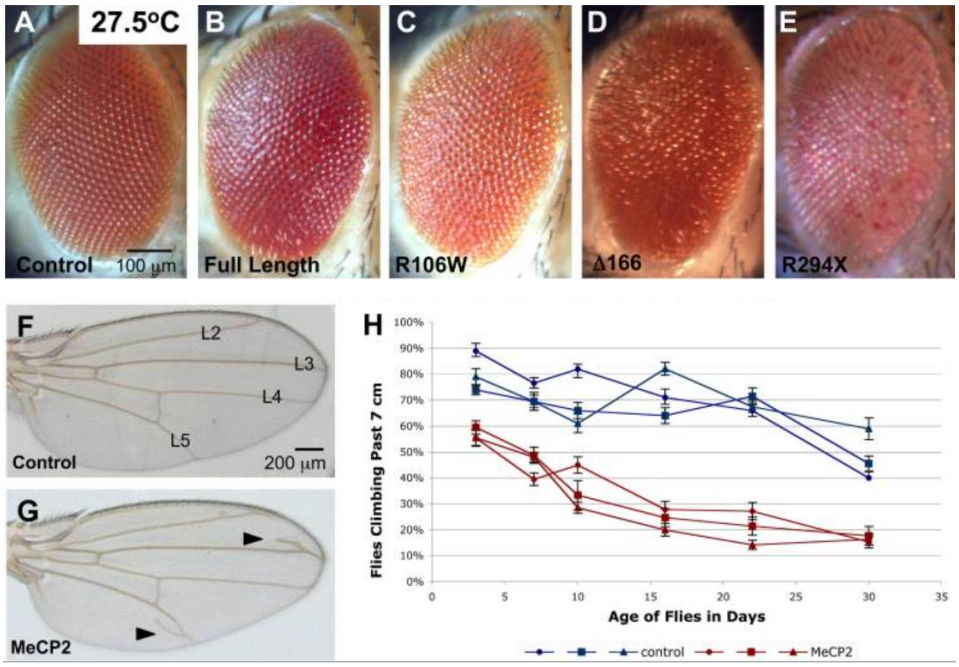

Figure V. Light microscope images (**A–E**) of fly eyes from controls or animals expressing MeCP2 driven by *GMR*-Gal4 driver at 27.5°C. External eyes of control flies show normal ommatidial organization, while eyes from animals expressing any of four distinct MeCP2 alleles show disruption in the structured pattern of the eye surface. **F–G**. The C5-Gal4 driver was used to drive either UAS-lacZ or full-length MeCP2 throughout the wing pouch at 25°C. Compared to controls, MeCP2 expressing flies have extra vein tissue (arrowheads) near L3 and L5. H. The neuronal driver Cha-Gal4 was used to drive expression of either UAS-eGFP or full-length MeCP2 at 25°C (Adapted from Cukier et al., 2008).

Importantly, flies expressing human *MECP2* displayed neurological phenotypes reminiscent of RTT features, including disrupted eye morphology, impaired climbing ability, and wing abnormalities (Fig. V).

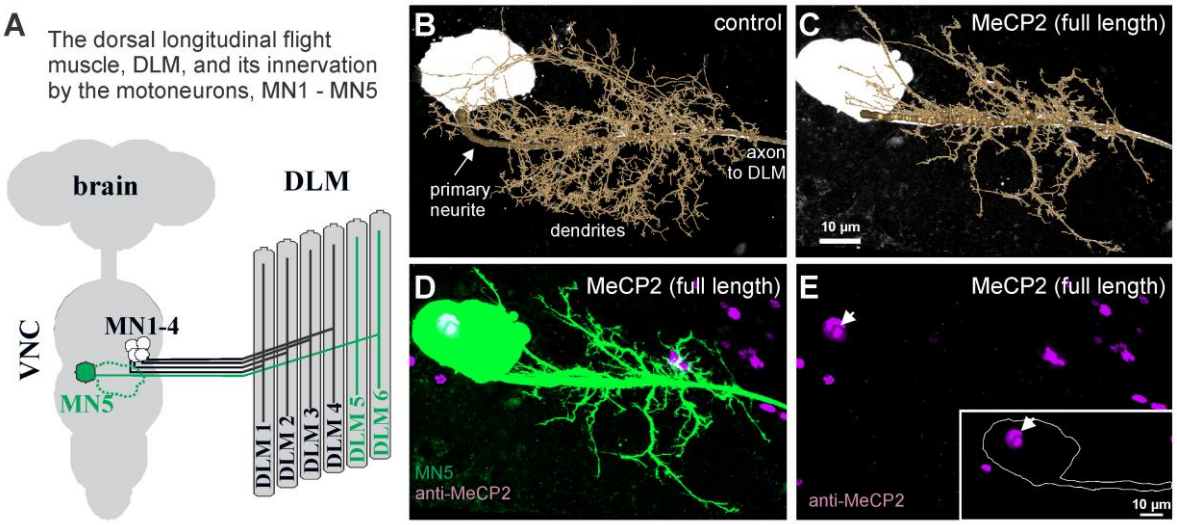

Figure VI. Heterologous expression of human *MECP2* in *Drosophila* motoneurons. (A) Schematic of MN1–5 and their innervation of dorsal longitudinal flight muscles (DLMs). (B) Normal dendritic structure of MN5. (C) Dendritic defects in MN5 upon *MECP2* expression. (D–E) MeCP2 immunostaining shows localization restricted to the MN5 nucleus, with no signal in dendritic processes (adapted from Vonhoff et al., 2012).

Vonhoff et al. (2012) first showed that neuronal overexpression of human *MECP2* in *Drosophila* leads to striking dendritic abnormalities, including a ~60% reduction in branch number and ~50% decrease in total dendritic length. Importantly, these defects required an intact methyl-CpG-binding domain (MBD), as mutant alleles lacking MBD function failed to elicit structural changes, indicating that the phenotypes arose from specific molecular actions rather than nonspecific toxicity. These dendritic impairments translated into severe motor dysfunctions: affected flies displayed drastically reduced flight capacity, with mean flight bout duration reduced by a factor of ~60, highlighting the functional consequences of MeCP2 dysregulation in motor circuits (Figure VI).

Building on these findings, the authors employed *Drosophila* as a high-throughput platform to identify genetic modifiers of MeCP2-induced phenotypes. Using both candidate gene and genetic screen approaches, they found that multiple chromatin remodeling genes (e.g., *osa, Asx, corto, Scm, trx*), the kinase *tricornered (trc)*, and the UBE3A target *pebble (pbl)* could either suppress or exacerbate MeCP2-dependent phenotypes. Notably, reduction of *osa* dosage ameliorated dendritic defects, suggesting that MeCP2 toxicity in flies may arise through aberrant chromatin remodeling rather than direct DNA methylation. These insights underscore the utility of the fly

model in uncovering conserved pathways and genetic interactions that modulate MeCP2 function.

Together, these studies highlight *Drosophila* as a powerful and genetically tractable system for modeling *MECP2* misexpression effects. While not recapitulating all aspects of RTT, the fly model provides unique advantages: rapid experimental turnaround, precise genetic manipulation, and the capacity to identify modifiers and therapeutic targets. Consequently, *Drosophila* represents an important complementary model for unraveling the molecular mechanisms underlying RTT and related neurodevelopmental disorders.

Building on the established validity of the *Drosophila* model for *MECP2* misexpression, it becomes particularly relevant to extend investigations beyond the nervous system. Given the bidirectional communication of the gut–brain axis and the presence of non-neurological symptoms in *MECP2*-related disorders, exploring muscle and gut phenotypes provides further insights into disease mechanisms.

1.3 Gut and muscles involvement in neurological diseases

1.3.1 Gut functionality and dysbiosis in neurological diseases

As in many other neurological diseases, RTT subjects frequently present with gastrointestinal manifestations such as constipation (Motil et al., 2012) and dysbiosis (Borghi & Vignoli, 2019), suggesting a dysregulation of the gut–brain axis (Figure VII).

The gut–brain axis is a bidirectional communication network that connects the gastrointestinal tract and the central nervous system through neural, endocrine, and immune pathways. Among the microbial factors that sustain this crosstalk, metabolites are key mediators. In particular, beneficial metabolites such as short-chain fatty acids (SCFAs - acetate, propionate, butyrate), generated by bacterial fermentation of dietary fiber, play crucial homeostatic roles (Sittipo et al., 2022).

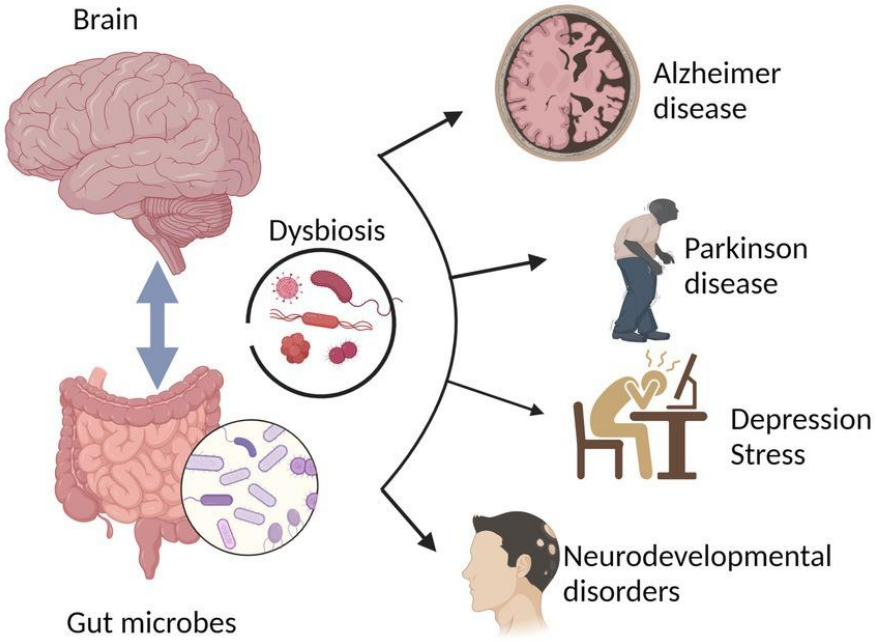

Figure VII. The physiological homeostasis attained during typical brain functioning is a result of the interactions between the brain and the gut-brain. Several brain disorders, including Parkinson's disease, neurodegenerative diseases, depression, stress, Alzheimer's disease, and neurodevelopmental disorders, have been linked to altered gut microbiota or gut dysbiosis (Ullah et al., 2023).

Altered microbiota composition has been associated with a variety of neurological disorders, including Alzheimer's disease, Parkinson's disease, autism spectrum disorder, and epilepsy. In these contexts, dysbiosis is linked to reduced SCFA levels, increased gut permeability, and microglial activation (Pedroza Matute & Iyavoo, 2023; Sittipo et al., 2022).

Recent research has identified significant alterations in gut microbiota composition in RTT patients, revealing a less diverse microbial community with enrichment in *Bacteroidaceae*, *Clostridium* spp., and *Sutterella* spp., alongside depletion in *Ruminococcaceae* (Borghi et al., 2017). These microbiota changes are associated with altered SCFA production and correlate with severe clinical outcomes (Borghi et al., 2017; Borghi & Vignoli, 2019).

1.3.2 Muscle issues in neurological diseases

On the other hand, muscle issues are prominent features across various neurological diseases, affecting both skeletal and potentially visceral muscles. Recent research provides compelling evidence that muscle defects in neurological disorders arise from intrinsic muscle-specific mechanisms rather than solely from denervation. In spinal muscular atrophy, muscle defects occur prior to and independently of motor neuron degeneration, with genetic rescue

experiments demonstrating muscle-specific requirements of disease-causing genes. Similarly, conditional ALS mouse models expressing muscle-specific mutant SOD1 mutants develop muscle atrophy accompanied primarily by muscle-intrinsic defects, with only mild and secondary alterations reported in motor neurons (Boyer et al., 2013). In Huntington's disease, R6/2 transgenic mice exhibit uniform muscle atrophy distinct from typical denervation patterns, along with progressive neuromuscular junction abnormalities and impaired trophic signaling between motor neurons and muscle (Ribchester et al., 2004). These findings demonstrate that muscle tissue plays an active pathological role across multiple neurodegenerative diseases (Duranti & Villa, 2024).

As mentioned before, both RTT and MDS present with hypotonia and muscle abnormalities (Collins & Neul, 2022; Ta et al., 2022). In the RTT mouse model, skeletal muscle exhibits disorganized architecture with hypotrophic fibers and tissue fibrosis, accompanied by alterations in the IGF-1/Akt/mTOR pathway (Conti et al., 2015). Additionally, mice RTT skeletal muscle demonstrates mitochondrial dysfunction, including reduced cytochrome c oxidase subunit I expression, decreased respiratory chain enzyme activity, and diminished glutathione levels, potentially contributing to progressive motor deterioration through oxidative stress (Gold et al., 2014). MDS similarly presents with hypotonia and gastrointestinal problems affecting visceral muscle function (Ta et al., 2022).

1.3.3 Energy Deficits and Chromatin Alterations as Drivers of Muscle Pathophysiology

Muscle morphological and functional defects can arise from both energetic impairments and alterations in chromatin structure.

With regard to energetic deficits, mitochondrial morphology is pivotal for muscle function: disrupted cristae, imbalanced fusion/fission dynamics, or altered mitochondrial networks reduce ATP production and compromise contractility. In *Drosophila* flight muscles, studies have demonstrated a tight coordination between mitochondrial architecture and myofibrillar structure, highlighting mechanical and energetic adaptations that optimize muscle performance (Vila et al., 2017).

In parallel, chromatin alterations exert a profound impact on muscle fiber morphology and function through multiple mechanisms. For example, during aging, skeletal muscle nuclei

undergo structural and molecular changes that affect chromatin organization, gene expression, and transcriptional activity, ultimately contributing to reduced muscle mass and function (Cisterna & Malatesta, 2024). Moreover, external mechanical cues can modulate transcription by remodeling chromatin structure, establishing a regulatory axis that links cellular morphology to nuclear architecture and gene expression (Vergani et al., 2004). Chromatin-modifying enzymes further regulate muscle gene expression by interacting with myogenic transcription factors, thereby influencing differentiation, hypertrophy, and fiber-type specification (McKinsey et al., 2002). Finally, skeletal muscle differentiation relies on highly coordinated epigenetic mechanisms - including chromatin remodeling enzymes and higher-order chromatin organization - that control the activation and repression of tissue-specific genes during myogenesis (Hernández-Hernández et al., 2020).

Taken together, these findings demonstrate that both mitochondrial dysfunction and chromatin structural changes directly contribute to muscle fiber development, maintenance, and function, providing a conceptual framework for investigating muscle pathology in *MECP2*-related diseases using *Drosophila* models.

1.3.4 The *Drosophila* Skeletal Muscles and Neuromuscular Junctions

As little is known about how muscle defects arise in MeCP2-related disorders, *Drosophila* provides a valuable model to investigate the developmental and physiological mechanisms underlying these abnormalities.

Larval muscle fibers are established during embryogenesis, whereas adult muscle fibers originate during metamorphosis, either through remodeling of larval fibers or *de novo* differentiation from muscle precursor cells, such as in the development of indirect flight muscles (Schultheis et al., 2019).

Drosophila melanogaster larvae possess a highly organized musculoskeletal system that integrates the exoskeletal cuticle, somatic body wall muscles, and visceral gut musculature to support locomotion, organ positioning, and digestion.

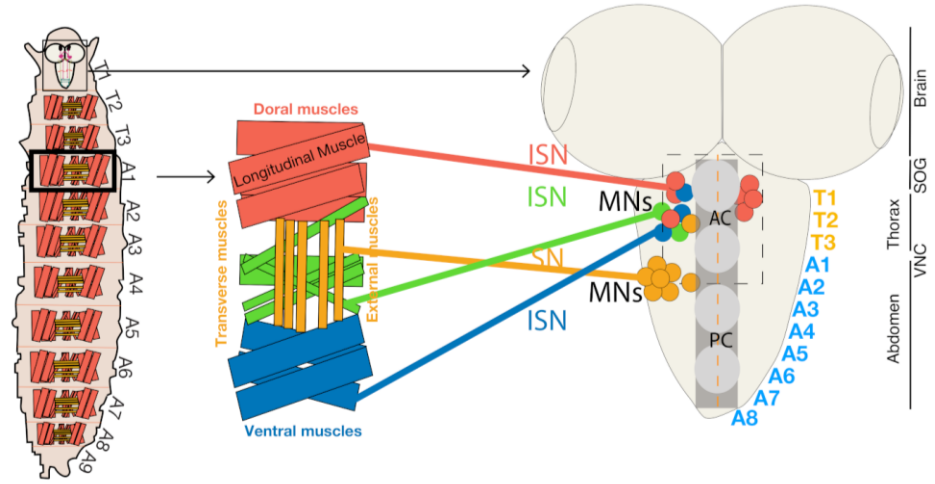

Figure VIII. Schematic of the *Drosophila* larval CNS and neuromuscular system, showing brain, subesophageal ganglia (SOG), and ventral nerve cord (VNC). Motor neurons (MNs) in the VNC innervate abdominal muscles via intersegmental (ISN) and segmental (SN) nerves, forming a myotopic map of motorneuron-to-muscle connectivity (adapted from Gowda et al., 2021)

The larval body wall includes specialized skeletal muscles, such as dorsal, ventral, and lateral groups, organized segmentally and innervated by defined motor neurons, which generate coordinated crawling movements through precisely timed contractions (Figure VIII; Ashley & Carrillo, 2025; Bate, 1990; Heckscher et al., 2012). Certain muscles, including alary muscles and thoracic alary-related muscles, connect the circulatory system and midgut to the exoskeleton, functioning as spring-like structures that maintain organ positioning during locomotion (Bataillé et al., 2015). These somatic muscles also act as developmental organizers, providing scaffolding for adult flight muscles during metamorphosis, with myoblast fusion and myotendinous junction formation regulated by factors such as fascin (Camuglia et al., 2018; Poovathumkadavil & Jagla, 2020; Roy & VijayRaghavan, 1998).

The *Drosophila* neuromuscular junctions (NMJ) serve as an excellent model system for studying synaptic transmission, sharing structural and functional similarities with human synapses (B. Zhang & Stewart, 2010). The larval body wall contains 30 muscles per hemisegment innervated by 35 motor neurons in a highly stereotyped pattern (Brent et al., 2009).

1.3.5 The *Drosophila* gastrointestinal system

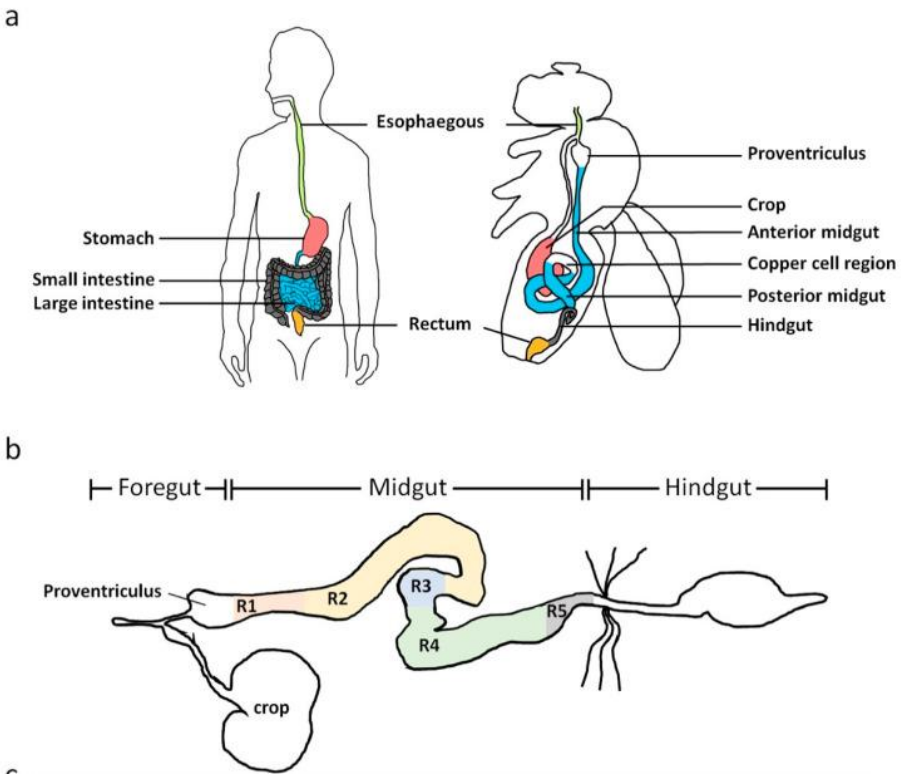

Figure IX. Comparison of human and *Drosophila* digestive tracts. (a) Major functional regions are conserved, including esophagus, midgut (anterior/posterior), hindgut, and stomach/crop. (b) *Drosophila* gut subregions, with foregut (crop, proventriculus), midgut (R1–R5), and hindgut (adapted from Chiang et al., 2022).

Figure IX highlights the gastrointestinal tract of adult *D. melanogaster*, with panel B showing the segmented gastrointestinal tract (R1–R5) (Chiang et al., 2022). Similar to humans, the fly possesses an esophagus, a crop, and mid and hindgut that perform digestive and defense

functions. The visceral musculature surrounds and supports the alimentary canal, providing the contractile framework that drives peristalsis.

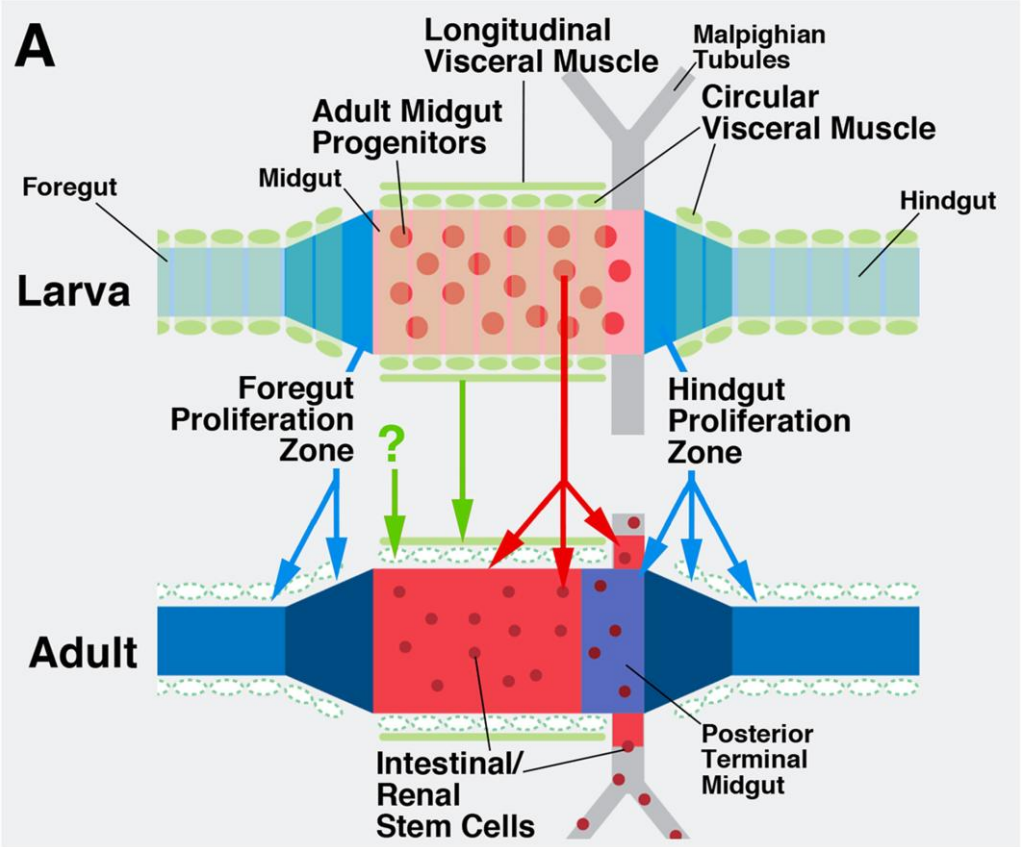

Figure X. Schematic representation of the *Drosophila* intestine, indicating ontogenetic relationship between larval and adult structures. (Adapted from Aghajanian et al., 2016)

The fly gut is encased by visceral musculature composed of longitudinal and circular syncytial fibers, which support peristalsis, digestion, and epithelial homeostasis (Figure X; Aghajanian et al., 2016; Klapper, 2000). Visceral muscles undergo extensive remodeling during metamorphosis, dedifferentiating into mononuclear myoblasts before redifferentiating to form the adult gut musculature (Aghajanian et al., 2016).

Gut motility is coordinated by specialized enteroendocrine cells expressing Diuretic Hormone 31 (DH31) and by somatic motor neurons innervating the hindgut and sphincter, enabling sequential defecation cycles (Lajeunesse et al., 2010; X. Zhang et al., 2014). Neurotransmitters such as proctolin and glutamate mediate precise neuromuscular signaling to circular muscle fibers, ensuring effective intestinal contractions (Anderson et al., 1988).

Functional studies have demonstrated that defects in skeletal or gut muscles, as seen in AMPK or drop-dead mutants, impair peristalsis and nutrient absorption, highlighting the essential interplay between muscle integrity and digestive function (Bland et al., 2010; Peller et al., 2009).

Together, the larval skeletal system and visceral musculature form an integrated framework that coordinates locomotion, organ protection, and gut physiology, providing a versatile platform for developmental and functional studies in *Drosophila* (Bataillé et al., 2015; Weitkunat & Schnorrer, 2014).

1.4 Short-Chain Fatty Acids (SCFAs)

Preclinical studies suggest that interventions such as supplementation with probiotics, prebiotics, synbiotics, dietary modulation, or fecal microbiota transplantation can mitigate neuroinflammation and improve neurological phenotypes (Loh et al., 2024; Zheng et al., 2023). Nevertheless, further clinical studies are required to validate these approaches and fully translate them into effective therapeutic strategies for human patients (Alves et al., 2025; Ashique et al., 2024; Hsieh et al., 2024; Wang et al., 2023).

1.4.1 Production and General Mechanisms

SCFAs, primarily acetate, propionate, and butyrate, are metabolites produced by gut microbiota via fermentation of dietary fibers (Canani et al., 2011; Dalile et al., 2019; DeCastro et al., 2022). Chemically, SCFAs are saturated aliphatic organic acids with fewer than six carbons; acetate (C2), propionate (C3), and butyrate (C4) are the most abundant and biologically significant (Cook & Sellin, 1998). As postbiotics, SCFAs act as functional microbial-derived molecules that directly modulate host physiology (Figure XI). They exert their effects through multiple mechanisms, including activation of specific G-protein-coupled receptors (GPR41, GPR43, GPR109A) and inhibition of histone deacetylases (HDACs), influencing energy metabolism, immune responses, and epigenetic regulation (Koh et al., 2016; Tan et al., 2014).

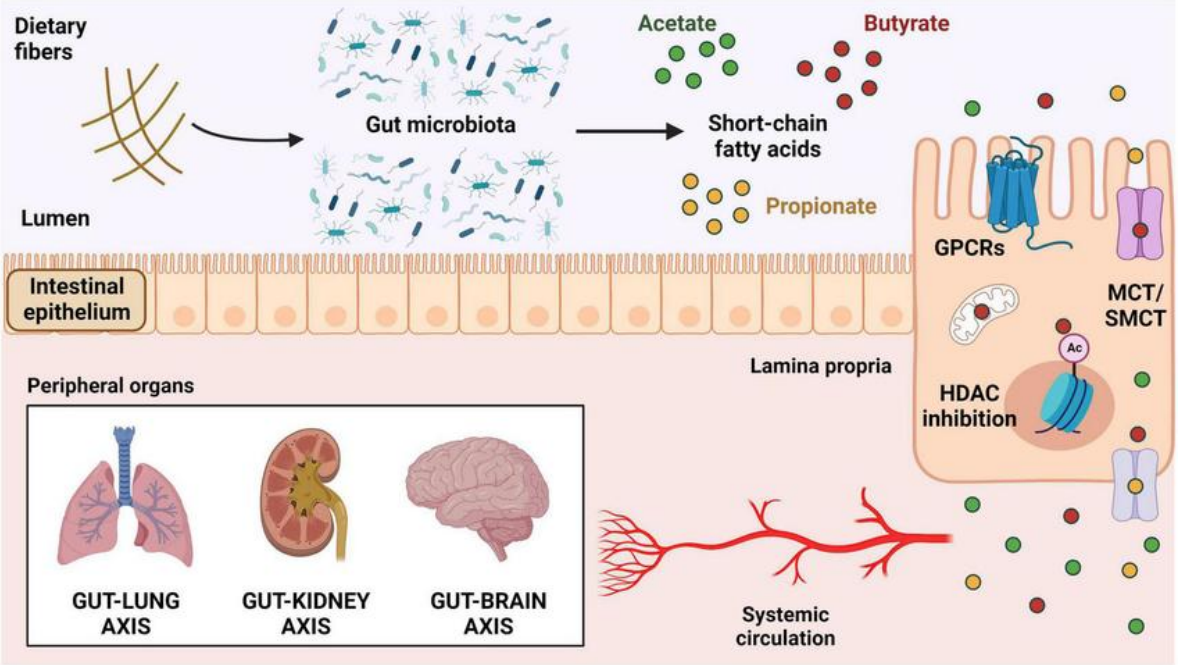

Figure XI. Mechanisms of actions of short-chain fatty acids. Production of SCFAs by bacterial fermentation of soluble dietary fibers in the colonic lumen. These metabolites can activate GPCRs expressed on the surface of intestinal epithelial cells (HCAR2/GPR109a, FFAR2/GPR43, and FFAR3/GPR41) or be internalized by cellular transporters (MCT and SMCT). Once inside the cells, SCFAs can be used in the mitochondria for ATP generation, act in the nucleus as HDAC inhibitors, or be transported outside of the cells into the intestinal lamina propria and subsequently into the bloodstream. Upon reaching systemic circulation, SCFAs can modulate the function of several target tissues, including lungs, kidneys, and brain. SCFAs, short-chain fatty acids; GPCRs, G-protein-coupled receptors; FFAR, free fatty acids receptor; HCAR2, hydroxycarboxylic acid receptor 2; MCT, proton-coupled monocarboxylate transporter; SMCT, sodium-coupled monocarboxylate transporter; HDAC, histone deacetylase (Correa et al., 2022).

1.4.2 Energetic Roles of Butyrate: Mitochondria and Muscle

Butyrate (NaB) serves as the primary energy source for colonocytes, supporting mitochondrial respiration and preventing autophagy in germ-free mice (Donohoe et al., 2011). In skeletal muscle and brown adipose tissue, supplementation enhances mitochondrial biogenesis, fatty acid β-oxidation, and respiratory function, protecting against diet-induced metabolic dysfunction and insulin resistance (C. L. Gao et al., 2011; Mollica et al., 2017; Rose et al., 2018).

The tight coupling between mitochondrial architecture and myofibrillar organization (Vila et al., 2017) supports the idea that modulating mitochondrial dynamics through NaB could help preserve muscle integrity (H. Liu et al., 2023).

Animal studies further validate the protective effects of NaB: in dexamethasone-induced muscle atrophy, it reduces proteolysis and downregulates atrophy-related genes (Zhao et al., 2025); in aging mice, it preserves fiber size, improves mitochondrial metabolism, and decreases oxidative stress (Walsh et al., 2015). These data highlight the central role of butyrate in supporting systemic energy homeostasis and skeletal muscle health.

1.4.3 Epigenetic Roles of Butyrate: HDAC Inhibition

Beyond metabolism, butyrate functions as a histone deacetylase (HDAC) inhibitor, promoting histone hyperacetylation and altering gene expression (Davie, 2003). This epigenetic modulation affects a subset of genes, particularly via Sp1/Sp3 binding sites, leading to anti-proliferative, pro-differentiative, and anti-inflammatory effects. In skeletal muscle cells, HDAC inhibition contributes to protection against insulin resistance and obesity-related phenotypes (Steliou et al., 2012).

In the nervous system, butyrate enhances neurogenesis, supports memory consolidation, and exhibits neuroprotective effects. For example, in Huntington's disease mouse models, it extends lifespan, improves motor function, and delays neuropathological progression (Ferrante et al., 2003). Moreover, NaB restores mitochondrial function in obesity-related neuroinflammation models, upregulates brain-derived neurotrophic factor (BDNF), and reduces oxidative stress in neurons and synapses (Cavaliere et al., 2023; Yan et al., 2024)

Collectively, SCFAs, and butyrate in particular, act as postbiotic molecules with integrated metabolic, epigenetic, and neuroprotective roles. Their ability to maintain mitochondrial integrity, modulate muscle function, and regulate gene expression positions them as promising therapeutic agents for neuromuscular and neurodegenerative disorders.

1.4.4 *Drosophila* for SCFA

Drosophila is also useful for studying the effects of supplements and pharmacological compounds. For example, feeding with 4-phenylbutyrate (a butyrate derivative) extends fly lifespan (Kang et al., 2002) by modifying histone acetylation, while addition of sodium butyrate mitigates motor deficits in a rotenone-induced Parkinson's model (St. Laurent et al., 2013), probably through its HDAC inhibitor activity. Moreover, the ease of raising large populations

of *Drosophila* at low cost and rapidly evaluating behavioural and physiological phenotypes makes it ideal for high-throughput screening of new drugs or nutrients. This approach tests antimicrobial and nutraceutical compounds (following the 3R paradigm) before moving to more complex models (Link & Bellen, 2020; Vidal et al., 2024).

2. Aims

The aim of my PhD thesis is to investigate the role of *MECP2* misexpression in non-neuronal tissues, with a focus on muscles in the *Drosophila melanogaster* model. A second objective is to use this model to test SCFAs, some of which are already in clinical trials, on the observed defects and to explore the mechanisms underlying their potential beneficial effects. The ultimate goal is to contribute to the understanding of non-neuronal symptoms in *MECP2*-related disorders - which are numerous and still poorly characterized - and to use the *Drosophila* model to dissect the mechanisms of action of promising therapeutic supplements that may also be applicable to other chromatin-related diseases.

3. Materials and Methods

3.1 *Drosophila* Husbandry, Crosses, and Strains

All strains were maintained on standard cornmeal-based food containing yeast, molasses, and agar at 25 °C, unless otherwise specified. Tissue-specific overexpression of human *MECP2* was achieved using the binary Gal4/UAS system (Brand and Perrimon, 1993). For temporal control of *Gal4* activity, *tub-Gal80^ts* was employed: at 18°C, Gal80^ts represses Gal4, whereas at 29 °C or above, it becomes inactive. Crosses were set at 25 °C, and progeny were shifted to 29 °C when higher *UAS*-driven expression was required.

The following genotypes were used:

3.1.1 *Gal4* Drivers

- *Act5C-Gal4 (in house)*
- *Tubulin-Gal4 (in house)*
- *elav-Gal4 (Grifoni Lab, Università dell'Aquila, Italy)*
- *D42-Gal4 (BDSC#8816)*
- *GMR-Gal4 (in house)*
- *Ilp-Gal4 (Aliaga Lab, Francis Crick Institute, UK)*
- *Mip-Gal4 (Aliaga Lab, Francis Crick Institute, UK)*
- *Mef2-Gal4 (Jafar-Nejad Lab, Baylor College of Medicine, TX)*
- *how24B-Gal4 (Jafar-Nejad Lab, Baylor College of Medicine, TX)*
- *c179-Gal4 (BDSC #6450)*
- *vm-Gal4 (BDSC #48547)*
- *r4-Gal4 (in house)*
- *cg-Gal4 (BDSC#7011)*
- *MyO-Gal4 (BDSC #83278)*
- *NP3270-Gal4 (DGRC#113192)*
- *NP3207-Gal4 (DGRC#113157)*
- *hand-Gal4 (BDSC #66795)*
- *tey-Gal4 (BDSC #2702)*
- *tub-Gal80^ts (BDSC #7108)*

3.1.2 *UAS* Responders

- *UAS-MECP2 (Botas Lab, Baylor College of Medicine, TX)*
- *UAS-MECP2-R294X (Botas Lab, Baylor College of Medicine, TX)*
- *UAS-MECP2-R106W (Botas Lab, Baylor College of Medicine, TX)*
- *UAS-MECP2-Δ166 (Botas Lab, Baylor College of Medicine, TX)*
- *UAS-GFP (BDSC #5431)*
- *UAS-nuclear LacZ (Vincent Lab, Francis Crick Institute, UK)*
- *UAS-RFP (BL#27391)*

3.1.3 Strains for Mutagenesis via Imprecise P-element Excision and RNA interference lines

- w+;Sp/CyO;Δ*2-3[ry+],Sb/TM6,Ubx* (transposase: in house)
- y[1] w[67c23]; P{y[+mDint2] w[+mC]=EPgy2}CG15439[EY01496] (P-element insertion: BDSC#20121)
- P{KK108167}VIE-260B (VDRC#110635)
- w1118; P{GD9021}v19490 (VDRC#19490)

BDSC: Bloomington *Drosophila* Stock Center; VDRC: Vienna *Drosophila* Resource Center; DGRC: *Drosophila* Genomics Resource Center

3.2 Temporal Control of *MECP2* Expression using Gal80^TS

To achieve temporal control of *MECP2* expression and circumvent the early lethality associated with constitutive expression under the *Mef2-Gal4* driver, we employed the temperature-sensitive Gal80 repressor (Gal80^ts). The Gal80^ts system is a well-established method for regulating Gal4/UAS-mediated gene expression in *Drosophila* in a temperature-dependent manner (Zeidler et al., 2004). Gal80 normally inhibits the transcriptional activator Gal4 (Ma & Ptashne, 1988); however, the Gal80^ts variant allows temporal modulation of this inhibition. At 18 °C (the permissive temperature), Gal80^ts binds and represses Gal4, thereby preventing UAS-driven transcription. Upon shifting to 25 °C (the restrictive temperature), Gal80^ts becomes inactive, releasing Gal4 and enabling expression of the UAS-linked transgene (Barwell et al., 2023).

In larval experiments, *Mef2*-Gal4 was used without Gal80^ts, resulting in constitutive expression of *MECP2* from the embryonic stage onward. For adult gut morphology analyses, temporal control was achieved using *tub*-Gal80^ts in combination with *Mef2*-Gal4. *MECP2* expression was induced either immediately after eclosion (10 days after egg laying, AEL) or after gut maturation (15 days AEL, corresponding to 5 days post-eclosion), by shifting flies from 18 °C to 25 °C. Crosses were performed using the same *Mef2*-Gal4 and UAS-*MECP2* lines described in the previous section.

3.3 Assessment of Tissue-specific Expression of Gal4 Rrivers

To validate the tissue specificity of the Gal4 drivers used in this study, we employed the UAS-GFP reporter system. Each driver line was crossed to a UAS-GFP responder line, and the resulting progeny was screened for GFP expression in vivo using fluorescence microscopy. GFP signal was evaluated at different developmental stages including larvae, and, when applicable, pupae and adult flies to capture dynamic expression patterns across tissues and time points.

Microscopy was performed on whole-mount individuals or dissected tissues, using appropriate filter sets to detect GFP fluorescence. To exclude potential artifacts due to tissue autofluorescence, each driver line was also crossed to a control lines (lacking the *UAS-GFP* transgene), and the same imaging settings were applied. Only GFP patterns distinguishable from background autofluorescence were considered specific. Representative images supporting these observations were collected (data not shown) and are available upon request.

3.4 Lethality Quantification

3.4.1 Quantification of Adult Lethality

To quantify the lethality associated with *MECP2* overexpression, we performed genetic crosses between tissue-specific Gal4 drivers (in heterozygosity and balanced over a dominant marker) and a homozygous *UAS-MECP2* responder line. For each cross, an equal number of virgin females and males (typically 10 of each) were mated in standard vials, and egg laying was synchronized over a 24-hour period to minimize variability in developmental timing. Progeny were scored approximately 12 days after egg laying, in parallel across all experimental conditions.

Under Mendelian inheritance, 50% of the progeny were expected to carry both the Gal4 driver and the *UAS-MECP2* transgene. We counted the total number of emerging adult flies and determined the percentage of *MECP2*-expressing individuals by identifying those carrying the Gal4 driver marker. This observed frequency was divided by the expected 50% to calculate a survival ratio (i.e., *observed% / expected%*). The lethality ratio was then defined as the reciprocal of the survival ratio (i.e., *lethality = 1 / survival ratio*) and used to quantify the severity of developmental lethality across genotypes. This approach allowed normalization of lethality values regardless of variations in total progeny numbers.

Synchronized egg collections were incubated at 25 °C on control or supplemented food. At 5 days AEL, the ratio of pupae to wandering L3 larvae was calculated. Pupae displaying rigid, elongated cuticle were scored as non-viable.

3.4.2 Developmental Staging of Lethality

To further characterize the developmental stage at which lethality occurred, we performed staging of all synchronized progeny 12 days after egg laying (AEL), a time point at which control flies had fully reached adulthood. All crosses were synchronized by allowing egg laying over a 24-hour period and incubated at 25°C on control or supplemented food. At day 12 AEL, progeny from all genotypes were examined, and their developmental stage was recorded based on external morphology.

For genotypes exhibiting partial lethality, particularly *Mef2>MECP2* and *how24B>MECP2*, we quantified the number of individuals still at the larval, early pupal, or late pupal stage. These counts were expressed as a percentage of the total number of progenies in the vial, allowing comparison across conditions and replicates. The resulting distribution was used to identify developmental delays or blocks and was graphically represented to complement the adult lethality data.

3.5 Larval and Gut Length Measurements

Larval length was measured in wandering third-instar larvae without anesthesia. Larvae were gently placed on a flat surface and immediately imaged under a stereomicroscope equipped with a calibrated scale. For each condition, a minimum of 10 larvae were imaged, and total body length was measured from the anterior mouth hooks to the posterior spiracles using Fiji (ImageJ).

Gut length was assessed in dissected whole guts from third-instar larvae and adults. After dissection in cold PBS, samples were fixed in 4% paraformaldehyde (PFA), mounted in PBS, and imaged at low magnification. The total gut length was measured from the proventriculus to the hindgut end/posterior ampulla with Fiji.

In addition to length, gut width was measured in a defined anatomical region immediately distal to the acid zone, where the midgut resumes a straight and regular morphology. The measurement was performed perpendicularly to the gut axis and normalized by always selecting the same segment across samples. A minimum of 5 guts per genotype and condition were analyzed.

3.6 Eye Roughness Phenotypes

To evaluate the impact of *MECP2* overexpression on eye development, flies carrying *UAS-MECP2* constructs were crossed with the *GMR-Gal4* driver line, which induces expression in the developing eye imaginal disc. Crosses were maintained at 29°C to enhance Gal4-driven expression. Adult flies (1–6 days after eclosion) were anesthetized using ice and imaged using a stereomicroscope equipped with a color camera. Eye morphology was assessed based on the disruption of ommatidial organization and loss of pigmentation, which are indicative of rough eye phenotypes. Representative images were acquired for each genotype.

3.7 Wing Phenotypes

To investigate wing abnormalities potentially associated with neuromuscular defects, *UAS-MECP2* lines were crossed to the *D42-Gal4* driver and *GMR-Gal4* to the *CG15439* RNAi line (#GD). All crosses were conducted at 29 °C to ensure robust transgene activation. Adult flies were anesthetized with CO_2 and their wings were imaged under a stereomicroscope. Wing morphology was examined and compared to control flies to identify deviations such as abnormal posture or structural defects. The penetrance and severity of the wing phenotype were quantified using a minimum of 15 flies per genotype.

3.8 Muscle Morphology and Immunofluorescence

3.8.1 Body-Wall Muscles

Third-instar larvae were dissected in cold PBS (Sigma-Aldrich#D8537)and fixed in 4% paraformaldehyde (PFA; Carlo Erba Reagents#415694) for 20 minutes at room temperature.

Samples were washed in 0.1% PBST (PBS + 0.1% Triton X-100) and blocked for 30 minutes in 3% BSA. Tissues were then incubated overnight at 4°C with rabbit anti-MECP2 antibody (Invitrogen PA1-887, 1:200) to assess MECP2 expression, and stained for 2 hours at room temperature with Alexa Fluor 488-conjugated anti-rabbit IgG (Jackson ImmunoResearch 111-545-003, 1:200), Phalloidin-TRITC (Sigma P1951, 1:1000) to visualize actin fibers, and 15 minutes with DAPI (Sigma-Aldrich#D9542, 1:5000) for nuclear counterstaining. Samples were mounted in antifade medium and imaged using a confocal microscope (Nikon A1R/AX laser scanning).

Quantitative analysis was carried out using Fiji (ImageJ). For each sample, muscle 6 and 7 were examined in abdominal segments A1–A3, and the width/length ratio was calculated for each muscle as a measure of muscle fiber thickness.

3.8.2 Neuromuscular Junction (NMJ)

To analyze NMJ morphology, dissected larval body-wall preparations (prepared as above) were additionally incubated overnight at 4°C with mouse anti-Bruchpilot (nc82) antibody (DSHB, 1:100), followed by Cy3-conjugated anti-HRP (Jackson 123-165-021, 1:200) and DAPI (Sigma D9542, 1:5000). Confocal images were acquired using a confocal microscope (Nikon A1R/AX laser scanning). NMJs located on muscles 6 and 7 in abdominal segments A1–A3 were analyzed. Quantification of neuromuscular junction (NMJ) morphology and synaptic architecture was performed using Fiji software. Bouton number was determined by manually counting boutons along muscles 6/7 in abdominal segment A1-A3, based on morphological criteria. Branch number was quantified by tracing distinct axonal branches extending from the main nerve terminal. Synaptic active zones were visualized by immunostaining with the presynaptic marker nc82 (anti-Bruchpilot), and their integrated density was calculated by measuring the sum of nc82-positive pixel intensities within the NMJ region of interest. For each genotype, values were normalized to muscle surface area to account for differences in muscle size.

3.8.3 Visceral Muscles

Visceral muscles were analyzed in both larval and adult midguts. Guts were dissected and fixed in 4% PFA for 40 minutes at room temperature, then permeabilized with 0.2% PBST and blocked in PBTN (PBS + 0.1% Triton X-100 + 4% horse serum) for 30 minutes.

Samples were stained with the following reagents:

- Phalloidin-Alexa Fluor 647 (Invitrogen A22287, 1:500) to visualize visceral muscle fibers
- Rabbit anti-MECP2 (Invitrogen PA1-887, 1:200), incubated overnight at 4°C
- Alexa Fluor 488-conjugated anti-rabbit IgG (Invitrogen A11008, 1:200) as secondary antibody

Samples were mounted in Vectashield with DAPI (Thermofisher#NC9524612) and imaged using confocal microscopy. Morphological evaluation focused on the muscle fibers in a defined region of the midgut, immediately distal to the acid zone, which was consistently used across samples. While no direct morphometric quantification was applied, fiber integrity and organization were assessed qualitatively and compared across genotypes.

3.8.4 Immunostaining of Embryos

Mef2>GFP and *c179>GFP Drosophila* lines were used to visualize skeletal and visceral muscles. Embryos of the appropriate stage were collected on apple juice agar plates, treated briefly with 100% bleach for 1–2 min to remove the chorion, and washed thoroughly with distilled water. Embryos were then dried on filter paper and transferred to clean tubes. Fixation was performed in a scintillation vial containing heptane, PBS, and 37% formaldehyde for 20 min with constant shaking. After removal of the aqueous layer, methanol was added, and embryos were vigorously shaken to separate those with intact vitelline membranes, which remained at the interface. Embryos were then transferred to Eppendorf tubes, washed at least twice with methanol, and stored at –20°C until staining.

Fixed embryos were stained with anti-GFP (Abcam #5450) to detect transgene expression, anti-FasIII (DSHB #7G10) to visualize visceral muscle membranes, and DAPI (Vectashield + DAPI, ThermoFisher#NC9524612) for nuclei. Stained samples were mounted in Vectashield and imaged using a confocal microscope.

3.9 Functional Locomotion assays

3.9.1 Larval Crawling Assay

To assess larval locomotor performance, individual wandering third-instar larvae (n = 20 per genotype) were gently transferred using a wet brush onto a Petri dish placed over graph paper with a 0.5 cm^2 grid. Larvae were allowed to acclimate for 30 seconds and repositioned at the center of the plate if necessary. Crawling behaviour was then recorded for 1 minute. The number of grid lines crossed during this period was manually counted, and the total distance travelled was calculated as the number of lines crossed multiplied by 0.5 cm. This value was used to estimate the average speed (cm/min) of each larva. This assay quantifies locomotor ability across genotypes and experimental conditions. Measurements were performed on 10–20 larvae per genotype. The protocol was kindly provided by Valentina Fajner (personal communication).

3.9.2 Larval Wandering Ability Assay

To evaluate larval locomotor behaviour associated with pupariation, we assessed the wandering ability of late third-instar (L3) larvae. Wandering is defined as the physiological crawling movement by which larvae leave the food substrate to pupariate on the side of the vial. For each genotype, larvae ($n \approx 30$) were allowed to wander naturally within their original food vials. The amount of food in each vial and the egg-laying time was carefully standardized to normalize larval density and minimize environmental biases. Locomotor ability was quantified by measuring, in millimeters, the linear distance between the food surface level and the final position of the pupal case along the vial wall. This assay provides a simple and quantitative measure of larval locomotor performance related to developmental progression.

3.9.3 Adult Climbing Assay

Female adult flies (10 per vial, $n = 4$ vials per genotype), raised on either control or supplemented diets, were tested for motor performance using a standard negative geotaxis (climbing) assay. Flies were gently tapped to the bottom of the vial and given 10 seconds to reach a 7 cm mark. The proportion of flies surpassing the mark was recorded. Each group was tested at four time points: 5, 10, 20, and 30 days post eclosion (dpe). For each vial at each time point, the climbing test was repeated 5 times, with 5-minute rest intervals between trials to

avoid fatigue. Videos were recorded for all trials and analyzed offline to ensure consistent and accurate scoring.

To reduce variability due to manual handling, a custom-designed rack allowing simultaneous mounting and tapping of up to 10 vials was used. This setup enabled parallel testing of all experimental conditions, ensuring synchronized tap-down and minimizing operator bias. The climbing index was calculated as the average proportion of flies that surpassed the mark across the five trials for each vial. Importantly, flies were not exposed to CO_2 anesthesia for at least 3 days prior to testing to avoid any confounding effects on motor performance. The assay protocol follows established methods widely used in *Drosophila* behavioural studies.

3.9.4 Adult Muscle Seizure Assay

To assess mechanically induced myoclonic seizures in adult flies, we developed a behavioural assay based on startle-induced seizure activity. This test was performed on the same individuals previously used in the climbing assay at 30 dpe. Flies of each genotype were mechanically stimulated by gently tapping the vial against a hard surface two to three times, eliciting a startle response. In susceptible flies, this stimulus triggered transient, involuntary myoclonic seizures, followed by spontaneous motor recovery. Ten seconds after stimulation, the number of flies still exhibiting seizure activity was recorded and normalized to the total number of individuals tested. Videos are available upon request.

3.9.5 Mouth Hook Contraction Assay

Third-instar wandering larvae of *Drosophila melanogaster* carrying either the *Mef2>GFP* control or *Mef2>MECP2* transgenes were synchronized by collecting eggs from equal numbers of parental flies (20–25 pairs per tube) on standard cornmeal–molasses medium. At approximately 96 hours post-egg laying, early wandering L3 larvae were gently harvested under a stereomicroscope using fine-tip forceps and transferred in groups of five into silicone-coated Petri dishes containing a thin layer (~2 mm) of 2% yeast solution. Following a 30-second acclimation period, larval movements were video-recorded at 10× magnification for 60 seconds. Individual body-wall contraction waves were subsequently counted from the recordings, and the mean contraction rate per minute was calculated for each group. Four independent biological replicates were performed for each genotype. Statistical comparison

between the *Mef2>GFP* and *Mef2>MECP2* cohorts was conducted using an unpaired two-tailed Student's *t*-test in GraphPad Prism. Videos are available upon request.

3.10 Gut motility assays

3.10.1 Gut Peristalsis

Gut peristalsis was assessed both in wandering third-instar larvae (L3) and adult flies. Larvae were gently washed in PBS prior to dissection to remove debris. Intact guts were carefully dissected in room temperature Schneider's *Drosophila* Medium (Thermo Fisher Scientific#21720-024). Dissection aimed to maintain all connected tissues while exposing only the apical gut region around the physiological constriction (approximate boundary at the start of the acidic zone).

After dissection, guts were transferred to fresh Schneider's medium at room temperature. The preparation was allowed to equilibrate until the first peristaltic contraction was observed. At that moment, a timer was started and peristaltic contractions were counted manually under a stereomicroscope for 1 minute.

3.10.2 Gut Clearance Assays

Two different gut clearance assays were performed on synchronized L3 larvae fed on a bromophenol blue (Merck#B8026)-supplemented diet (0.0005%) to compare genotypes and evaluate dietary supplementation effects.

- **Blue Larvae Percentage Assay (Genotype Comparison):** Larvae were placed on Whatman paper soaked with 20% sucrose in PBS containing a blue dye. The percentage of larvae displaying blue gut content was recorded at defined time points as a readout of clearance efficiency.

- **Food Retention Index (Dietary Supplementation):** For a more quantitative assessment, larvae (10 per replicate, 5 replicates per genotype) were similarly exposed to the dyed sucrose solution, and residual gut content was scored at 8, 24, and 36 hours post-exposure. The food retention index (FRI) was calculated as:

  $$FRI = (No\ discharge \times 1 + Semi\ discharge \times 0.5 + Full\ discharge \times 0) / Total\ larvae\ scored$$

This index allowed finer quantification of gut clearance differences across dietary conditions.

3.11 Diet Supplementation Protocols

All supplementation experiments were conducted using standard *Drosophila* medium (cornmeal-agar-yeast) as the base diet. Each supplement was prepared by first creating a stock solution, which was then diluted into the diet after it had cooled to 65°C to prevent degradation of the compounds. The mixture was thoroughly homogenized to ensure even distribution. Eggs were laid on the supplemented medium, allowing the progeny to develop from embryo to adulthood under the specific dietary conditions.

Supplementation Details:

- **Sodium Butyrate (NaB):** (Sigma-Aldrich#B5887). A 20 mM stock solution was prepared and diluted 1:10 into the diet, resulting in a final concentration of 2 mM.
- **Valproic Acid (VPA):** (Merck#P4543). Final concentrations of 1 mM and 2.5 mM were used, prepared by diluting the stock solution into the diet.
- **Propionic Acid (PA):** Propionic acid is present in the standard diet at 0.7% as a preservative. To achieve a final concentration of 0%, the existing propionic acid was removed, and additional propionic acid was added accordingly to reach the final concentration of 2.5%.
- **Acetic Acid (AcOH):** (Sigma-Aldrich#27221). A final concentration of 0.75% was used, based on the protocol by Martelli et al., (2024).
- **Lalbaay®** (KOLFARMA SRL#982845036): This commercial product contains sodium butyrate, among other components. The amount added was calculated to provide a final concentration of sodium butyrate equivalent to that used in the sodium butyrate supplementation. Lalbaay also contains maltodextrins, alpha-lactalbumin, inulin, fructooligosaccharides, flavorings, sucralose (a sweetener), and polysorbate 80 (an emulsifier).

Outcome Measures:

- **Developmental Progression**: Assessed by the pupation rate, calculated as the percentage of pupae over total larvae 5 days after egg laying (AEL).

- **Lethality during Larval-Pupa Transition**: Viability was expressed as the percentage of pupae reaching adulthood.
- **Survival Ratio**: Calculated as the observed versus expected ratio of progeny for each genotype, based on Mendelian expectations due to the use of a balancer chromosome. For normalization, the average survival of the control was set to 1 in each condition.

3.12 Electron Microscopy and Mitochondria Analysis

Body wall tissues from *Drosophila melanogaster* were dissected and immediately washed in cold 1× PBS. Samples were fixed for 3 hours at room temperature in 2.5% glutaraldehyde prepared in 0.1 M sodium cacodylate buffer, then post-fixed in 4% osmium tetroxide (cat.19140, Electron Microscopy Sciences, Hatfield, PA, USA) for 2 hours, followed by incubation in 1% aqueous uranyl acetate (cat.22400-1, Electron Microscopy Sciences) for 1 hour at room temperature. After dehydration through a graded ethanol series, specimens were treated with propylene oxide (cat. P021, TAAB Laboratories Equipment, Aldermaston, UK) and embedded in epoxy resin (Poly-Bed; cat.08792-1, Polysciences, Warrington, PA, USA). Polymerization was carried out overnight at 42 °C and then for 48 hours at 60 °C. Semithin sections (200 nm) were obtained and stained with toluidine blue for initial assessment of tissue orientation and preservation. Ultrathin sections (50 nm) were collected on copper grids, counterstained with 1% uranyl acetate, and imaged using a HT7800 120 kV transmission electron microscope (Hitachi) equipped with a Megaview III digital camera and Radius 2.0 software (EMSIS, Muenster, Germany). Mitochondrial morphology was evaluated in transverse sections of muscle fibers. For morphometric analysis, individual mitochondria were manually segmented and measured using the line tool in Radius 2.0 software. Measurements included mitochondrial number and cristae organization and were performed on twenty MIA (multiple image alignment) micrographs for each condition at 20k magnification, on three biologically independent samples (N = 3).

3.13 Generation and Validation of CG15439 Deletion Alleles

3.13.1 Imprecise Excision of a P-element in the 5'UTR of *CG15439*

To generate deletion alleles of *CG15439* (the *Drosophila* ortholog of *PHF14*), we performed imprecise excision of a P-element inserted in the 5' untranslated region (5'UTR) of the gene. Flies carrying this P-element were crossed to a transposase-expressing strain to induce

mobilization. Progeny was screened for loss of red eye pigmentation, a visible marker of excision events.

Candidate excision lines were isolated and maintained as balanced stocks. These lines were then subjected to molecular validation to characterize the nature and extent of the induced genomic alterations.

3.13.2 Genomic DNA Extraction and PCR-based Screening

Genomic DNA was extracted from pools of five whole L3 larvae per genotype using the QIAamp DNA Mini and Blood Mini Kit (QIAGEN, Cat. No. 51104), following the manufacturer's protocol. DNA quantity and purity were assessed with a spectrophotometer (NanoDrop One, Thermo Fisher Scientific).

PCR-based screening was then performed to detect deletions or rearrangements at the excision site. A total of three forward and three reverse primers were designed using Benchling (www.benchling.com), positioned approximately 100, 500, and 1000 base pairs upstream and downstream of the P-element insertion site, respectively. Primer sequences are reported in Table III.

Table III. Primer sequences used for PCR screening of CG15439 excision alleles. Forward (F) and reverse (R) primers flanking the original P-element insertion site were designed at three distances (~100 bp, ~500 bp, ~1000 bp) upstream and downstream, respectively.

Primer Name	Sequence (5'–3')
F1000	TTCGATAAGAAAGCCGGCCA
F500	GAGCACTAGACAGCTGAAGT
F100	TGCGTAGTAATCTTCGGCTG
R100	ACTATTCTGTCCGTGTCATCGC
R500	TGTCGCAGTCGCACTCTAAT
R1000	CCATTGTGCGATTCCGTCTT

Primer design followed standard criteria for specificity, melting temperature, and amplicon length, aiming to balance sensitivity and resolution of potential deletions. Genotyping PCR was carried out using GoTaq® G2 DNA Polymerase (Promega#M7841). Reactions were prepared in a final volume of 50 µL containing 10 µL of 5× Green GoTaq Reaction Buffer, 1 µL of

dNTP mix (10 mM each), 1 μL of each primer (10 μM), 0.25 μL of polymerase (5 U/μL), <500 ng of template DNA, and nuclease-free water up to volume. Cycling conditions were: initial denaturation at 95 °C for 2 min; 25–35 cycles of 95 °C for 30 s, annealing for 30 s (2 °C below the lowest melting temperature of the primer pair), 72 °C for 1 min/kbp; final extension at 72 °C for 5 min; and hold at 4 °C. PCR products were resolved on agarose gels at concentrations ranging from 1% to 2% depending on the expected amplicon size. Gels were stained with DNA Gel Stain and visualized using a gel documentation system. Amplicons showing size shifts compared to controls were considered indicative of potential excision events and were selected for Sanger sequencing.

3.13.3 Sequencing and Analysis of Excision Events

To confirm the molecular nature of excision events, selected PCR amplicons were purified using the Monarch® Genomic DNA Purification Kit (New England Biolabs#T3010) and submitted for Sanger sequencing (Eurofins Genomics). Sequencing data were analyzed using Benchling's alignment tools, comparing each sequence to the *Drosophila melanogaster* reference genome to identify insertions, deletions, or rearrangements near the original P-element insertion site.

3.14 Statistical Analysis

Data are presented as mean ± standard deviation or mean ± standard error, unless otherwise indicated. Each data point corresponds to the mean of technical replicates within a single biological replicate, unless otherwise indicated. Statistical analyses and graph generation were performed using GraphPad Prism 8. Comparisons between two groups were conducted using two-tailed unpaired Student's t-tests. For comparisons involving three or more groups, one-way analysis of variance (ANOVA). Statistical significance thresholds were set as follows and indicated on graphs by asterisks: $p < 0.05$ (*), $p < 0.01$ (**), $p < 0.001$ (***), and $p < 0.0001$ (****).

4. Results

Figures related to this section are provided from page 86 onwards

4.1 Validation of a *Drosophila* Model for *MECP2*-Related Disorders with Tissue-Specific Overexpression

Since *MECP2* is ubiquitously expressed in human tissues - including skeletal and smooth muscle, according to The Human Protein Atlas (proteinatlas.org) - we sought to examine the consequences of its misexpression in different tissues. To this end, we employed the *Drosophila UAS–Gal4* system, which enables tissue-specific gene expression and has previously been used to investigate *MECP2*-related conditions (Cukier et al., 2008). A panel of tissue-specific *Gal4* drivers was therefore tested and selected to drive expression of human *MECP2* together with a GFP reporter (Fig. 1A; Table 1).

As an initial validation, we reproduced established phenotypes resulting from neuronal *MECP2* expression. The overexpression of *MECP2* with the *GMR-Gal4* driver produced a strong rough eye phenotype (Fig. 1B, left panel), consistent with previous observations (Cukier et al., 2008). In addition, expression under the neuronal driver *D42-Gal4* caused developmental abnormalities, including defective wing morphology (Fig. 1B, right panel). Although *D42-Gal4* is primarily a neuronal driver, similar wing defects have been reported when it was used to overexpress a mitochondrial transcription factor (Cagin et al., 2015), suggesting that the phenotype may, at least in part, result from indirect neuronal effects.

Table 1. Expression patterns and lethality associated with different GAL4 drivers in *Drosophila.* GAL4 drivers are grouped according to their main expression domain (ubiquitous, enteric neurons, neurological, mesodermal and enterocytes). For each driver, the larval (L3) expression pattern is shown, indicating the specific tissues in which expression was detected. The last column reports the percentage of lethality at adult stage (12 days AEL), calculated as the inverse of survival based on the expected Mendelian ratio in flies expressing human *MECP2*.

Driver type	Driver	Tested tissue(s) targeted	*MECP2* adult lethality
Ubiquitous drivers	*actin*	whole body	100%
Neurological drivers	*elav*	brain	0%
	D42	nervous system	4%
	GMR	eye discs	63%
Enteric neurons	*ilp*	anterior enteric neurons	0%
	Mip	anterior enteric neurons	0%
Mesodermal drivers	*Mef2*	body wall, visceral muscles, salivary glands	100%

	how24B	body wall, visceral muscles, trachea, salivary glands	100%
	c179	body wall, visceral muscles, salivary glands	83%
	vm	body wall, visceral muscles	100%
	cg	fat bodies	85%
Enterocytes	*Myo*	enterocytes	3%
	NP3270	gut (enterocytes)	0%
	NP3207	gut (enterocytes)	0%
	mex1	gut (enterocytes)	0%

4.2 Developmental Lethality Screening Reveals Muscle as a Site of *MECP2* Misexpression Toxicity

We next assessed the ability of different drivers to induce lethality during development or adulthood, as an indicator of pathological perturbation. Interestingly, *MECP2* expression in the mesoderm, which gives rise to muscles, caused the most pronounced lethality (Table 1). Notably, MECP2 overexpression in the fat body using the cg-Gal4 driver also resulted in substantial lethality (85%), consistent with previous evidence that MeCP2 levels in peripheral metabolic tissues critically influence organismal viability and energy homeostasis (C. Liu et al., 2020). Given the gastrointestinal motility impairments and movement defects observed in patients, we specifically focused on investigating the impact of *MECP2* misexpression in *Drosophila* musculature. To this end, we primarily used *Mef2*-Gal4 and *how24B*-Gal4, two muscle-specific drivers previously validated with a UAS-GFP reporter. Both drivers showed robust expression in skeletal and visceral musculature (Fig. 1C) and led to 100% lethality at the adult stage (Table 1). Immunostaining against MeCP2 confirmed its nuclear localization in both muscle types, consistent with expected chromatin targeting, as previously reported by Cukier et al. (Fig. 1D).

To analyse the effects of MeCP2 in muscles, we quantified survival at 12 days after egg laying (AEL), considering this time point as representative of full adult eclosion under standard conditions. Flies expressing *MECP2* in muscle via *Mef2-GAL4* driver displayed strong developmental lethality, with the majority of individuals arrested at larval or early pupal stages. In contrast, *how24B>MECP2* flies progressed further in development, with most animals

arrested as late pupae, reflecting the later onset of *how-24B* driver expression (Fig. 2A; Galeone et al., 2020).

To further characterize these phenotypes, we visually documented morphological abnormalities across developmental stages. *Mef2 > MECP2* larvae appeared elongated compared to controls with 27% of cases exhibiting pronounced shape distortions suggestive of systemic defects. In contrast, *how24B > MECP2* did not show any morphological defects at either the larval or pupal stage (Fig. 2B-C). These results confirm that muscle tissue is highly sensitive to *MECP2*-induced perturbation and that the developmental timing of expression plays a crucial role in determining the severity of the phenotype.

4.3 Structural and Functional Defects in Larval Skeletal Muscles upon *MECP2* Misexpression

To further investigate the consequences of *MECP2* misexpression in the mesoderm, we focused on larval skeletal muscles, which are highly organized and well-characterized in *Drosophila*. To ensure consistency, we focused on the morphology of muscle 6 and 7 of larval segment A1, 2 and 3 (Fig. 3A). We found that compared with controls, muscle 6 of *Mef2 > MECP2* animals is significantly reduced in thickness compared to control larvae (*Mef2>GFP*) (Fig. 3B). We note that UAS-MECP2 larvae are fully viable and display normal skeletal muscles (Fig. S1), confirming that muscle defects and lethality in *Mef2>MECP2* and *how24B>MECP2* animals result specifically from Gal4-driven overexpression.

To assess muscle functionality, we employed a series of behavioural assays that reflect the performance of the larval and adult muscular system. Larvae expressing *MECP2* in muscles showed significantly reduced crawling speed compared to control larvae (Fig. 3C) and impaired wandering ability compared to controls (Fig. 3D). To obtain data at the adult stage, we employed the later-onset muscle driver *c179* (Fig. S2), as *MECP2* misexpression driven by *Mef2* is fully lethal (Table 1). The *c179* driver allows a fraction of animals to reach adulthood and be assessed for locomotor performance (see Table 1 for lethality rates). Adult flies displayed progressive locomotor decline compared to control, as measured by climbing ability over time relative to age-matched *c179>GFP* flies (Fig. 3E') and abnormal, involuntary myoclonic seizures at the adult stage upon mechanical stimulation, characterized by rapid, repetitive muscle contractions, which were not observed in control adults (Fig. 3E").

Considering the critical role of mitochondria in sustaining muscle function, we analyzed mitochondrial ultrastructure in the body wall muscles of L3 larvae overexpressing *MECP2* in muscles (*Mef2>MECP2*) compared to controls (*Mef2>GFP*). Transmission electron microscopy (TEM) analysis revealed a notable increase in the number of mitochondria, accompanied by a higher incidence of altered cristae morphology (Fig. 3F). The mitochondria accumulation might reflect a compensatory response to energy imbalance in *MECP2*-overexpressing muscles, consistent with previous data in other *Mecp2* KO models (Gold et al., 2014).

Finally, we verified that these defects were not simply due to reduced feeding ability. By measuring mouth hook contractions, even though with higher variability, we found no significant differences between *Mef2>MECP2* larvae and controls (Fig. S3A).

Together, these findings demonstrate that muscle-specific *MECP2* misexpression compromises both the structural integrity as well as the functionality of the skeletal musculature, suggesting that alteration of MeCP2 in patients might affect directly the muscle system.

4.4 MeCP2 Mutant Phenotypes in *Drosophila* (R106W, R294X)

Given the clinical relevance of different *MECP2* mutations in Rett syndrome, we next asked how specific Rett-associated variants modulate the phenotypes observed upon wild-type *MECP2* overexpression. R294X is a nonsense mutation that creates a premature stop codon, converting arginine at position 294 to a stop codon generating a complete deletion of the TRD (Ananiev et al., 2011; Chae et al., 2002). It is reported in several large studies as a pathogenic *MECP2* mutation that generally leads to milder clinical features, including lower clinical severity scores, better preservation of walking ability and hand use, and later onset of stereotyped movements (Cuddapah et al., 2014). One report, however, describes severe intellectual disability associated with R294X (Jara-Ettinger et al., 2021). In contrast, R106W is a missense mutation that affects the highly conserved MBD of MeCP2. This mutation involves a C→T transition at a CpG hotspot, representing one of the recurrent spontaneous mutations identified in RTT patients (Wan et al., 1999). It is consistently associated with a severe phenotype, with patients showing higher clinical severity scores and greater motor

impairments; skewed X-inactivation may contribute to the observed severity in some cases (Mietto et al., 2025)(Figure 4A).

Having established the effects of wild-type *MECP2* (WT) overexpression on skeletal muscle structure and function, we next investigated how these specific variants modulate such phenotypes in *Drosophila*. To this end, we analyzed the above mentioned alleles (R106W, R294X) in assays measuring pupal and muscle morphology and eye phenotype, , following the interpretative framework proposed by Chen et al. (2025). In this model, a variant that behaves like the reference protein or enhancing the phenotype is considered function-retaining (less pathogenic), whereas one that fails to reproduce the reference phenotype (suppressing or "rescuing" it) is classified as loss-of-function (more pathogenic).

Interestingly, compared to *Mef2>MECP2*, *Mef2>MECP2*^{R106W} animals survived to adulthood. In sheer contrast, *Mef2>MECP2*^{R294X} animals survived less than *Mef2>MECP2* animals (Figure 4B). Consistent with this, pupae expressing *MECP2*^{R106W} were of normal size, while those expressing *MECP2*^{R294X} failed to pupariate and elongated as MECP2-expressing larvae (Figure 4C, quantified in C'). As previously shown in Fig. 1, overexpression of wild-type *MECP2* under the *GMR*-Gal4 driver induced a rough-eye phenotype compared to the control *GMR>GFP*. Expression of *MECP2*^{R294X} caused lethality before the eye phenotype could be fully assessed. In contrast, *MECP2*^{R106W} allele resulted in a morphology similar to that of the control (Figure 4D).Visualization of body-wall muscles revealed that MeCP2^{R106W} did not induce muscle thinning while MeCP2^{R294X} induced a strong thinning and degeneration (Figure 4E). Thus, our genetic analysis indicates that gain of function phenotypes of mesodermal MeCP2 expression are not recapitulated by the loss of function MeCP2^{R106W} variant, while the partially function-retaining variant MeCP2^{R294X} yields gain of function phenotypes that are even stronger that of MeCP2.

These results are consistent with the pathogenicity reported in the literature for the *MECP2* variants tested. In particular, the loss-of-function effect for *MECP2*^{R106W} align with its association with more severe phenotypes compared to *MECP2*^{R294X}, which is instead linked to milder clinical presentations (Wen et al., 2020).

4.5 Altered Visceral Muscle Function

Having established the vulnerability of skeletal muscles to *MECP2* misexpression, we next asked whether visceral muscles, which surround the gut are responsible for its motility, were similarly affected. To address this, we expressed *MECP2* using the *Mef2* driver and evaluated gut functionality using two complementary assays: gut clearance and gut peristalsis (Fig. 5A).

To assess gut clearance, we fed third-instar larvae a standard diet supplemented with a blue dye and monitored the natural discharge of food over a 24-hour period, which normally precedes pupariation. In control *Mef2>GFP* animals, nearly all larvae showed proper clearance, transitioning from blue to pale-blue and ultimately white abdomens within 24 hours (Fig. 5B, panels a–c; B'). In contrast, approximately 50% of *Mef2>MECP2* larvae failed to discharge the ingested blue food compared to nearly 100% clearance in control larvae (*Mef2>GFP*) (Fig. 5B, panels d–f; B'). In several cases, dye retention persisted even after the formation of the pupal cuticle, suggesting a failed food discharge. Similar but milder phenotypes in gut discharge defects – due to the later onset expression – were observed with *how24B* driver (Fig. S3B).

Consistent with these findings, the peristaltic activity observed in dissected larvae was strongly impaired in *Mef2>MECP2* animals. Quantification of gut contractions per minute revealed a dramatic reduction in contraction frequency compared to controls (Fig. 5C). Together, these results demonstrate that *MECP2* misexpression in muscles disrupts gut motility, leading to food retention.

4.6 *MECP2* Overexpression Impairs Visceral Muscle Fibers Organization and Gut Structure

Following the observed defects in visceral muscle functionality, we next investigated whether these impairments were associated with structural abnormalities in visceral muscle organization. We first assessed the gross morphology of the gut, and morphometric analysis revealed a significant reduction in gut length in *Mef2>MECP2* larval guts compared to *Mef2>GFP* controls, while gut width remained unchanged, when compared to control guts (Fig. 6A-B). These data indicate that a shortening of the intestinal tract that was not due to the larval size, which on the contrary we found increased in *Mef2>MECP2* animals, relative to control (Fig. 2B).

To examine visceral muscle fiber organization, we performed phalloidin staining and found that approximately 60% of *Mef2>MECP2* larval guts exhibited fragmentation of circular muscle fibers while 0% of control guts showed this phenotype (Fig. 6C). We then extended the analysis to adult visceral muscles using drivers specific for circular (*Hand-Gal4*) and longitudinal (*Tey-Gal4*) fibers, both of which permit adult eclosion. *MECP2* misexpression under these drivers caused structural abnormalities compared to respective driver>*GFP* controls: *Tey>MECP2* resulted in reduced longitudinal fiber thickness (Fig. 6D), while *Hand>MECP2* led to disrupted, net-like patterning of visceral muscle fibers (Fig. 6E). In both conditions, gut length was significantly reduced compared to controls (Fig. 6D',E').

These structural defects were not merely morphological, as *Hand>MECP2* adults also displayed impaired gut peristalsis relative to control adults (Fig. 6F), confirming functional consequences.

Together, these findings demonstrate that *MECP2* misexpression disrupts visceral muscle architecture in both larval and adult stages.

4.7 Temporal Requirement of *MECP2* Expression for Gut–Muscle Phenotypes

To determine whether *MECP2* misexpression affects visceral muscles specifically during their developmental phase or also at later stages, we added to our genetic background a temperature-sensitive repressor of Gal4 activity (Gal80^ts) (Fig. 7A,E). This manipulation allows temporal control of *MECP2* expression under the *Mef2* driver.

We first induced *MECP2* expression immediately after adult eclosion, a stage when the visceral muscles have developed but are still immature. In this condition, we observed prominent gut morphological alterations, including a marked increase in gut width with preserved length compared to age-matched control adults (Fig. 7B), as well as disruption of muscle fiber organization as visualized by phalloidin staining (Fig. 7C). These structural defects were accompanied by significantly impaired gut peristalsis relative to controls (Fig. 7D).

In contrast, when *MECP2* expression was delayed until five days after eclosion, a time when visceral muscles are fully mature, no major macroscopic alterations were observed, except for a

mild reduction in gut length compared to controls (Fig. 7F). Microscopic analysis revealed only subtle disruptions in fiber organization relative to controls (Fig. 7G).

These findings indicate that *MECP2* misexpression has a stronger impact during the developmental phase of visceral muscle formation, while fully differentiated adult visceral muscles are less vulnerable. This highlights a critical temporal window during which *MECP2* expression must be tightly regulated to ensure proper muscle architecture and function.

4.8 The Fly Muscle Defects Associated with *MECP2* Misexpression are Tissue Autonomous

We next tested whether the functional defects observed in *Mef2>MECP2* animals could also arise when *MECP2* is misexpressed in the nervous system. For this purpose, we overexpressed *MECP2* using the pan-neuronal driver *Elav-Gal4*. This was particularly relevant as *Elav*-driven expression had previously shown no lethality (Table 1), suggesting that neuronal misexpression might have a limited impact compared to the severe muscle phenotypes described above. Morphological analysis of skeletal muscle fibers confirmed the lack of muscle effects upon neuronal misexpression. No significant differences were detected in the width/length ratio of muscle 6 and 7 between *Elav>MECP2* and controls (Fig.8A). Furthermore, gut clearance assays showed no significant impairment of intestinal function in *Elav>MECP2* animals (Fig. 8B), in contrast with the profound defects seen with *Mef2*-driven expression (Fig.3B).

Finally, to address whether the movement defects previously reported (reduced larval motility and adult climbing ability; Figures 3C-E) could be secondary to alterations in neuromuscular junction (NMJ) integrity, we analyzed NMJ morphology in *Mef2>MECP2* larvae. No significant differences were observed in neuronal branching, bouton number, or active zone area compared to controls (Fig. 8C). These data demonstrate that *MECP2* misexpression in muscles does not disrupt NMJ structure and that the locomotor and visceral muscle phenotypes we observed cannot be achieved autonomously by *MECP2* misexpression in the nervous system.

4.9 SCFA Supplementations: Beneficial Effects of Butyrate in *MECP2*-Overexpressing Flies

Given the dual role of SCFAs as microbial metabolites and chromatin remodelers, we tested whether dietary supplementation could modulate the phenotypes observed upon *MECP2* misexpression in muscle (Fig. 9A).

To test the functional relevance of different SCFAs in our model, we first focused on propionate (Fig. 9B), which is already present in *Drosophila* standard diet as a preservative due to its antimicrobial properties, at a concentration of 0.7%. Increasing its concentration to 2.5% led to a significantly reduced survival ratio in *c179>MECP2* animals compared to those reared on either 0.7% or 0% propionate, between which no difference was observed. This suggests that propionate, at higher levels, exerts a detrimental effect, possibly due to excessive depletion of commensal microbes that contribute to endogenous SCFA production.

We next investigated whether supplementation with acetate or butyrate, including a butyrate-rich supplement (Lalbaay®), could improve viability in flies expressing *MECP2* under the muscle-specific *c179* driver. In the representative image of the vials (Fig. 9C), control animals (*c179>GFP*) on standard diet show normal development, with numerous adults accumulated at the top of the vial. In contrast, vials with *c179>MECP2* flies raised on standard diet show a dramatic developmental defect, with very few or no visible adults at the same time point. Notably, all the supplemented conditions (acetate, sodium butyrate, and Lalbaay®) resulted in improved eclosion compared to unsupplemented *c179>MECP2* flies, visually evidenced by the presence of emerged adults, especially prominent in the Lalbaay® and NaB groups. This reflects a partial rescue of the developmental lethality. Quantification of adult survival at day 12 (Fig. 9C') confirms these observations: although only butyrate reached statistical significance, all three supplements increased adult viability compared to the unsupplemented condition. Together, these results suggest that microbial-derived metabolites may alleviate the developmental and survival defects caused by *MECP2* overexpression in muscle. In line with this, Lalbaay® and sodium butyrate showed comparable effects, consistent with the fact that the amount of butyrate was normalized between the two treatments. Acetate also showed a mild beneficial effect, though to a lesser extent, supporting a SCFA-specific contribution to the phenotype.

Finally, to test whether Lalbaay® could improve developmental progression and muscular function, we evaluated wandering behaviour in *Mef2>MECP2* larvae, which fail to reach pupation. Supplementation with Lalbaay® significantly improved wandering ability compared to unsupplemented *c179>MECP2* larvae (Fig. 9D), suggesting a positive impact on motor function and/or overall larval health.

These findings highlight the key role of butyrate among SCFAs in rescuing *MECP2*-induced muscle defects, likely through its epigenetic activity as an HDAC inhibitor. The comparable effect of sodium butyrate and the butyrate-rich postbiotic Lalbaay®, at least on some of our assays, further suggests a microbiota-mediated contribution to this beneficial outcome. Importantly, Lalbaay® differs from pure sodium butyrate in that it represents a postbiotic formulation, potentially linking its efficacy to microbiota-mediated delivery mechanisms rather than direct metabolite supplementation alone.

4.10 Butyrate Rescues Morphological and Functional Muscle and Gut Defects Involving Epigenetic Mechanisms

Thus, we decided to focus on butyrate and strikingly, we found that butyrate treatment significantly restored skeletal muscle morphology in *Mef2>MECP2* animals, increasing fiber thickness in both abdominal muscle 6 and 7 (Figure 10A). In adults, climbing ability which we found impaired in *MECP2*-overexpressing flies, was also rescued upon butyrate treatment (Figure 10B). We next assessed visceral muscle function and found that butyrate supplementation partially rescued both gut clearance and peristaltic activity (Figure 10 C–D).

To distinguish between the potential trophic effect of butyrate as a SCFA and the epigenetic effect as a HDAC inhibitor (HDACi), we supplemented the diet with sodium valproate (VPA), a broad-spectrum HDACi lacking nutritional properties. Remarkably, VPA recapitulated the beneficial effects of butyrate, improving both developmental progression and survival (Figure 10 E–F). These findings support the idea that butyrate exerts its effects primarily via epigenetic rescue of altered deacetylation. While a potential trophic role of butyrate as an SCFA cannot be excluded, the comparable effects of VPA strongly support HDAC inhibition as the predominant mechanism.

Altogether, these data suggest that the functional and structural defects caused by *MECP2* misexpression in muscle tissue can be ameliorated by HDAC inhibition, highlighting a potential therapeutic role for epigenetic modulators such as butyrate.

4.11 Exploring a MeCP2 Interactor: Preliminary Characterization of PHF14/CG15439

Prompted by recent findings highlighting new MeCP2 interactors, we explored the potential role of the *Drosophila* ortholog of *PHF14*, a gene implicated in a Rett-like neurodevelopmental phenotypes. In a study by Zhou and colleagues, a missense mutation in human *PHF14* was identified in a patient with Rett-like features. Functional analyses revealed that this mutation abolished the interaction between PHF14 and MeCP2, suggesting that the PHF14–TCF20 complex may contribute to MeCP2-related pathology (Zhou et al., 2022).

Drosophila melanogaster harbors an ortholog of PHF14, annotated as CG15439, which remains functionally uncharacterized. To investigate its function, we tested two available RNAi lines targeting this gene (GD9021 and KK108167), driven by either a ubiquitous (Act5C-Gal4) or muscle-specific (*Mef2*-Gal4) driver. Consistent with the lethality observed upon *MECP2* overexpression using the *Mef2* driver (Table 1), expression of the GD9021 RNAi line also resulted in complete lethality under both ubiquitous and muscle-specific conditions, whereas KK108167 did not induce detectable phenotypes, likely reflecting differences in RNAi efficiency or insertion site between GD and KK lines.

To assess potential tissue-specific effects, we used the *GMR*-Gal4 driver, which is commonly employed for eye-specific expression but also shows activity in other imaginal tissues, including the wing disc (Li et al., 2012). No eye defects were observed, but nearly all animals analyzed ($N \approx 30$) exhibited consistent wing malformations (Fig. 11A), reminiscent of phenotypes previously reported upon *MECP2* overexpression in neurons (Fig. 1B right panel).

To further characterize the role of CG15439 and generate genetic tools for interaction studies with MeCP2, we performed imprecise excision of a P-element insertion located near the gene. Progeny from crosses with a transposase-expressing strain were screened based on the loss of eye pigmentation, and three candidate genotypes (Δ5, Δ6, and Δ7) were selected for molecular validation (Fig. 11B). We subsequently expanded the mutant collection by including an additional set of 22 potential excision lines for further screening and characterization.

PCR analysis using primers flanking the insertion site revealed distinct band patterns: Δ6 and Δ7 showed amplicons comparable to the parental line, consistent with possible excision of the transposon or presence of small mismatches. In contrast, Δ5 retained a longer fragment, suggesting partial retention of P-element sequences (Fig. 11C). Sequencing of PCR products confirmed multiple mismatches near the excision site (Fig. 11D), consistent with insertion–deletion events or small mutations. These data support the successful generation of candidate alleles of *CG15439*, which may provide useful tools for future epistasis experiments and modifier screens to test potential functional interactions between CG15439 and MeCP2 *in vivo*.

5. Discussion

5.1 Reproducing Patient-like Muscle Defects in *Drosophila*

Clinical and epidemiological studies show that Rett syndrome (RTT) and *MECP2*-related disorders commonly involve extensive musculoskeletal and gastrointestinal pathology (Brunetti & Lumsden, 2020; Galán-Olleros et al., 2024; Motil et al., 2012). Mouse and other models reproduce critical aspects of this peripheral phenotype: Mecp2-null mice show hypotrophic fibers, fibrosis and altered IGF-1/Akt/mTOR signalling (Conti et al., 2015), while heterologous *MECP2* expression in *Drosophila* produces anatomical and motor defects and engages conserved chromatin-remodelling modifiers (Cukier et al., 2008; Vonhoff et al., 2012).

In our *Drosophila* muscle-specific misexpression model we recapitulated several patient-relevant features: strong developmental lethality with early (*Mef2*) drivers, overt larval/pupal arrest, clear structural muscle abnormalities and impaired locomotor outputs in surviving larvae/adults. Morphological analysis revealed mitochondrial alterations in muscle and disorganization of intestinal tissues.

Together, the clinical literature and our *Drosophila* data strengthen the concept that *MECP2* dysregulation yields peripheral muscle pathology that mirrors patient comorbidities. Our work validates *Drosophila* as a tractable system to model peripheral *MECP2* effects, to test genetic modifiers identified in screens and to link molecular signatures (e.g., mitochondrial changes) to organismal phenotypes. This supports the argument that studies of *MECP2* should extend beyond the CNS to include muscle and visceral compartments when seeking therapeutic interventions.

5.2 Variant Interpretation and Genetic Value of the *Drosophila* Model

Given the clinical heterogeneity of *MECP2* mutations, several studies have highlighted how distinct variants differentially affect molecular function and phenotypic severity (Mietto et al., 2025; Ortega-Alarcon et al., 2020; Yusufzai & Wolffe, 2000). In particular, missense mutations in the MBD such as R106W impair DNA binding, whereas truncations like R294X disrupt TRD, thus, transcriptional repression and protein stability, aligning with their classification as functionally divergent alleles. Recent interpretative frameworks (E. Chen et al., 2025) propose that variants acting as phenotype enhancers in overexpression assays retain pathogenic activity

(gain-of-function), whereas those failing to reproduce reference phenotypes reflect loss of function properties.

Our data fit within this scheme: consistent with the pioneering work of Cukier et al. (2008), who first characterized the functional consequences of MECP2 variants in *Drosophila* eyes, our data confirm the pathogenicity of R106W and the relatively milder effects of R294X. In particular, our findings expand these observations by systematically testing multiple tissues, revealing that the impact of MECP2 variants is highly tissue-specific. While R106W consistently acted as a loss-of-function pathogenic allele, R294X behaved predominantly as a benign variant with occasional context-dependent toxicity, and Δ166 showed strong enhancing effects outside the nervous system. These results therefore extend previous knowledge by highlighting that MECP2 variant behaviour cannot be generalized but rather depends on the tissue in which it is expressed (Cuddapah et al., 2014; Cukier et al., 2008; Jara-Ettinger et al., 2021).

Although the *Drosophila* model may be viewed primarily as a genetic system rather than a fully conserved functional homolog: as *MECP2* is a dosage-sensitive gene where both loss (RTT) and gain (MDS) produce overlapping phenotypes (Collins & Neul, 2022; Pascual-Alonso et al., 2023), overexpression in flies provides a tractable entry point to interrogate variant pathogenicity relevant to both syndromes. Overall, while requiring careful validation in mammalian systems, our results illustrate that *Drosophila* genetic assays can functionally stratify *MECP2* variants into loss- versus gain-of-function classes, thereby complementing mammalian models and providing an efficient discovery platform for downstream mechanistic and therapeutic studies.

One caveat is the low DNA methylation content in *Drosophila*, which could limit modeling of MeCP2 as a methyl-CpG binding protein. However, MeCP2 also binds unmethylated DNA structures and regulates chromatin independently of DNA methylation (Galvão & Thomas, 2005; Hansen et al., 2010; Yakabe et al., 2008). Its high nuclear abundance and binding dynamics (Meehan et al., 1992) indicate broader chromatin functions, consistent with our ability to capture variant-specific effects in flies.

5.3 Gain-of-Function versus Dominant-Negative Effects of Human *MECP2* in *Drosophila*

Although we cannot fully exclude the possibility that overexpression of human *MECP2* in *Drosophila* may produce non-specific protein–protein interactions, multiple lines of evidence suggest that this is not the case. In fact, previous studies have shown that human MeCP2 associates with chromatin and is phosphorylated at Ser423 in flies, interacts genetically with conserved chromatin remodeling factors (osa, corto, trithorax) and with the Super Elongation Complex (SEC, including AFF4), and requires an intact MBD to induce neuronal dendritic defects (Cukier et al., 2008; Sonn et al., 2024; Vonhoff et al., 2012). Transcriptomic analyses further identify conserved target genes downstream of MeCP2 that are altered only upon expression of wild-type, but not MBD-mutant hR106W MeCP2 (Williams et al., 2016). In our muscle-specific model, overexpressed *MECP2* localizes to nuclei of skeletal and visceral muscles (Fig. 1D) and induces clear structural defects (Figure 4). These defects result in lethality that depend on the MBD domain, as it is not observed upon expression of $MECP^{R206W}$, suggesting that these effects depend on chromatin regulation, rather than being non-specific. Moreover, preliminary analyses of PHF14, a recently identified MeCP2 interactor (Zhou et al., 2017), provide a tractable genetic entry point for future studies to probe direct *MECP2* interactions in *Drosophila*. Collectively, these data suggest that the phenotypes observed in our model are amenable to future mechanistic dissection through modifier and epistasis approaches, and are possibly relevant to RTT.

5.4 Timing of *MECP2* Expression: Windows of Vulnerability and Experimental Control

Multiple studies demonstrate that timing of *MECP2* expression is critical: embryonic/transcriptional defects precede overt neurological symptoms in mouse models (Bedogni et al., 2016). Reactivation or re-expression of *Mecp2* in symptomatic adult mice produces robust morphological and functional recovery, demonstrating reversibility in murine systems (Guy et al., 2007; Robinson et al., 2012). *Drosophila* provides powerful temporal control (GAL4/GAL80ts and refined expression cassettes) to separate embryonic, larval and adult

effects, a major advantage for modelling regression and dissecting developmental versus degenerative contributions (Meireles-Filho et al., 2014; Filho et al., 2014; Pfeiffer et al., 2010).

We exploited multiple muscle drivers (*Mef2* - earliest; *how24B* - embryonic but later; *c179* - larval) and a Gal80ts adult-repression system to map the relationship between MeCP2 onset and severity. Early *Mef2*-driven misexpression produced the most severe developmental lethality and structural defects, whereas later or adult-restricted expression reduced lethality and permitted adult phenotypes. These manipulations reveal a graded sensitivity to timing.

Our temporal dissection indicates that MeCP2 misexpression impacts muscle development most strongly during early myogenic windows, consistent with the idea that developmental impairment (rather than pure late degeneration) contributes substantially to the peripheral phenotype. This interpretation is concordant with clinical observations that hypotonia and gastrointestinal dysmotility are common early features in RTT patients (Baikie et al., 2014; Motil et al., 2012), supporting the concept of a shared systemic window of vulnerability beyond the CNS. *Drosophila*'s inducible toolkit therefore offers a unique opportunity to model patient-like regression and to test whether late interventions can ameliorate established peripheral deficits.

5.5 Tissue Autonomy: Muscle-Intrinsic vs Neuron-Dependent Mechanisms

A long-standing question in the MECP2 field is whether muscle abnormalities arise from muscle-intrinsic defects or from non-autonomous, neuron-dependent mechanisms. Mouse studies generally support the latter: muscle-specific *Mecp2* deletion results in largely normal muscle morphology and function, indicating that most skeletal muscle abnormalities in Rett models are secondary to altered neuronal input or systemic dysregulation (Conti et al., 2015). However, Ross et al. (2016) showed that some peripheral phenotypes, such as reduced stamina, exercise intolerance and skeletal defects, persist even when neuronal *Mecp2* is intact, pointing to non-neuronal tissue-specific contributions. Complementary evidence from peripheral and mesodermal tissues further supports this: *Mecp2* regulates mitochondrial genes in fibroblasts through YY1–ANT1 repression (Forlani et al., 2010), perturbs cardiac development and gene expression when overexpressed (Alvarez-Saavedra et al., 2010), and is

required for proper cardiomyocyte differentiation, transcriptional identity and structural integrity (Hara et al., 2015).

Human data may also point to an additional layer of complexity, suggesting possible species differences in MECP2 dosage within muscle tissue. In mice, MECP2 levels in skeletal muscle are reported to be very low—consistent with the relatively mild consequences of muscle-specific Mecp2 deletion (Ross et al., 2016). In humans, by contrast, both RNA and protein abundance appear higher in skeletal muscle according to the Human Protein Atlas, raising the possibility that human muscle could be more sensitive to MECP2 perturbations. Although still speculative, this difference in baseline expression might partly explain why peripheral MECP2 dysfunction could have a more pronounced cell-autonomous impact in humans than in mice.

In sheer contrast, our *Drosophila* results provide a clearer readout of muscle autonomy. Muscle-specific *MECP2* misexpression (*Mef2>MECP2*) induces robust structural and mitochondrial defects, whereas neuron-directed expression (*Elav>MECP2*) fails to produce comparable muscular changes, and no signs of NMJ degeneration were observed. These results contrast with the predominantly non-autonomous phenotypes seen in mice but are consistent with models where MeCP2 dosage affects mesodermal tissues directly. The divergence likely reflects species-specific differences in chromatin context, developmental compensation, and the degree to which systemic or neuronal circuits mask tissue-intrinsic vulnerabilities. Thus, while mouse data suggest that major muscle defects are largely neuro-dependent, both mammalian and human evidence indicate peripheral *MECP2* sensitivity, and our fly model unambiguously demonstrates a muscle-autonomous pathogenic potential when *MECP2* levels are perturbed.

5.6 Therapeutic Avenues: SCFAs, Nutrition, Microbiota And Symptomatic Care

Clinical management of RTT remains largely symptomatic, with limited success from previous metabolic trials, though emerging genetic therapies - such as adeno-associated virus-mediated gene replacement, genome and RNA editing, and reactivation of the silent *MECP2* allele - offer promising disease-modifying strategies supported by preclinical and early clinical studies (Palmieri et al., 2023; Percy, 2002). Nevertheless, several limitations must be considered, including dosage sensitivity, potential off-target effects, and challenges in achieving cell type–

specific expression. On the other hand, growing evidence highlights the therapeutic potential of SCFAs, which can modulate mitochondrial function, HDAC activity, and metabolic signaling (Z. Gao et al., 2009; Hu et al., 2020; Rose et al., 2018). Gut microbiota studies in RTT report altered composition and SCFA profiles, potentially contributing to gastrointestinal and systemic symptoms (Borghi et al., 2017; Strati et al., 2016; Thapa et al., 2021). Clinical guidelines for constipation favor established laxative strategies, while evidence for routine probiotic use remains limited (Bautista-Casasnovas, 2011; Vale San Gomes & de Morais, 2020).

In our *Drosophila* model, SCFAs interventions partially rescued skeletal muscle morphology and visceral muscle functionality, providing a mechanistic link between SCFA exposure and muscle deficits in *MECP2* disorders. Comparative analysis further revealed that high propionate exacerbated lethality in *c179>MECP2* flies, whereas sodium butyrate and a butyrate-rich postbiotic (Lalbaay®) improved eclosion and wandering behaviour. This suggests an involvement of the microbiota, as propionate may act as an antibacterial agent in this context and can be neurotoxic at high concentrations, potentially causing symptoms such as lethargy, abnormal behaviour, and motor impairments, whereas butyrate promotes a healthy microbiota (X. Chen et al., 2025). These findings align with a broader range of microbiota-targeted interventions - including probiotics, prebiotics, synbiotics, and postbiotic formulations—that aim to modulate microbial communities and leverage SCFA-mediated benefits for host physiology (Loh et al., 2024; Mirzaei et al., 2021; Sherwin et al., 2018).

Finally, emerging clinical studies are beginning to translate these concepts. A recent single-center, randomized, cross-over trial (NCT05420805) is testing pre- and postbiotic supplementation in RTT patients carrying *MECP2* mutations, using two commercial products (Lalbaay Monofasico® and Bizetaflox Pediatrico®) containing SCFA-related components such as alpha-lactalbumin and butyric acid. Outcomes include intestinal inflammation, seizure frequency and severity, and overall quality of life. Together with our preclinical results, these developments highlight the translational potential of SCFA-based strategies, suggesting that modulation of the microbiota–gut–brain axis may represent a novel therapeutic avenue in RTT.

Notably, the gut–brain axis involvement in RTT appears to share commonalities with other neurodevelopmental disorders such as autism and Down syndrome (Borghi & Vignoli, 2019), underscoring the relevance of microbiota reshaping strategies - via diet, pre/probiotics or postbiotics - for systemic and neurological manifestations (Borghi et al., 2017; Ivy & Standridge, 2021).

5.7 Epigenetic Rescue of *MECP2*-associated Peripheral Defects

Histone deacetylase inhibitors (HDACi), including short-chain fatty acids such as butyrate and valproic acid (VPA), have shown promising therapeutic effects across neurodevelopmental and neuromuscular disease models by modulating gene expression through epigenetic mechanisms (Berni Canani et al., 2012; Ferrante et al., 2003; Kilgore et al., 2010; Monti et al., 2010). In MeCP2-deficient *in vitro* systems, HDAC inhibition via VPA increases the expression of MeCP2 and its downstream target proteins, including BDNF and chromatin remodeling factors (Vecsler et al., 2010). In the *in vivo* mice model for Duchenne Muscular Dystrophy, the HDACi givinostat (ITF2357) provided functional and histological rescue by promoting the formation of muscles (increased cross-sectional area, reduction of fibrotic scars, fatty infiltration, and inflammatory infiltrate) and resulting in an overall enhancement of endurance performance during treadmill tests, thereby providing the preclinical basis for immediate translation into clinical studies (Consalvi et al., 2013).

In our *Mef2>MECP2 Drosophila* model, VPA supplementation, similarly to NaB supplementation, partially rescued developmental delay and lethality. Since VPA lacks the metabolic impact of butyrate, these results suggest that butyrate's rescue of muscle phenotypes is mediated via HDAC inhibition, modulating transcriptional networks essential for muscle differentiation, maturation, and systemic development, and complementing metabolic interventions.

The convergence of these preclinical findings and our rescue data highlights HDAC inhibition as a mechanistically plausible therapeutic avenue for *MECP2* disorders. Future translational studies should integrate epigenetic biomarkers - such as HDAC activity, histone acetylation patterns, and target gene expression - alongside functional endpoints, to systematically evaluate peripheral benefits of SCFA and VPA interventions in RTT.

5.8 Energetic and Mitochondrial Defects: Historic and Contemporary Evidence

Ultrastructural mitochondrial abnormalities in RTT muscle were reported decades ago (dumbbell/swollen mitochondria; Cardaioli et al., 1999; Eeg-Olofsson et al., 1988; Wakai et al., 1990). Contemporary studies confirm functional mitochondrial defects in Mecp2 models (reduced complex activities, oxidative stress; Gold et al., 2014; Kriaucionis et al., 2006), and large-scale proteomics reveal systemic metabolic derailment (Cortelazzo et al., 2017; Zlatic et al., 2024) .

Considering the critical role of mitochondria in sustaining muscle function, we analyzed structural and functional features in our *MECP2*-overexpressing *Drosophila* model (*Mef2>MECP2*). Transmission electron microscopy of body wall muscles revealed increased mitochondrial number and frequent cristae abnormalities, while locomotor assays and gut clearance/peristalsis tests showed impaired skeletal and visceral muscle performance, consistent with energy deficits. These data support the hypothesis that altered bioenergetics contributes to peripheral muscle dysfunction in *MECP2* disorders.

The convergence of historical biopsy reports, model-based functional data and our molecular profiles indicate mitochondrial dysfunction as a targetable component of *MECP2* peripheral pathology. Interventions that enhance mitochondrial biogenesis/function (e.g., butyrate-related pathways) merit prioritized preclinical-to-clinical translation, with standardized energetic biomarkers incorporated as endpoints.

An open question is whether SCFA supplementation, beyond improving muscle morphology, could directly restore mitochondrial integrity and function, linking metabolic and epigenetic rescue mechanisms.

5.9 Genetic Interactions and the Utility of PHF14 in *Drosophila*

MeCP2 functions within chromatin regulatory networks; genetic modifier screens in *Drosophila* have identified conserved interactors (osa, Sin3a, REST) and suggest practical conservation despite absence of a direct fly ortholog (Cukier et al., 2008; Gupta et al., 2016; Vonhoff et al., 2012). PHF14 is a critical component of the MeCP2-interacting chromatin regulatory complex that also includes TCF20, RAI1, and HMG20A (Dominguez et al., 2024). This complex is

essential for epigenetic and transcriptional regulation in the mammalian brain and is disrupted by Rett-causing *MECP2* mutations, underscoring its direct involvement in neurodevelopmental pathogenesis. In particular, a missense mutation in PHF14 has been identified in a patient with Rett-like neurological features, which abolished the MeCP2-PHF14-TCF20 interaction (Zhou et al., 2022).

In this context, we investigated the uncharacterized *Drosophila* ortholog CG15439. RNAi-mediated knockdown revealed strong phenotypic effects with one line causing lethality under ubiquitous and muscle drivers, and wing malformations under *GMR* control, while a second RNAi line remained phenotypically silent, likely reflecting differential knockdown efficiency. To expand the available toolkit, we generated imprecise excision alleles at the CG15439 locus, recovering candidate mutants with insertion–deletion events validated by sequencing.

These genetic resources set the stage for future epistasis experiments aimed at probing potential CG15439–MeCP2 interactions. The combination of overexpression and mutant designs in *Drosophila* offers a tractable framework to explore such relationships, providing rapid organismal readouts and opportunities for mechanistic follow-up. Although ultimate validation will require mammalian systems, the conserved chromatin machinery and established modifier logic underscore the utility of *Drosophila* as a discovery platform.

Future directions include testing isoform-selective HDAC inhibitors, detailed mitochondrial rescue assays, and systematic epistasis screens with our new PHF14 alleles, which may clarify the role of the PHF14–TCF20–MeCP2 complex in Rett and Rett-like syndromes (Zhou et al., 2022).

6. Conclusions

Our study establishes *Drosophila* as a powerful system to model peripheral consequences of *MECP2* dysregulation, capturing key features of patient pathology such as muscle defects, visceral involvement, and mitochondrial abnormalities. Through temporal and tissue-specific misexpression, we demonstrated that developmental timing critically shapes phenotype severity and that muscle-autonomous mechanisms contribute alongside potential systemic influences. Variant analyses further revealed distinct behaviours of clinically relevant alleles, supporting the utility of flies for functional stratification. Importantly, rescue by short-chain fatty acids, valproic acid, and postbiotic supplementation highlights the potential of metabolic and epigenetic interventions to ameliorate peripheral defects, providing mechanistic links to emerging microbiota–gut–brain axis therapies in RTT.

Despite limitations - including ectopic expression patterns, low endogenous DNA methylation, and the need for mammalian validation - our findings underscore the value of flies for rapid genetic dissection and for preclinical exploration of therapeutic strategies. Future directions include isoform-selective HDAC inhibitors, detailed mitochondrial rescue assays, and epistasis screens with PHF14 alleles to clarify conserved chromatin interactions. Together, these insights reinforce the concept that *MECP2* pathology extends beyond the CNS and that combined genetic, metabolic, and microbiota-targeted approaches may yield novel avenues for therapy.

References

Aghajanian, P., Takashima, S., Paul, M., Younossi-Hartenstein, A., & Hartenstein, V. (2016). Metamorphosis of the Drosophila visceral musculature and its role in intestinal morphogenesis and stem cell formation. *Developmental Biology*, *420*(1). https://doi.org/10.1016/j.ydbio.2016.10.011

Akaba, Y., & Takahashi, S. (2025). MECP2 duplication syndrome: Recent advances in pathophysiology and therapeutic perspectives. *Brain and Development*, *47*(4), 104371. https://doi.org/10.1016/J.BRAINDEV.2025.104371

Alvarez-Saavedra, M., Carrasco, L., Sura-Trueba, S., Aiello, V. D., Walz, K., Neto, J. X., & Young, J. I. (2010). Elevated expression of MeCP2 in cardiac and skeletal tissues is detrimental for normal development. *Human Molecular Genetics*, *19*(11), 2177–2190. https://doi.org/10.1093/HMG/DDQ096

Alves, S. de M., Lisboa-Filho, P. N., Zilli Vieira, C. L., & Piacenti-Silva, M. (2025). Alzheimer's disease and gut-brain axis: Drosophila melanogaster as a model. In *Frontiers in Neuroscience* (Vol. 19). Frontiers Media SA. https://doi.org/10.3389/fnins.2025.1543826

Ananiev, G., Williams, E. C., Li, H., & Chang, Q. (2011). Isogenic pairs of wild type and mutant induced pluripotent stem cell (iPSC) lines from rett syndrome patients as In Vitro disease model. *PLoS ONE*, *6*(9). https://doi.org/10.1371/journal.pone.0025255

Anderson, M. S., Halpern, M. E., & Keshishian, H. (1988). Identification of the neuropeptide transmitter proctolin in Drosophila larvae: Characterization of muscle fiber-specific neuromuscular endings. *Journal of Neuroscience*, *8*(1). https://doi.org/10.1523/jneurosci.08-01-00242.1988

Armstrong, M. J., Jin, Y., Vattathil, S. M., Huang, Y., Schroeder, J. P., Bennet, D. A., Qin, Z. S., Wingo, T. S., & Jin, P. (2023). Role of TET1-mediated epigenetic modulation in Alzheimer's disease. *Neurobiology of Disease*, *185*. https://doi.org/10.1016/j.nbd.2023.106257

Ashique, S., Mohanto, S., Ahmed, M. G., Mishra, N., Garg, A., Chellappan, D. K., Omara, T., Iqbal, S., & Kahwa, I. (2024). Gut-brain axis: A cutting-edge approach to target neurological disorders and potential synbiotic application. In *Heliyon* (Vol. 10, Issue 13). Elsevier Ltd. https://doi.org/10.1016/j.heliyon.2024.e34092

Ashley, J., & Carrillo, R. A. (2025). The Drosophila Larval Neuromuscular Junction: Developmental Overview. *Cold Spring Harbor Protocols*, *2025*(7). https://doi.org/10.1101/pdb.top108449

Baikie, G., Ravikumara, M., Downs, J., Naseem, N., Wong, K., Percy, A., Lane, J., Weiss, B., Ellaway, C., Bathgate, K., & Leonard, H. (2014). Gastrointestinal dysmotility in rett

syndrome. *Journal of Pediatric Gastroenterology and Nutrition*, *58*(2). https://doi.org/10.1097/MPG.0000000000000200

Bajikar, S. S., Anderson, A. G., Zhou, J., Durham, M. A., Trostle, A. J., Wan, Y. W., Liu, Z., & Zoghbi, H. Y. (2023). MeCP2 regulates Gdf11, a dosage-sensitive gene critical for neurological function. *ELife*, *12*. https://doi.org/10.7554/eLife.83806

Bakhoum, M. F., & Jackson, G. R. (2011). Demise of the flies: Why Drosophila models still matter. In *Progress in Molecular Biology and Translational Science* (Vol. 100). https://doi.org/10.1016/B978-0-12-384878-9.00011-X

Balicza, P., Gezsi, A., Fedor, M., Sagi, J. C., Gal, A., Varga, N. A., & Molnar, M. J. (2023). Multilevel evidence of MECP2-associated mitochondrial dysfunction and its therapeutic implications. *Frontiers in Psychiatry*, *14*, 1301272. https://doi.org/10.3389/FPSYT.2023.1301272/BIBTEX

Barwell, T., Geld, S., & Seroude, L. (2023). Comparison of GAL80ts and Tet-off GAL80 transgenes. *MicroPublication Biology*, *2023*. https://doi.org/10.17912/micropub.biology.000770

Bataillé, L., Frendo, J. L., & Vincent, A. (2015). Hox control of Drosophila larval anatomy; The Alary and Thoracic Alary-Related Muscles. In *Mechanisms of Development* (Vol. 138). https://doi.org/10.1016/j.mod.2015.07.005

Bate, M. (1990). The embryonic development of larval muscles in Drosophila. *Development*, *110*(3). https://doi.org/10.1242/dev.110.3.791

Bautista-Casasnovas, A. L. (2011). Estreñimiento. *Anales de Pediatria Continuada*, *9*(4), 201–208. https://doi.org/10.1016/S1696-2818(11)70030-0

Bedogni, F., Gigli, C. C., Pozzi, D., Rossi, R. L., Scaramuzza, L., Rossetti, G., Pagani, M., Kilstrup-Nielsen, C., Matteoli, M., & Landsberger, N. (2016). Defects during Mecp2 Null Embryonic Cortex Development Precede the Onset of Overt Neurological Symptoms. *Cerebral Cortex*, *26*(6). https://doi.org/10.1093/cercor/bhv078

Berni Canani, R., Di Costanzo, M., & Leone, L. (2012). The epigenetic effects of butyrate: Potential therapeutic implications for clinical practice. In *Clinical Epigenetics* (Vol. 4, Issue 1). https://doi.org/10.1186/1868-7083-4-4

Bland, M. L., Lee, R. J., Magallanes, J. M., Foskett, J. K., & Birnbaum, M. J. (2010). AMPK supports growth in Drosophila by regulating muscle activity and nutrient uptake in the gut. *Developmental Biology*, *344*(1). https://doi.org/10.1016/j.ydbio.2010.05.010

Boggio, E. M., Lonetti, G., Pizzorusso, T., & Giustetto, M. (2010). Synaptic determinants of Rett syndrome. In *Frontiers in Synaptic Neuroscience* (Issue AUG). https://doi.org/10.3389/fnsyn.2010.00028

Bolus, H., Crocker, K., Boekhoff-Falk, G., & Chtarbanova, S. (2020). Modeling neurodegenerative disorders in drosophila melanogaster. In *International Journal of Molecular Sciences* (Vol. 21, Issue 9). https://doi.org/10.3390/ijms21093055

Borghi, E., Borgo, F., Severgnini, M., Savini, M. N., Casiraghi, M. C., & Vignoli, A. (2017). Rett syndrome: A focus on gut microbiota. *International Journal of Molecular Sciences*, *18*(2). https://doi.org/10.3390/ijms18020344

Borghi, E., & Vignoli, A. (2019). Rett syndrome and other neurodevelopmental disorders share common changes in gut microbial community: A descriptive review. In *International Journal of Molecular Sciences* (Vol. 20, Issue 17). https://doi.org/10.3390/ijms20174160

Boyer, J. G., Ferrier, A., & Kothary, R. (2013). More than a bystander: The contributions of intrinsic skeletal muscle defects in motor neuron diseases. In *Frontiers in Physiology: Vol. 4 DEC*. https://doi.org/10.3389/fphys.2013.00356

Brent, J. R., Werner, K. M., & McCabe, B. D. (2009). Drosophila larval NMJ dissection. *Journal of Visualized Experiments*, *24*. https://doi.org/10.3791/1107

Brunetti, S., & Lumsden, D. E. (2020). Rett Syndrome as a movement and motor disorder – A narrative review. In *European Journal of Paediatric Neurology* (Vol. 28). https://doi.org/10.1016/j.ejpn.2020.06.020

Cagin, U., Duncan, O. F., Gatt, A. P., Dionne, M. S., Sweeney, S. T., & Bateman, J. M. (2015). Mitochondrial retrograde signaling regulates neuronal function. *Proceedings of the National Academy of Sciences*, **112**(44). https://doi.org/10.1073/pnas.1505036112

Camuglia, J. M., Mandigo, T. R., Moschella, R., Mark, J., Hudson, C. H., Sheen, D., & Folker, E. S. (2018). An RNAi based screen in Drosophila larvae identifies fascin as a regulator of myoblast fusion and myotendinous junction structure. *Skeletal Muscle*, *8*(1). https://doi.org/10.1186/s13395-018-0159-9

Cardaioli, E., Dotti, M. T., Hayek, G., Zappella, M., & Federico, A. (1999). Studies on mitochondrial pathogenesis of Rett syndrome: Ultrastructural data from skin and muscle biopsies and mutational analysis at mtDNA nucleotides 10463 and 2835. *Journal of Submicroscopic Cytology and Pathology*, *31*(2).

Casas-Tintó, S. (2024). Drosophila as a Model for Human Disease: Insights into Rare and Ultra-Rare Diseases. In *Insects* (Vol. 15, Issue 11). Multidisciplinary Digital Publishing Institute (MDPI). https://doi.org/10.3390/insects15110870

Cavaliere, G., Catapano, A., Trinchese, G., Cimmino, F., Penna, E., Pizzella, A., Cristiano, C., Lama, A., Crispino, M., & Mollica, M. P. (2023). Butyrate Improves Neuroinflammation and Mitochondrial Impairment in Cerebral Cortex and Synaptic Fraction in an Animal Model of Diet-Induced Obesity. *Antioxidants*, *12*(1). https://doi.org/10.3390/antiox12010004

Chae, J. H., Yong, Hwang, S., Ki, Kim, J., Chae, D., Hwang, K.), & Kim, K. J. (2002). *Mutation Analysis of MECP2 and Clinical Characterization in Korean Patients With Rett Syndrome*. https://doi.org/https://doi.org/10.1093/NAR%2F28.21.4172

Chahrour, M., & Zoghbi, H. Y. (2007). The Story of Rett Syndrome: From Clinic to Neurobiology. In *Neuron* (Vol. 56, Issue 3). https://doi.org/10.1016/j.neuron.2007.10.001

Chan, H. Y. E., & Bonini, N. M. (2000). Drosophila models of human neurodegenerative disease. In *Cell Death and Differentiation* (Vol. 7, Issue 11). https://doi.org/10.1038/sj.cdd.4400757

Chen, E., Schmitt, J., McIntosh, G., Young, B. P., Lian, T., Liu, J., Chen, K. K., Liston, J. B., MacDonald, L., Wang, B., Medina Giro, S., Boehme, B., Das, M., Indran, S., Chao, J. T., Rogic, S., Pavlidis, P., Allan, D. W., & Loewen, C. J. R. (2025). Revealing function-altering MECP2 mutations in individuals with autism spectrum disorder using yeast and Drosophila . *GENETICS*. https://doi.org/10.1093/genetics/iyaf121

Chen, X., Cheng, Q., & Zhang, G. F. (2025). Elevated propionate and its association with neurological dysfunctions in propionic acidemia. In *Frontiers in Molecular Neuroscience* (Vol. 18). Frontiers Media SA. https://doi.org/10.3389/fnmol.2025.1499376

Chen, Y., Liang, R., Li, Y., Jiang, L., Ma, D., Luo, Q., & Song, G. (2024). Chromatin accessibility: biological functions, molecular mechanisms and therapeutic application. In *Signal Transduction and Targeted Therapy* (Vol. 9, Issue 1). Springer Nature. https://doi.org/10.1038/s41392-024-02030-9

Chiang, M. H., Ho, S. M., Wu, H. Y., Lin, Y. C., Tsai, W. H., Wu, T., Lai, C. H., & Wu, C. L. (2022). Drosophila Model for Studying Gut Microbiota in Behaviours and Neurodegenerative Diseases. In *Biomedicines* (Vol. 10, Issue 3). https://doi.org/10.3390/biomedicines10030596

Chouhan, A. K., Guo, C., Hsieh, Y. C., Ye, H., Senturk, M., Zuo, Z., Li, Y., Chatterjee, S., Botas, J., Jackson, G. R., Bellen, H. J., & Shulman, J. M. (2016). Uncoupling neuronal death and dysfunction in Drosophila models of neurodegenerative disease. *Acta Neuropathologica Communications*, *4*(1). https://doi.org/10.1186/s40478-016-0333-4

Chua, G. N. L., & Liu, S. (2024). Differential dynamics specify MeCP2 function at nucleosomes and methylated DNA. *Biophysical Journal*, *123*(3). https://doi.org/10.1016/j.bpj.2023.11.1433

Cicaloni, V., Pecorelli, A., Tinti, L., Rossi, M., Benedusi, M., Cervellati, C., Spiga, O., Santucci, A., Hayek, J., Salvini, L., Tinti, C., & Valacchi, G. (2020). Proteomic profiling reveals mitochondrial alterations in Rett syndrome. *Free Radical Biology and Medicine*, *155*, 37–48. https://doi.org/10.1016/J.FREERADBIOMED.2020.05.014

Cisterna, B., & Malatesta, M. (2024). Molecular and Structural Alterations of Skeletal Muscle Tissue Nuclei during Aging. In *International Journal of Molecular Sciences* (Vol. 25, Issue 3). Multidisciplinary Digital Publishing Institute (MDPI). https://doi.org/10.3390/ijms25031833

Collins, B. E., & Neul, J. L. (2022). Rett Syndrome and MECP2 Duplication Syndrome: Disorders of MeCP2 Dosage. In *Neuropsychiatric Disease and Treatment* (Vol. 18). https://doi.org/10.2147/NDT.S371483

Connelly, J. C., Cholewa-Waclaw, J., Webb, S., Steccanella, V., Waclaw, B., & Bird, A. (2021). Absence of MeCP2 binding to non-methylated GT-rich sequences in vivo. *Nucleic Acids Research*, *48*(7). https://doi.org/10.1093/NAR/GKAA102

Consalvi, S., Mozzetta, C., Bettica, P., Germani, M., Fiorentini, F., Del Bene, F., Rocchetti, M., Leoni, F., Monzani, V., Mascagni, P., Puri, P. L., & Saccone, V. (2013). Preclinical studies in the mdx mouse model of duchenne muscular dystrophy with the histone deacetylase inhibitor givinostat. *Molecular Medicine*, *19*(1). https://doi.org/10.2119/molmed.2013.00011

Conti, V., Gandaglia, A., Galli, F., Tirone, M., Bellini, E., Campana, L., Kilstrup-Nielsen, C., Rovere-Querini, P., Brunelli, S., & Landsberger, N. (2015). MeCP2 affects skeletal muscle growth and morphology through non cell-autonomous mechanisms. *PLoS ONE*, *10*(6). https://doi.org/10.1371/journal.pone.0130183

Cook, S. I., & Sellin, J. H. (1998). Review article: Short chain fatty acids in health and disease. In *Alimentary Pharmacology and Therapeutics* (Vol. 12, Issue 6). https://doi.org/10.1046/j.1365-2036.1998.00337.x

Cortelazzo, A., De Felice, C., De Filippis, B., Ricceri, L., Laviola, G., Leoncini, S., Signorini, C., Pescaglini, M., Guerranti, R., Timperio, A. M., Zolla, L., Ciccoli, L., & Hayek, J. (2017). Persistent Unresolved Inflammation in the Mecp2-308 Female Mutated Mouse Model of Rett Syndrome. *Mediators of Inflammation*, *2017*. https://doi.org/10.1155/2017/9467819

Cuddapah, V. A., Pillai, R. B., Shekar, K. V., Lane, J. B., Motil, K. J., Skinner, S. A., Tarquinio, D. C., Glaze, D. G., McGwin, G., Kaufmann, W. E., Percy, A. K., Neul, J. L., & Olsen, M. L. (2014). Methyl-CpG-binding protein 2 (MECP2) mutation type is associated with

disease severity in rett syndrome. *Journal of Medical Genetics*, *51*(3). https://doi.org/10.1136/jmedgenet-2013-102113

Cukier, H. N., Perez, A. M., Collins, A. L., Zhou, Z., Zoghbi, H. Y., & Botas, J. (2008a). Genetic modifiers of MeCP2 function in Drosophila. *PLoS Genetics*, *4*(9). https://doi.org/10.1371/journal.pgen.1000179

Davie, J. R. (2003). Inhibition of histone deacetylase activity by butyrate. *Journal of Nutrition*, *133*(7 SUPPL.). https://doi.org/10.1093/jn/133.7.2485s

Deal, S. L., & Yamamoto, S. (2019). Unraveling novel mechanisms of neurodegeneration through a large-scale forward genetic screen in Drosophila. In *Frontiers in Genetics* (Vol. 10, Issue JAN). https://doi.org/10.3389/fgene.2018.00700

D'Mello, S. R. (2021). MECP2 and the biology of MECP2 duplication syndrome. In *Journal of Neurochemistry* (Vol. 159, Issue 1, pp. 29–60). John Wiley and Sons Inc. https://doi.org/10.1111/jnc.15331

Dominguez, G., Wu, Y., & Zhou, J. (2024). Epigenetic Regulation and Neurodevelopmental Disorders: From MeCP2 to the TCF20/PHF14 Complex. In *Genes* (Vol. 15, Issue 12). Multidisciplinary Digital Publishing Institute (MDPI). https://doi.org/10.3390/genes15121653

Donohoe, D. R., Garge, N., Zhang, X., Sun, W., O'Connell, T. M., Bunger, M. K., & Bultman, S. J. (2011). The microbiome and butyrate regulate energy metabolism and autophagy in the mammalian colon. *Cell Metabolism*, *13*(5). https://doi.org/10.1016/j.cmet.2011.02.018

Duranti, E., & Villa, C. (2024). From Brain to Muscle: The Role of Muscle Tissue in Neurodegenerative Disorders. In *Biology* (Vol. 13, Issue 9). Multidisciplinary Digital Publishing Institute (MDPI). https://doi.org/10.3390/biology13090719

Eeg-Olofsson, O., Al-Zuhair, A. G., Teebi, A. S., & Al-Essa, M. M. (1988). Abnormal mitochondria in the Rett syndrome. *Brain and Development*, *10*(4). https://doi.org/10.1016/S0387-7604(88)80010-X

Einspieler, C., & Marschik, P. B. (2019). Regression in Rett syndrome: Developmental pathways to its onset. In *Neuroscience and Biobehavioural Reviews* (Vol. 98). https://doi.org/10.1016/j.neubiorev.2019.01.028

Elovsson, G., Bergkvist, L., & Brorsson, A. C. (2021). Exploring aβ proteotoxicity and therapeutic candidates using drosophila melanogaster. In *International Journal of Molecular Sciences* (Vol. 22, Issue 19). https://doi.org/10.3390/ijms221910448

Elovsson, G., Klingstedt, T., Nilsson, K. R. P., & Brorsson, A. C. (2025). Diversity of Aβ aggregates produced in a gut-based Drosophila model of Alzheimer's disease. *PLOS ONE*, *20*(7 July). https://doi.org/10.1371/journal.pone.0314832

Fasolino, M., & Zhou, Z. (2017). The crucial role of DNA methylation and MeCP2 in neuronal function. In *Genes* (Vol. 8, Issue 5). https://doi.org/10.3390/genes8050141

Fernius, J., Starkenberg, A., Pokrzywa, M., & Thor, S. (2017). Human TTBK1, TTBK2 and MARK1 kinase toxicity in Drosophila melanogaster is exacerbated by co-expression of human Tau. *Biology Open*, *6*(7). https://doi.org/10.1242/bio.022749

Fernius, J., Starkenberg, A., & Thor, S. (2017). Bar-coding neurodegeneration: Identifying subcellular effects of human neurodegenerative disease proteins using Drosophila leg neurons. *DMM Disease Models and Mechanisms*, *10*(8). https://doi.org/10.1242/dmm.029637

Ferrante, R. J., Kubilus, J. K., Lee, J., Ryu, H., Beesen, A., Zucker, B., Smith, K., Kowall, N. W., Ratan, R. R., Luthi-Carter, R., & Hersch, S. M. (2003). Histone Deacetylase Inhibition by Sodium Butyrate Chemotherapy Ameliorates the Neurodegenerative Phenotype in Huntington's Disease Mice. *Journal of Neuroscience*, *23*(28). https://doi.org/10.1523/jneurosci.23-28-09418.2003

Forlani, G., Giarda, E., Ala, U., di Cunto, F., Salani, M., Tupler, R., Kilstrup-Nielsen, C., & Landsberger, N. (2010). The MeCP2/YY1 interaction regulates ANT1 expression at 4q35: novel hints for Rett syndrome pathogenesis. *Human Molecular Genetics*, *19*(16), 3114. https://doi.org/10.1093/HMG/DDQ214

Galán-Olleros, M., González-Alguacil, E., Soto-Insuga, V., Vara-Arias, M. T., Ortiz-Cabrera, N. V., Egea-Gámez, R. M., García-Peñas, J. J., & Martínez-Caballero, I. (2024). Prevalence of orthopaedic conditions in Rett syndrome: a systematic review and meta-analysis. In *Journal of Intellectual Disability Research* (Vol. 68, Issue 12, pp. 1331–1343). John Wiley and Sons Inc. https://doi.org/10.1111/jir.13193

Galvão, T. C., & Thomas, J. O. (2005). Structure-specific binding of MeCP2 to four-way junction DNA through its methyl CpG-binding domain. *Nucleic Acids Research*, *33*(20). https://doi.org/10.1093/nar/gki971

Gao, C. L., Liu, G. L., Liu, S., Chen, X. H., Ji, C. B., Zhang, C. M., Xia, Z. K., & Guo, X. R. (2011). Overexpression of PGC-1β improves insulin sensitivity and mitochondrial function in 3T3-L1 adipocytes. *Molecular and Cellular Biochemistry*, *353*(1–2). https://doi.org/10.1007/s11010-011-0789-2

Gao, Z., Yin, J., Zhang, J., Ward, R. E., Martin, R. J., Lefevre, M., Cefalu, W. T., & Ye, J. (2009). Butyrate improves insulin sensitivity and increases energy expenditure in mice. *Diabetes*, *58*(7). https://doi.org/10.2337/db08-1637

Gatto, C. L., & Broadie, K. (2011). Drosophila modeling of heritable neurodevelopmental disorders. In *Current Opinion in Neurobiology* (Vol. 21, Issue 6). https://doi.org/10.1016/j.conb.2011.04.009

Geiman, T. M., & Robertson, K. D. (2002). Chromatin remodeling, histone modifications, and DNA methylation - How does it all fit together? In *Journal of Cellular Biochemistry* (Vol. 87, Issue 2). https://doi.org/10.1002/jcb.10286

Gold, W. A., Williamson, S. L., Kaur, S., Hargreaves, I. P., Land, J. M., Pelka, G. J., Tam, P. P. L., & Christodoulou, J. (2014). Mitochondrial dysfunction in the skeletal muscle of a mouse model of Rett syndrome (RTT): Implications for the disease phenotype. *Mitochondrion*, *15*(1). https://doi.org/10.1016/j.mito.2014.02.012

Gomez, A., Gonzalez, S., Oke, A., Luo, J., Duong, J. B., Esquerra, R. M., Zimmerman, T., Capponi, S., Fung, J. C., & Nystul, T. G. (2024). A High-Throughput Method for Quantifying Drosophila Fecundity. *Toxics*, *12*(9). https://doi.org/10.3390/toxics12090658

Gowda, S. B. M., Salim, S., & Mohammad, F. (2021). Anatomy and neural pathways modulating distinct locomotor behaviours in Drosophila larva. In *Biology* (Vol. 10, Issue 2). https://doi.org/10.3390/biology10020090

Guidera, K. J., Borrelli, J., Raney, E., Thompson-Rangel, T., & Ogden, J. A. (1991). Orthopaedic manifestations of rett syndrome. *Journal of Pediatric Orthopaedics*, *11*(2). https://doi.org/10.1097/01241398-199103000-00013

Gupta, T., Morgan, H. R., Bailey, J. A., & Certel, S. J. (2016). Functional conservation of MBD proteins: MeCP2 and Drosophila MBD proteins alter sleep. *Genes, Brain and Behaviour*, *15*(8). https://doi.org/10.1111/gbb.12314

Guy, J., Gan, J., Selfridge, J., Cobb, S., & Bird, A. (2007). Reversal of neurological defects in a mouse model of Rett syndrome. *Science*, *315*(5815). https://doi.org/10.1126/science.1138389

Hagberg, B., Aicardi, J., Dias, K., & Ramos, O. (1983). A progressive syndrome of autism, dementia, ataxia, and loss of purposeful hand use in girls: Rett's syndrome: Report of 35 cases. *Annals of Neurology*, *14*(4). https://doi.org/10.1002/ana.410140412

Hansen, J. C., Ghosh, R. P., & Woodcock, C. L. (2010). Binding of the Rett syndrome protein, MeCP2, to methylated and unmethylated DNA and chromatin. In *IUBMB Life* (Vol. 62, Issue 10). https://doi.org/10.1002/iub.386

Hara, M., Takahashi, T., Mitsumasu, C., Igata, S., Takano, M., Minami, T., Yasukawa, H., Okayama, S., Nakamura, K., Okabe, Y., Tanaka, E., Takemura, G., Kosai, K. I., Yamashita, Y., & Matsuishi, T. (2015). Disturbance of cardiac gene expression and

cardiomyocyte structure predisposes Mecp2-null mice to arrhythmias. *Scientific Reports 2015 5:1*, *5*(1), 11204-. https://doi.org/10.1038/srep11204

Heckman, L. D., Chahrour, M. H., & Zoghbi, H. Y. (2014). Rett-causing mutations reveal two domains critical for MeCP2 function and for toxicity in MECP2 duplication syndrome mice. *ELife*, *3*. https://doi.org/10.7554/elife.02676

Heckscher, E. S., Lockery, S. R., & Doe, C. Q. (2012). Characterization of Drosophila larval crawling at the level of organism, segment, and somatic body wall musculature. *Journal of Neuroscience*, *32*(36). https://doi.org/10.1523/JNEUROSCI.0222-12.2012

Hernández-Hernández, O., Ávila-Avilés, R. D., & Hernández-Hernández, J. M. (2020). Chromatin Landscape During Skeletal Muscle Differentiation. In *Frontiers in Genetics* (Vol. 11). Frontiers Media S.A. https://doi.org/10.3389/fgene.2020.578712

Hsieh, C. C. Jung, Lo, Y. C., Wang, H. H., Shen, H. Y., Chen, Y. Y., & Lee, Y. C. (2024). Amelioration of the brain structural connectivity is accompanied with changes of gut microbiota in a tuberous sclerosis complex mouse model. *Translational Psychiatry*, *14*(1). https://doi.org/10.1038/s41398-024-02752-y

Hu, S., Kuwabara, R., de Haan, B. J., Smink, A. M., & de Vos, P. (2020). Acetate and butyrate improve β-cell metabolism and mitochondrial respiration under oxidative stress. *International Journal of Molecular Sciences*, *21*(4). https://doi.org/10.3390/ijms21041542

Ip, J. P. K., Mellios, N., & Sur, M. (2018). Rett syndrome: Insights into genetic, molecular and circuit mechanisms. *Nature Reviews Neuroscience*, *19*(6). https://doi.org/10.1038/s41583-018-0006-3

Ivy, A. S., & Standridge, S. M. (2021). Rett Syndrome: A Timely Review From Recognition to Current Clinical Approaches and Clinical Study Updates. In *Seminars in Pediatric Neurology* (Vol. 37). https://doi.org/10.1016/j.spen.2021.100881

Jara-Ettinger, A. C., Suárez-Hortiales, S., & De la Torre-García, O. (2021). Rett syndrome: Report of a new pathogenic variant and review of the literature regarding two clinical cases. *Boletin Medico Del Hospital Infantil de Mexico*, *78*(4). https://doi.org/10.24875/BMHIM.20000121

Kang, H. L., Benzer, S., & Min, K. T. (2002). Life extension in Drosophila by feeding a drug. *Proceedings of the National Academy of Sciences of the United States of America*, *99*(2). https://doi.org/10.1073/pnas.022631999

Kilgore, M., Miller, C. A., Fass, D. M., Hennig, K. M., Haggarty, S. J., Sweatt, J. D., & Rumbaugh, G. (2010). Inhibitors of class 1 histone deacetylases reverse contextual memory deficits in a mouse model of alzheimer's disease. *Neuropsychopharmacology*, *35*(4). https://doi.org/10.1038/npp.2009.197

Kitani-Morii, F., Friedland, R. P., Yoshida, H., & Mizuno, T. (2021). Drosophila as a Model for Microbiota Studies of Neurodegeneration. In *Journal of Alzheimer's Disease* (Vol. 84, Issue 2). https://doi.org/10.3233/JAD-215031

Klapper, R. (2000). The longitudinal visceral musculature of Drosophila melanogaster persists through metamorphosis. *Mechanisms of Development*, 95(1-2), 47–54. https://doi.org/10.1016/S0925-4773(00)00328-2

Koh, A., De Vadder, F., Kovatcheva-Datchary, P., & Bäckhed, F. (2016). From dietary fiber to host physiology: Short-chain fatty acids as key bacterial metabolites. In *Cell* (Vol. 165, Issue 6). https://doi.org/10.1016/j.cell.2016.05.041

Kriaucionis, S., Paterson, A., Curtis, J., Guy, J., MacLeod, N., & Bird, A. (2006). Gene Expression Analysis Exposes Mitochondrial Abnormalities in a Mouse Model of Rett Syndrome. *Molecular and Cellular Biology*, *26*(13). https://doi.org/10.1128/mcb.01665-05

Lajeunesse, D. R., Johnson, B., Presnell, J. S., Catignas, K. K., & Zapotoczny, G. (2010). Peristalsis in the junction region of the Drosophila larval midgut is modulated by DH31 expressing enteroendocrine cells. *BMC Physiology*, *10*(1). https://doi.org/10.1186/1472-6793-10-14

Li, L., Chen, R., Zhang, H., Li, J., Huang, H., Weng, J., Tan, H., Guo, T., Wang, M., & Xie, J. (2024). The epigenetic modification of DNA methylation in neurological diseases. In *Frontiers in Immunology* (Vol. 15). Frontiers Media SA. https://doi.org/10.3389/fimmu.2024.1401962

Link, N., & Bellen, H. J. (2020). Using Drosophila to drive the diagnosis and understand the mechanisms of rare human diseases. *Development (Cambridge)*, *147*(21). https://doi.org/10.1242/dev.191411

Liu, C., Wang, J., Wei, Y., Zhang, W., Geng, M., Yuan, Y., Chen, Y., Sun, Y., Chen, H., Zhang, Y., Xiong, M., Li, Y., Zheng, L., & Huang, K. (2020). Fat-Specific Knockout of Mecp2 Upregulates Slpi to Reduce Obesity by Enhancing Browning. *Diabetes*, *69*(1), 35–47. https://doi.org/10.2337/DB19-0502

Liu, H., Zhao, J., Zhang, W., & Nie, C. (2023). Impacts of sodium butyrate on intestinal mucosal barrier and intestinal microbial community in a weaned piglet model. *Frontiers in Microbiology*, *13*. https://doi.org/10.3389/fmicb.2022.1041885

Liu, Y., Flamier, A., Bell, G. W., Diao, A. J., Whitfield, T. W., Wang, H. C., Wu, Y., Schulte, F., Friesen, M., Guo, R., Mitalipova, M., Liu, X. S., Vos, S. M., Young, R. A., & Jaenisch, R. (2024). MECP2 directly interacts with RNA polymerase II to modulate transcription in human neurons. *Neuron*, *112*(12), 1943-1958.e10. https://doi.org/10.1016/j.neuron.2024.04.007

Liu, Y., Whitfield, T. W., Bell, G. W., Guo, R., Flamier, A., Young, R. A., & Jaenisch, R. (2025). Exploring the complexity of MECP2 function in Rett syndrome. In *Nature Reviews Neuroscience* (Vol. 26, Issue 7, pp. 379–398). Springer Nature. https://doi.org/10.1038/s41583-025-00926-1

Loh, J. S., Mak, W. Q., Tan, L. K. S., Ng, C. X., Chan, H. H., Yeow, S. H., Foo, J. B., Ong, Y. S., How, C. W., & Khaw, K. Y. (2024). Microbiota–gut–brain axis and its therapeutic applications in neurodegenerative diseases. In *Signal Transduction and Targeted Therapy* (Vol. 9, Issue 1). https://doi.org/10.1038/s41392-024-01743-1

Lyst, M. J., Ekiert, R., Ebert, D. H., Merusi, C., Nowak, J., Selfridge, J., Guy, J., Kastan, N. R., Robinson, N. D., De Lima Alves, F., Rappsilber, J., Greenberg, M. E., & Bird, A. (2013). Rett syndrome mutations abolish the interaction of MeCP2 with the NCoR/SMRT co-repressor. *Nature Neuroscience*, *16*(7). https://doi.org/10.1038/nn.3434

Ma, J., & Ptashne, M. (1988). Converting a eukaryotic transcriptional inhibitor into an activator. *Cell*, *55*(3). https://doi.org/10.1016/0092-8674(88)90030-X

Marballi, K., & MacDonald, J. L. (2021). Proteomic and transcriptional changes associated with MeCP2 dysfunction reveal nodes for therapeutic intervention in Rett syndrome. *Neurochemistry International*, *148*. https://doi.org/10.1016/j.neuint.2021.105076

Martelli, F., Quig, A., Mele, S., Lin, J., Fulton, T. L., Wansbrough, M., Barlow, C. K., Schittenhelm, R. B., Johnson, T. K., & Piper, M. D. W. (2024). A defined diet for pre-adult Drosophila melanogaster. *Scientific Reports*, *14*(1). https://doi.org/10.1038/s41598-024-57681-z

McKinsey, T. A., Zhang, C. L., & Olson, E. N. (2001). Identification of a Signal-Responsive Nuclear Export Sequence in Class II Histone Deacetylases. *Molecular and Cellular Biology*, *21*(18). https://doi.org/10.1128/mcb.21.18.6312-6321.2001

McKinsey, T. A., Zhang, C. L., & Olson, E. N. (2002). Signaling chromatin to make muscle. *Current Opinion in Cell Biology*, *14*(6), 763–772. https://doi.org/10.1016/S0955-0674(02)00389-7

Meehan, R., Lewis, J. D., & Bird, A. P. (1992). Characterization of MECP2, a vertebrate DNA binding protein with affinity for methylated DNA. *Nucleic Acids Research*, *20*(19). https://doi.org/10.1093/nar/20.19.5085

Meireles-Filho, A. C. A., Bardet, A. F., Yáñez-Cuna, J. O., Stampfel, G., & Stark, A. (2014). Cis-regulatory requirements for tissue-specific programs of the circadian clock. *Current Biology*, *24*(1). https://doi.org/10.1016/j.cub.2013.11.017

Mel B. Feany & Welcome W. Bender. (2000). A Drosophila model of Parkinson's disease. *NATURE*, *404*, 395–398.

Michno, K., van de Hoef, D., Wu, H., & Boulianne, G. L. (2005). Modeling Age-Related Diseases in Drosophila: Can this Fly? In *Current Topics in Developmental Biology* (Vol. 71). https://doi.org/10.1016/S0070-2153(05)71006-1

Mietto, M., Montanari, S., Falzarano, M. S., Manzati, E., Rimessi, P., Fabris, M., Selvatici, R., Gualandi, F., Neri, M., Fortunato, F., Rosa, M., Foti, S., Bigoni, S., Gessi, M., Vacca, M., Torelli, S., Hayek, J., & Ferlini, A. (2025). *MECP2 mRNA Profile in Brain Tissues from a Rett Syndrome Patient and Three Human Controls: Mutated Allele Preferential Transcription and In Situ RNA Mapping*. https://doi.org/10.3390/biom

Mirzaei, R., Afaghi, A., Babakhani, S., Sohrabi, M. R., Hosseini-Fard, S. R., Babolhavaeji, K., Khani Ali Akbari, S., Yousefimashouf, R., & Karampoor, S. (2021). Role of microbiota-derived short-chain fatty acids in cancer development and prevention. In *Biomedicine and Pharmacotherapy* (Vol. 139). https://doi.org/10.1016/j.biopha.2021.111619

Mirzoyan, Z., Sollazzo, M., Allocca, M., Valenza, A. M., Grifoni, D., & Bellosta, P. (2019). Drosophila melanogaster: A model organism to study cancer. In *Frontiers in Genetics* (Vol. 10). https://doi.org/10.3389/fgene.2019.00051

Mollica, M. P., Raso, G. M., Cavaliere, G., Trinchese, G., De Filippo, C., Aceto, S., Prisco, M., Pirozzi, C., Di Guida, F., Lama, A., Crispino, M., Tronino, D., Vaio, P. Di, Canani, R. B., Calignano, A., & Meli, R. (2017). Butyrate regulates liver mitochondrial function, efficiency, and dynamics in insulin-resistant obese mice. *Diabetes*, *66*(5). https://doi.org/10.2337/db16-0924

Monti, B., Polazzi, E., & Contestabile, A. (2010). Biochemical, Molecular and Epigenetic Mechanisms of Valproic Acid Neuroprotection. *Current Molecular Pharmacology*, *2*(1). https://doi.org/10.2174/1874467210902010095

Moog, U., Smeets, E. E. J., Van Roozendaal, K. E. P., Schoenmakers, S., Herbergs, J., Schoonbrood-Lenssen, A. M. J., & Schrander-Stumpel, C. T. R. M. (2003). Neurodevelopmental disorders in males related to the gene causing Rett syndrome in females (MECP 2). In *European Journal of Paediatric Neurology* (Vol. 7, Issue 1). https://doi.org/10.1016/S1090-3798(02)00134-4

Motil, K. J., Caeg, E., Barrish, J. O., Geerts, S., Lane, J. B., Percy, A. K., Annese, F., McNair, L., Skinner, S. A., Lee, H. S., Neul, J. L., & Glaze, D. G. (2012). Gastrointestinal and nutritional problems occur frequently throughout life in girls and women with rett syndrome. *Journal of Pediatric Gastroenterology and Nutrition*, *55*(3). https://doi.org/10.1097/MPG.0b013e31824b6159

Nagai, Y., Mizuno, H., Fujikake, N., & Wada, K. (2011). α-Synuclein transgenic Drosophila as a model of Parkinson's disease and related synucleinopathies. In *Parkinson's Disease*. https://doi.org/10.4061/2011/212706

Nakhal, M. M., Yassin, L. K., Alyaqoubi, R., Saeed, S., Alderei, A., Alhammadi, A., Alshehhi, M., Almehairbi, A., Al Houqani, S., BaniYas, S., Qanadilo, H., Ali, B. R., Shehab, S., Statsenko, Y., Meribout, S., Sadek, B., Akour, A., & Hamad, M. I. K. (2024). The Microbiota–Gut–Brain Axis and Neurological Disorders: A Comprehensive Review. In *Life* (Vol. 14, Issue 10). Multidisciplinary Digital Publishing Institute (MDPI). https://doi.org/10.3390/life14101234

Nan, X., Campoy, F. J., & Bird, A. (1997). MeCP2 is a transcriptional repressor with abundant binding sites in genomic chromatin. *Cell*, *88*(4). https://doi.org/10.1016/S0092-8674(00)81887-5

Neul, J. L., Kaufmann, W. E., Glaze, D. G., Christodoulou, J., Clarke, A. J., Bahi-Buisson, N., Leonard, H., Bailey, M. E. S., Schanen, N. C., Zappella, M., Renieri, A., Huppke, P., & Percy, A. K. (2010). Rett syndrome: Revised diagnostic criteria and nomenclature. *Annals of Neurology*, *68*(6). https://doi.org/10.1002/ana.22124

Nitta, Y., & Sugie, A. (2022). Studies of neurodegenerative diseases using Drosophila and the development of novel approaches for their analysis. In *Fly* (Vol. 16, Issue 1). https://doi.org/10.1080/19336934.2022.2087484

Ortega-Alarcon, D., Claveria-Gimeno, R., Vega, S., Jorge-Torres, O. C., Esteller, M., Abian, O., & Velazquez-Campoy, A. (2020). Molecular context-dependent effects induced by rett syndrome-associated mutations in mecp2. *Biomolecules*, *10*(11). https://doi.org/10.3390/biom10111533

Palmieri, M., Pozzer, D., & Landsberger, N. (2023). Advanced genetic therapies for the treatment of Rett syndrome: state of the art and future perspectives. In *Frontiers in Neuroscience* (Vol. 17). https://doi.org/10.3389/fnins.2023.1172805

Pascual-Alonso, A., Xiol, C., Smirnov, D., Kopajtich, R., Prokisch, H., & Armstrong, J. (2023). Identification of molecular signatures and pathways involved in Rett syndrome using a multi-omics approach. *Human Genomics*, *17*(1). https://doi.org/10.1186/s40246-023-00532-1

Pedroza Matute, S., & Iyavoo, S. (2023). Exploring the gut microbiota: lifestyle choices, disease associations, and personal genomics. In *Frontiers in Nutrition* (Vol. 10). https://doi.org/10.3389/fnut.2023.1225120

Peller, C. R., Bacon, E. M., Bucheger, J. A., & Blumenthal, E. M. (2009). Defective gut function in drop-dead mutant Drosophila. *Journal of Insect Physiology*, *55*(9). https://doi.org/10.1016/j.jinsphys.2009.05.011

Peña, C. J. (2025). Epigenetic regulation of brain development, plasticity, and response to early-life stress. In *Neuropsychopharmacology*. Springer Nature. https://doi.org/10.1038/s41386-025-02179-z

Percy, A. K. (2002). Rett syndrome: Current status and new vistas. In *Neurologic Clinics* (Vol. 20, Issue 4). https://doi.org/10.1016/S0733-8619(02)00022-1

Percy, A. K., Lee, H. S., Neul, J. L., Lane, J. B., Skinner, S. A., Geerts, S. P., Annese, F., Graham, J., McNair, L., Motil, K. J., Barrish, J. O., & Glaze, D. G. (2010). Profiling scoliosis in rett syndrome. *Pediatric Research*, *67*(4). https://doi.org/10.1203/PDR.0b013e3181d0187f

Pfeiffer, B. D., Ngo, T. T. B., Hibbard, K. L., Murphy, C., Jenett, A., Truman, J. W., & Rubin, G. M. (2010). Refinement of tools for targeted gene expression in Drosophila. *Genetics*, *186*(2). https://doi.org/10.1534/genetics.110.119917

Poovathumkadavil, P., & Jagla, K. (2020). Genetic control of muscle diversification and homeostasis: Insights from drosophila. In *Cells* (Vol. 9, Issue 6). https://doi.org/10.3390/cells9061543

Ramocki, M. B., Tavyev, Y. J., & Peters, S. U. (2010). The MECP2 duplication syndrome. In *American Journal of Medical Genetics, Part A* (Vol. 152, Issue 5, pp. 1079–1088). https://doi.org/10.1002/ajmg.a.33184

Ribchester, R. R., Thomson, D., Wood, N. I., Hinks, T., Gillingwater, T. H., Wishart, T. M., Court, F. A., & Morton, A. J. (2004). Progressive abnormalities in skeletal muscle and neuromuscular junctions of transgenic mice expressing the Huntington's disease mutation. *European Journal of Neuroscience*, *20*(11). https://doi.org/10.1111/j.1460-9568.2004.03783.x

Robinson, L., Guy, J., McKay, L., Brockett, E., Spike, R. C., Selfridge, J., De Sousa, D., Merusi, C., Riedel, G., Bird, A., & Cobb, S. R. (2012). Morphological and functional reversal of phenotypes in a mouse model of Rett syndrome. *Brain*, *135*(9). https://doi.org/10.1093/brain/aws096

Rose, S., Bennuri, S. C., Davis, J. E., Wynne, R., Slattery, J. C., Tippett, M., Delhey, L., Melnyk, S., Kahler, S. G., MacFabe, D. F., & Frye, R. E. (2018). Butyrate enhances mitochondrial function during oxidative stress in cell lines from boys with autism. *Translational Psychiatry*, *8*(1). https://doi.org/10.1038/s41398-017-0089-z

Ross, P. D., Guy, J., Selfridge, J., Kamal, B., Bahey, N., Elizabeth Tanner, K., Gillingwater, T. H., Jones, R. A., Loughrey, C. M., McCarroll, C. S., Bailey, M. E. S., Bird, A., & Cobb, S. (2016). Exclusive expression of MeCP2 in the nervous system distinguishes between brain and peripheral Rett syndrome-like phenotypes. *Human Molecular Genetics*, *25*(20). https://doi.org/10.1093/hmg/ddw269

Roy, S., & VijayRaghavan, K. (1998). Patterning muscles using organizers: Larval muscle templates and adult myoblasts actively interact to pattern the dorsal longitudinal flight

muscles of Drosophila. *Journal of Cell Biology*, *141*(5). https://doi.org/10.1083/jcb.141.5.1135

Schultheis, D., Schwirz, J., & Frasch, M. (2019). RNAi screen in tribolium reveals involvement of F-BAR proteins in myoblast fusion and visceral muscle morphogenesis in insects. *G3: Genes, Genomes, Genetics*, *9*(4). https://doi.org/10.1534/g3.118.200996

Sherwin, E., Dinan, T. G., & Cryan, J. F. (2018). Recent developments in understanding the role of the gut microbiota in brain health and disease. In *Annals of the New York Academy of Sciences* (Vol. 1420, Issue 1). https://doi.org/10.1111/nyas.13416

Shulman, J. M., & Feany, M. B. (2003). Genetic Modifiers of Tauopathy in Drosophila. *Genetics*, *165*(3). https://doi.org/10.1093/genetics/165.3.1233

Sittipo, P., Choi, J., Lee, S., & Lee, Y. K. (2022). The function of gut microbiota in immune-related neurological disorders: a review. In *Journal of Neuroinflammation* (Vol. 19, Issue 1). https://doi.org/10.1186/s12974-022-02510-1

Smirnov, K., Stroganova, T., Molholm, S., & Sysoeva, O. (2021). Reviewing evidence for the relationship of eeg abnormalities and rtt phenotype paralleled by insights from animal studies. In *International Journal of Molecular Sciences* (Vol. 22, Issue 10). https://doi.org/10.3390/ijms22105308

Smrt, R. D., Eaves-Egenes, J., Barkho, B. Z., Santistevan, N. J., Zhao, C., Aimone, J. B., Gage, F. H., & Zhao, X. (2007). Mecp2 deficiency leads to delayed maturation and altered gene expression in hippocampal neurons. *Neurobiology of Disease*, *27*(1). https://doi.org/10.1016/j.nbd.2007.04.005

Sonn, J. Y., Kim, W., Iwanaszko, M., Aoi, Y., Li, Y., Parkitny, L., Brissette, J. L., Weiner, L., Al-Ramahi, I., Botas, J., Shilatifard, A., & Zoghbi, H. Y. (2024). MeCP2 Interacts with the Super Elongation Complex to Regulate Transcription. *BioRxiv*, 2024.06.30.601446. https://doi.org/10.1101/2024.06.30.601446

St. Laurent, R., O'Brien, L. M., & Ahmad, S. T. (2013). Sodium butyrate improves locomotor impairment and early mortality in a rotenone-induced Drosophila model of Parkinson's disease. *Neuroscience*, *246*. https://doi.org/10.1016/j.neuroscience.2013.04.037

Steliou, K., Boosalis, M. S., Perrine, S. P., Sangerman, J., & Faller, D. V. (2012). Butyrate histone deacetylase inhibitors. *BioResearch Open Access*, *1*(4). https://doi.org/10.1089/biores.2012.0223

Strati, F., Cavalieri, D., Albanese, D., De Felice, C., Donati, C., Hayek, J., Jousson, O., Leoncini, S., Pindo, M., Renzi, D., Rizzetto, L., Stefanini, I., Calabrò, A., & De Filippo, C. (2016). Altered gut microbiota in Rett syndrome. *Microbiome*, *4*. https://doi.org/10.1186/s40168-016-0185-y

Ta, D., Downs, J., Baynam, G., Wilson, A., Richmond, P., & Leonard, H. (2022). A brief history of MECP2 duplication syndrome: 20-years of clinical understanding. In *Orphanet Journal of Rare Diseases* (Vol. 17, Issue 1). https://doi.org/10.1186/s13023-022-02278-w

Tan, J., McKenzie, C., Potamitis, M., Thorburn, A. N., Mackay, C. R., & Macia, L. (2014). The Role of Short-Chain Fatty Acids in Health and Disease. In *Advances in Immunology* (Vol. 121). https://doi.org/10.1016/B978-0-12-800100-4.00003-9

Thapa, P., Jayasuriya, R., Hall, J. J., Beek, K., Mukherjee, P., Gudi, N., & Narasimhan, P. (2021). Role of informal healthcare providers in tuberculosis care in low- And middle-income countries: A systematic scoping review. In *PLoS ONE* (Vol. 16, Issue 9 September). https://doi.org/10.1371/journal.pone.0256795

Ugur, B., Chen, K., & Bellen, H. J. (2016). Drosophila tools and assays for the study of human diseases. In *DMM Disease Models and Mechanisms* (Vol. 9, Issue 3). https://doi.org/10.1242/dmm.023762

Ullah, H., Arbab, S., Tian, Y., Liu, C. Q., Chen, Y., Qijie, L., Khan, M. I. U., Hassan, I. U., & Li, K. (2023). The gut microbiota–brain axis in neurological disorder. In *Frontiers in Neuroscience* (Vol. 17). https://doi.org/10.3389/fnins.2023.1225875

Vale San Gomes, D. O., & de Morais, M. B. (2020). Gut microbiota and the use of probiotics in constipation in children and adolescents: Systematic review. In *Revista Paulista de Pediatria* (Vol. 38). https://doi.org/10.1590/1984-0462/2020/38/2018123

Van Esch, H., Bauters, M., Ignatius, J., Jansen, M., Raynaud, M., Hollanders, K., Lugtenberg, D., Bienvenu, T., Jensen, L. R., Gécz, J., Moraine, C., Marynen, P., Fryns, J. P., & Froyen, G. (2005). Duplication of the MECP2 region is a frequent cause of severe mental retardation and progressive neurological symptoms in males. *American Journal of Human Genetics*, *77*(3). https://doi.org/10.1086/444549

Vecsler, M., Simon, A. J., Amariglio, N., Rechavi, G., & Gak, E. (2010). MeCP2 deficiency downregulates specific nuclear proteins that could be partially recovered by valproic acid in vitro. *Epigenetics*, *5*(1). https://doi.org/10.4161/epi.5.1.10630

Vergani, L., Grattarola, M., & Nicolini, C. (2004). Modifications of chromatin structure and gene expression following induced alterations of cellular shape. *The International Journal of Biochemistry & Cell Biology*, *36*(8), 1447–1461. https://doi.org/10.1016/J.BIOCEL.2003.11.015

Vicentini, F. A., Keenan, C. M., Wallace, L. E., Woods, C., Cavin, J. B., Flockton, A. R., Macklin, W. B., Belkind-Gerson, J., Hirota, S. A., & Sharkey, K. A. (2021). Intestinal microbiota shapes gut physiology and regulates enteric neurons and glia. *Microbiome*, *9*(1). https://doi.org/10.1186/s40168-021-01165-z

Vidal, M., Arch, M., Fuentes, E., & Cardona, P. J. (2024). Drosophila melanogaster experimental model to test new antimicrobials: a methodological approach. In *Frontiers in Microbiology* (Vol. 15). Frontiers Media SA. https://doi.org/10.3389/fmicb.2024.1478263

Vila, M. C., Rayavarapu, S., Hogarth, M. W., Van Der Meulen, J. H., Horn, A., Defour, A., Takeda, S., Brown, K. J., Hathout, Y., Nagaraju, K., & Jaiswal, J. K. (2017). Mitochondria mediate cell membrane repair and contribute to Duchenne muscular dystrophy. *Cell Death and Differentiation*, *24*(2). https://doi.org/10.1038/cdd.2016.127

Vonhoff, F., Williams, A., Ryglewski, S., & Duch, C. (2012a). Drosophila as a model for MECP2 gain of function in neurons. *PLoS ONE*, *7*(2). https://doi.org/10.1371/journal.pone.0031835

Vonhoff, F., Williams, A., Ryglewski, S., & Duch, C. (2012b). Drosophila as a Model for MECP2 Gain of Function in Neurons. *PLoS ONE*, *7*(2), e31835. https://doi.org/10.1371/JOURNAL.PONE.0031835

Vuu, Y. M., Roberts, C. T., & Rastegar, M. (2023). MeCP2 Is an Epigenetic Factor That Links DNA Methylation with Brain Metabolism. In *International Journal of Molecular Sciences* (Vol. 24, Issue 4). https://doi.org/10.3390/ijms24044218

Wahba, G., Schock, S. C., Claridge, E., Bettolli, M., Grynspan, D., Humphreys, P., & Staines, W. A. (2015). MeCP2 in the enteric nervous system. *Neurogastroenterology and Motility*, *27*(8). https://doi.org/10.1111/nmo.12605

Wahba, G., Schock, S. C., Cudd, S., Grynspan, D., Humphreys, P., & Staines, W. A. (2016). Activity and MeCP2-dependent regulation of nNOS levels in enteric neurons. *Neurogastroenterology and Motility*, *28*(11). https://doi.org/10.1111/nmo.12873

Wakai, S., Kameda, K., Ishikawa, Y., Miyamoto, S., Nagaoka, M., Okabe, M., Minami, R., & Tachi, N. (1990). Rett syndrome: findings suggesting axonopathy and mitochondrial abnormalities. *Pediatric Neurology*, *6*(5). https://doi.org/10.1016/0887-8994(90)90028-Y

Walsh, M. E., Bhattacharya, A., Sataranatarajan, K., Qaisar, R., Sloane, L., Rahman, M. M., Kinter, M., & Van Remmen, H. (2015). The histone deacetylase inhibitor butyrate improves metabolism and reduces muscle atrophy during aging. *Aging Cell*, *14*(6). https://doi.org/10.1111/acel.12387

Wan, M., Sung, S., Lee, J., Zhang, X., Houwink-Manville, I., Song, H.-R., Amir, R. E., Budden, S., Naidu, S., Luiz, J., Pereira, P., Lo, I. F. M., Zoghbi, H. Y., Schanen, N. C., & Francke, U. (1999). Rett Syndrome and Beyond: Recurrent Spontaneous and Familial MECP2 Mutations at CpG Hotspots. In *Am. J. Hum. Genet* (Vol. 65).

Wang, Q., Yang, Q., & Liu, X. (2023). The microbiota–gut–brain axis and neurodevelopmental disorders. In *Protein and Cell* (Vol. 14, Issue 10). https://doi.org/10.1093/procel/pwad026

Weitkunat, M., & Schnorrer, F. (2014). A guide to study Drosophila muscle biology. *Methods*, *68*(1). https://doi.org/10.1016/j.ymeth.2014.02.037

Williams, A. A., White, R., Siniard, A., Corneveaux, J., Huentelman, M., & Duch, C. (2016). MECP2 impairs neuronal structure by regulating KIBRA. *Neurobiology of Disease*, *91*, 284–291. https://doi.org/10.1016/J.NBD.2016.03.019

Wittmann, C. W., Wszolek, M. F., Shulman, J. M., Salvaterra, P. M., Lewis, J., Hutton, M., & Feany, M. B. (2001). Tauopathy in Drosophila: Neurodegeneration without neurofibrillary tangles. *Science*, *293*(5530). https://doi.org/10.1126/science.1062382

Yakabe, S., Soejima, H., Yatsuki, H., Tominaga, H., Zhao, W., Higashimoto, K., Joh, K., Kudo, S., Miyazaki, K., & Mukai, T. (2008). MeCP2 knockdown reveals DNA methylation-independent gene repression of target genes in living cells and a bias in the cellular location of target gene products. *Genes and Genetic Systems*, *83*(2). https://doi.org/10.1266/ggs.83.199

Yamamoto, T., Shimojima, K., Shimada, S., Yokochi, K., Yoshitomi, S., Yanagihara, K., Imai, K., & Okamoto, N. (2014). Clinical impacts of genomic copy number gains at Xq28. In *Human Genome Variation* (Vol. 1). https://doi.org/10.1038/hgv.2014.1

Yan, S., Ji, Q., Ding, J., Liu, Z., Wei, W., Li, H., Li, L., Ma, C., Liao, D., He, Z., & Ai, S. (2024). Protective effects of butyrate on cerebral ischaemic injury in animal models: a systematic review and meta-analysis. In *Frontiers in Neuroscience* (Vol. 18). https://doi.org/10.3389/fnins.2024.1304906

Yusufzai, T. M., & Wolffe, A. P. (2000). Functional consequences of Rett syndrome mutations on human MeCP2. *Nucleic Acids Research*, *28*(21). https://doi.org/10.1093/nar/28.21.4172

Zeidler, M. P., Tan, C., Bellaiche, Y., Cherry, S., Häder, S., Gayko, U., & Perrimon, N. (2004). Temperature-sensitive control of protein activity by conditionally splicing inteins. *Nature Biotechnology*, *22*(7). https://doi.org/10.1038/nbt979

Zhang, B., & Stewart, B. (2010). Electrophysiological recording from Drosophila larval body-wall muscles. *Cold Spring Harbor Protocols*, *5*(9). https://doi.org/10.1101/pdb.prot5487

Zhang, X., Koolhaas, W. H., & Schnorrer, F. (2014). A versatile two-step CRISPR- and RMCE-based strategy for efficient genome engineering in Drosophila. *G3: Genes, Genomes, Genetics*, *4*(12). https://doi.org/10.1534/g3.114.013979

Zhao, X., Zhu, M., Wang, Z., Gao, M., Long, Y., Zhou, S., & Wang, W. (2025). The Alleviative Effect of Sodium Butyrate on Dexamethasone-Induced Skeletal Muscle Atrophy. *Cell Biology International*, *49*(5), 508–521. https://doi.org/10.1002/cbin.70003

Zheng, Y., Bonfili, L., Wei, T., & Eleuteri, A. M. (2023). Understanding the Gut–Brain Axis and Its Therapeutic Implications for Neurodegenerative Disorders. In *Nutrients* (Vol. 15, Issue 21). https://doi.org/10.3390/nu15214631

Zhou, A., Han, S., & Zhou, Z. J. (2017). Molecular and genetic insights into an infantile epileptic encephalopathy–CDKL5 disorder. *Frontiers in Biology,* 12(1), 1–15. https://doi.org/10.1007/s11515-016-1438-7

Zhou, J., Hamdan, H., Yalamanchili, H. K., Pang, K., Pohodich, A. E., Lopez, J., Shao, Y., Oses-Prieto, J. A., Li, L., Kim, W., Durham, M. A., Bajikar, S. S., Palmer, D. J., Ng, P., Thompson, M. L., Bebin, E. M., Müller, A. J., Kuechler, A., Kampmeier, A., … Zoghbi, H. Y. (2022). Disruption of MeCP2–TCF20 complex underlies distinct neurodevelopmental disorders. *Proceedings of the National Academy of Sciences of the United States of America*, *119*(4). https://doi.org/10.1073/pnas.2119078119

Zlatic, S. A., Werner, E., Surapaneni, V., Lee, C. E., Gokhale, A., Singleton, K., Duong, D., Crocker, A., Gentile, K., Middleton, F., Dalloul, J. M., Liu, W. L. Y., Patgiri, A., Tarquinio, D., Carpenter, R., & Faundez, V. (2024). Systemic proteome phenotypes reveal defective metabolic flexibility in Mecp2 mutants. *Human Molecular Genetics*, *33*(1). https://doi.org/10.1093/hmg/ddad154

Zysman, L., Lotan, M., & Ben-Zeev, B. (2006). Osteoporosis in Rett syndrome: A study on normal values. In *TheScientificWorldJournal* (Vol. 6). https://doi.org/10.1100/tsw.2006.266

Figures

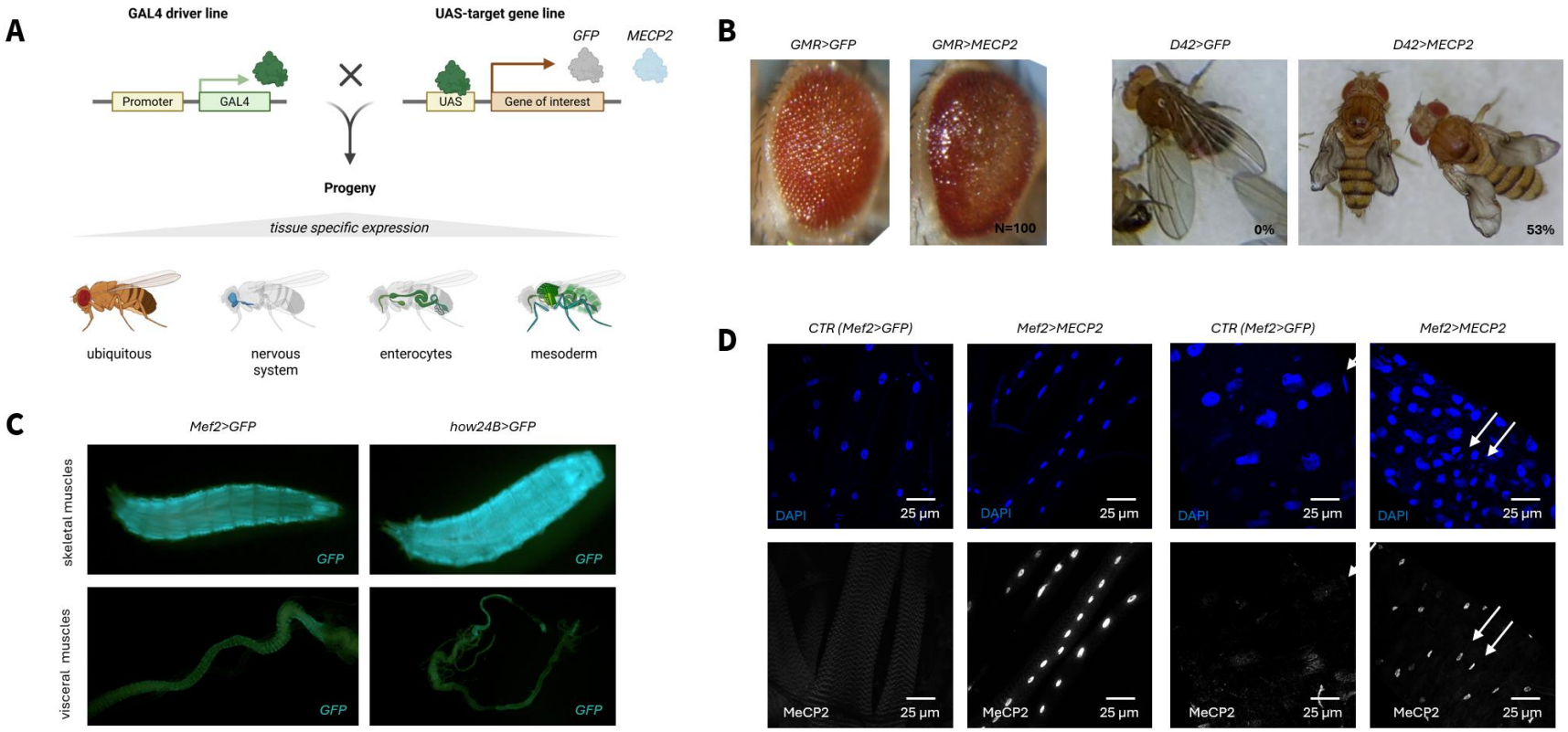

Fig. 1 Validation of *MECP2* overexpressing *Drosophila* model for *MECP2*-related diseases. (A) Schematic of the *UAS-GAL4* system and tissues targeted for *MECP2* expression. **(B)** Eye roughness phenotype induced by *MECP2* WT overexpression under GMR-GAL4 driver (N=100); quantification of wing defects and penetrance using D42-GAL4 (N=15). **(C)** GFP fluorescence showing larval expression pattern of the indicated muscle drivers in skeletal and visceral muscles. **(D)** Immunostaining of nuclei with DAPI (blue) and MeCP2 (white) in larval body wall muscles (left) and gut (right). The arrows indicate the colocalization of MeCP2 with the muscle cells nuclei.

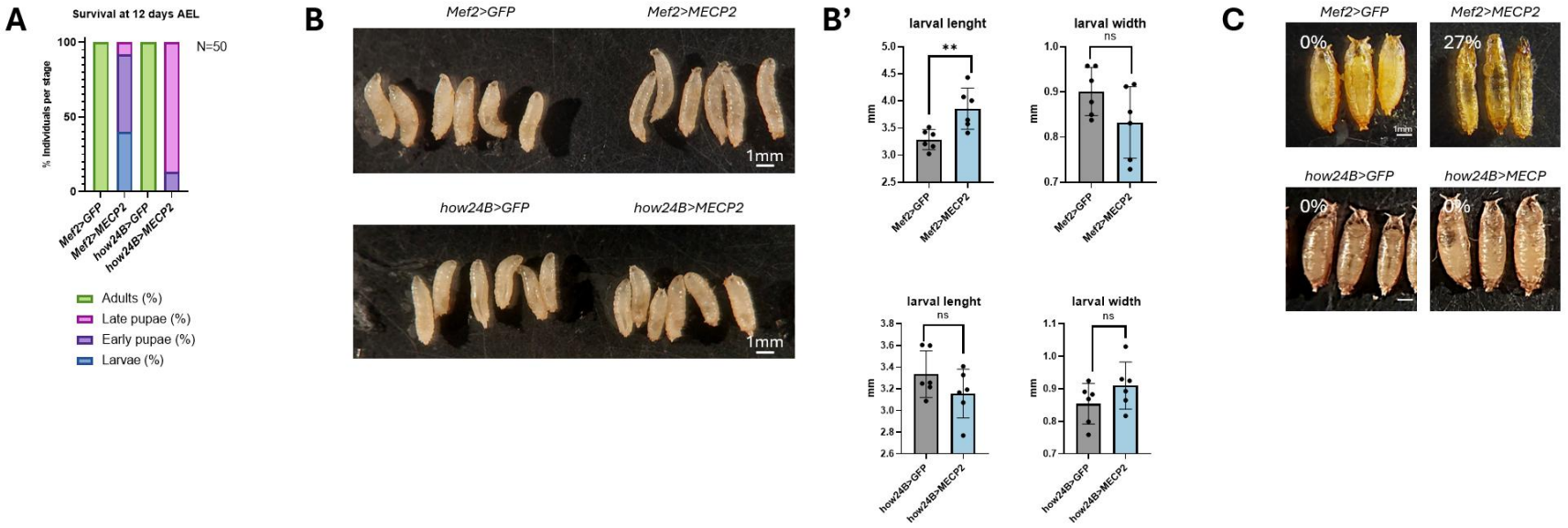

Fig. 2 Developmental lethality and morphological phenotypes upon *MECP2* misexpression in muscle. (A) Bar graph showing the proportion of animals arrested at different developmental stages at 12 days after egg laying (AEL), for each genotype. All bars represent 100% of individuals scored per genotype. In *Mef2 > GFP* (control), all animals reached adulthood (green). In *Mef2 > MECP2*, animals were arrested predominantly at the larval (blue) and early pupal stages (purple). In *how24B > MECP2*, animals mostly arrested at the late pupal stage (pink), with a smaller fraction at the early pupal stage (purple). **(B)** Representative images of five individual larvae per genotype and related quantification of length and width in B'. **(C)** Representative images of three pupae per genotype and percentage of the misshape phenotype indicated as the mean of the percentage of three independent biological replicates.

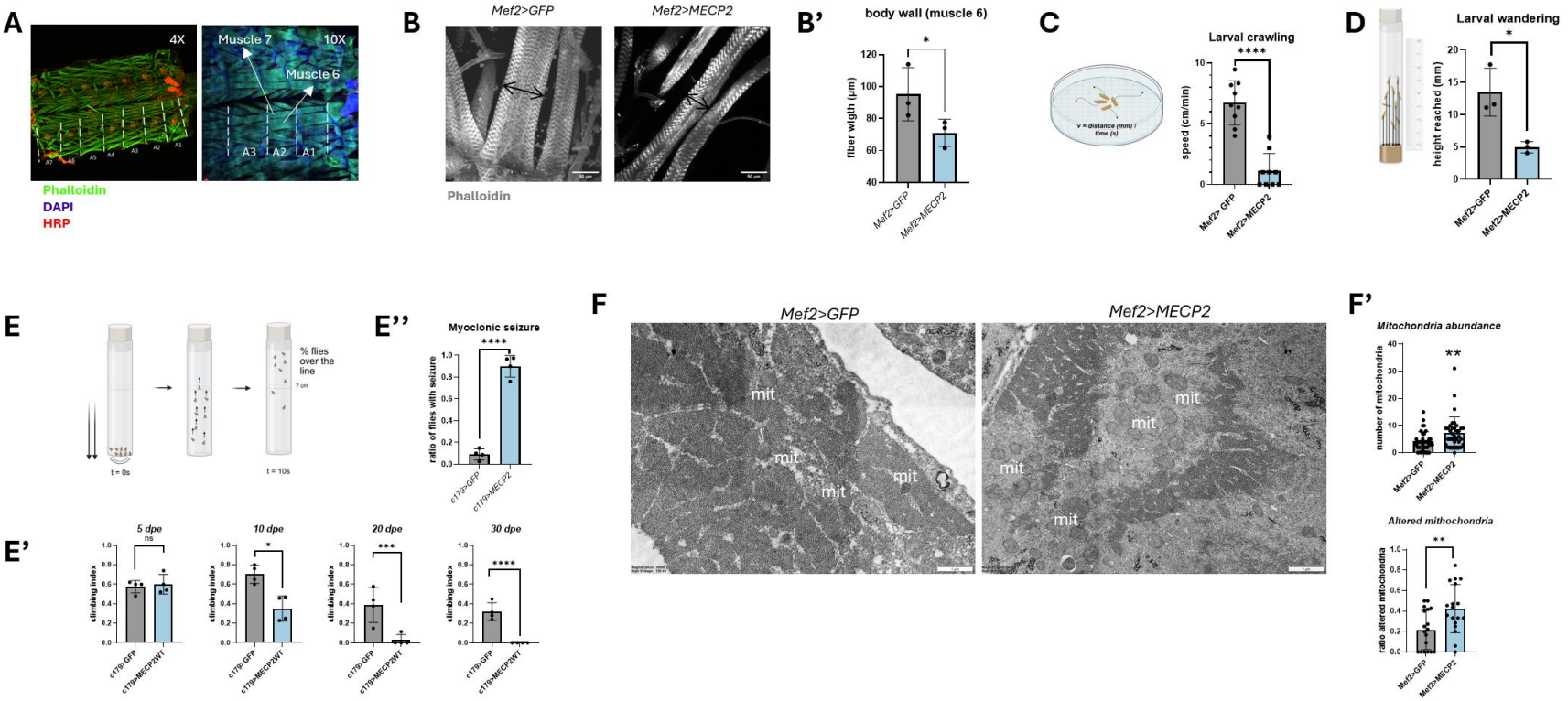

Fig. 3 *MECP2* misexpression in muscle impairs skeletal muscle morphology, mitochondrial integrity, and motor function. (A) Immunofluorescence images of larval body wall muscles in control flies. Left: low magnification (4×) showing the segmented pattern of the larval body wall (segments A1–A7). Right: higher magnification (10×) highlighting segments A6 and A7, with reference muscles 6 and 7 indicated. **(B)** Phalloidin staining of reference muscle 6 in *Mef2 > MECP2* and control larvae. *MECP2* misexpression leads to reduced muscle thickness. **(B')** Quantification of muscle 6 thickness. Data represent mean ± SD; individual data points are shown. **(C–F)** Functional assays in larvae. **(C)** Crawling speed and **(D)** larval wandering ability are significantly reduced in *Mef2 > MECP2* compared to controls. For the larval crawling each point represents a larva while for the wandering ability each point is the average of 30 pupal case. Schematic illustrations of the assays are shown on the left; quantification on the right. **(E)** Schematic of the climbing assay for adult muscle phenotypes observed upon late-onset misexpression of *MECP2* using the *c179* muscle driver. **(E')** Progressive impairment in climbing ability is observed at 5, 10, 20, and 30 days post-eclosion (dpe). Each point represent the average of technical replicates quantifying the ratio of larvae overcoming a 7 cm height after 10 s. Genotypes used: *c179 > MECP2* and *c179 > GFP* as control. Data

represent mean ± SD from multiple replicates. **(E")** Quantification of *c179 > MECP2* adults exhibiting mechanically induced myoclonic seizures upon stimulation. **(F)** Transmission electron microscopy (TEM) images of L3 larval body wall muscles from control (*Mef2>GFP*) and *MECP2*-overexpressing (*Mef2>MECP2*) *Drosophila*. Individual mitochondria are indicated by the label "mit". Scale bar: 500 nm. **(F')** Quantification of mitochondrial number per muscle section and percentage of mitochondria with altered cristae. Morphometric analysis was performed on 20 aligned TEM micrographs per genotype (magnification 20k), from three biologically independent samples (N = 3).

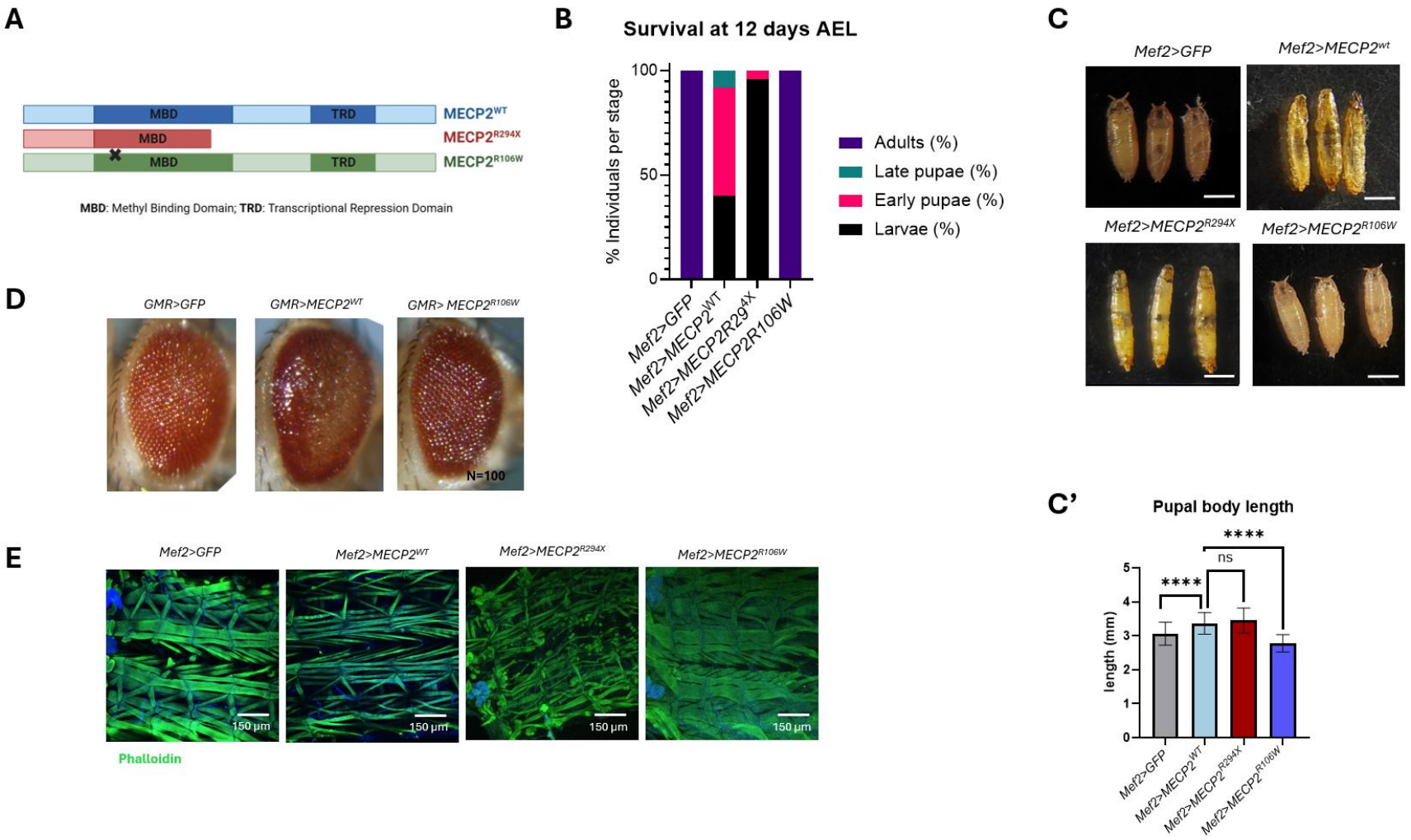

Fig. 4 *MECP2* mutant phenotypes in *Drosophila* (R106W, R294X) (A) Schematic representation of the MeCP2 protein (WT and mutant forms), showing the location of RTT–

associated mutations R106W, R294X. The two main functional domains - MBD and TRD - are indicated and color-coded consistently with subsequent panels. **(B)** 100% stacked bar chart showing the proportion of animals at each developmental stage (larvae, early pupae, late pupae, adults) at 12 days AEL for each genotype (N=30; single experiment). **(C)** Representative images of three early pupae selected at different time points due to the developmental delay (around 7 days AEL for GFP and R106W and after 10 days AEL for WT and R294X). Scale bar: 1 mm. **(C')** Quantification of pupal length for the indicated genotypes. Bars denote mean ± SD across replicates (N=50). **(D)** Eye roughness phenotype induced by *MECP2* WT and mutants overexpression under GMR-GAL4 driver (N=100). **(E)** Confocal images of larval body wall muscles stained with phalloidin (green) and DAPI (blue), showing muscle morphology alterations upon *MECP2* expression. Scale bar: 150 μm.

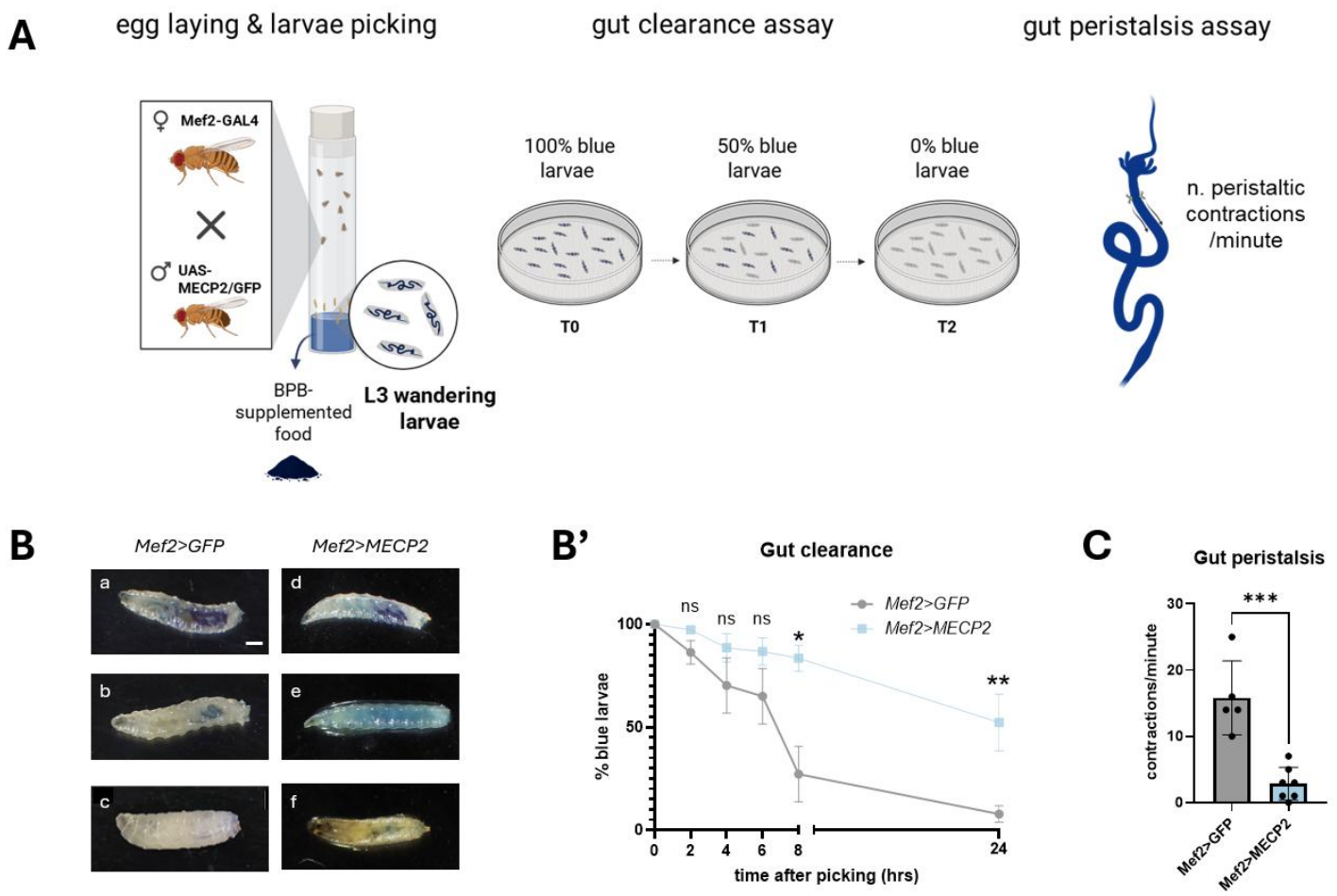

Fig. 5 *MECP2* overexpression in muscle impairs intestinal function in *Drosophila* larvae. (A) Schematic overview of the experimental setup. Larvae are obtained from genetic crosses and raised from the embryonic stage on food supplemented with bromophenol blue. At the wandering L3 stage, larvae displaying a blue gut were selected for two functional assays: *gut clearance* and *gut peristalsis*. The gut clearance assay is illustrated aside through representative images of the same Petri dish at three different time points and quantified as shown in B'. The peristalsis assay (right) shows the larval gut and the region where the number of peristaltic contractions were quantified per minute. **(B)** Representative brightfield images of

larvae at different time points: T0 (a-d), T1 (b-e) and T2 (c-f) of the indicated genotypes **(B')** Quantification of gut clearance over time. The percentage of larvae retaining blue dye was measured at several time points after picking. Control larvae (gray line) progressively cleared the dye, reaching nearly 0% at 24 hours, whereas *MECP2*-overexpressing larvae (blue line) retained blue coloration (~50%). Data are expressed as mean ± SEM. Approximately 30 larvae were analyzed per experiment, across ~9 independent experiments. Statistical analysis indicates no significant differences up to 6 hours post-picking, followed by significant differences at 8 and 24 hours. **(C)** Gut peristalsis is reduced in *MECP2*-overexpressing larvae. Scatter plot showing the number of peristaltic contractions per minute in individual animals. Each dot represents one larva.

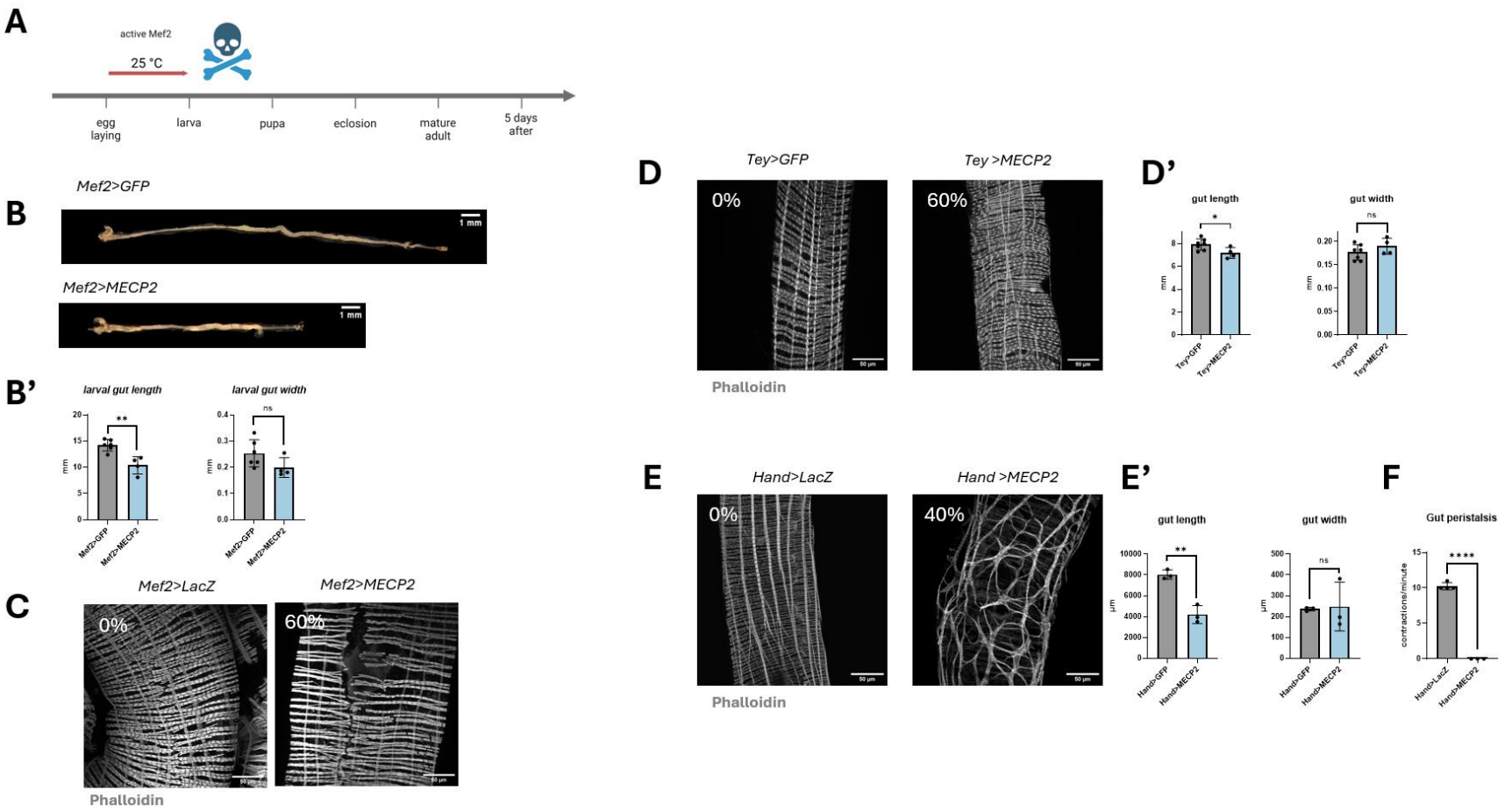

Fig. 6 *MECP2* overexpression impairs visceral muscle fibers and gut structure. (A) Schematic illustrating *MECP2* expression under the *Mef2* driver throughout larval development, resulting in lethality during the larva-to-pupa transition. **(B)** Brightfield images of dissected larval guts from the indicated genotypes. **(B')** Quantification of gut length and width of the indicated genotypes. Each point represent a gut. **(C)** Confocal images of larval guts stained with phalloidin to visualize visceral muscle fibers. The percentage of affected larvae (phenotype penetrance) is indicated. larvae per genotype. **(D)** Confocal images of adult guts stained with phalloidin under Tey>MECP2 and control conditions. Phenotype penetrance is indicated (N≈ 15). **(D')** Quantification of gut length and width in *Tey>MECP2* and control adults (N≈ 15*).* **(E)** Confocal images of adult guts stained with phalloidin in Hand>MECP2 and control

animals. Phenotype penetrance is indicated (N ≈ 15). **(E')** Quantification of gut length and width in *Hand>MECP2* and control adults (N ≈ 15). **(F)** Number of peristaltic contractions per minute in adult guts of the indicated genotypes. Each point represents a gut.

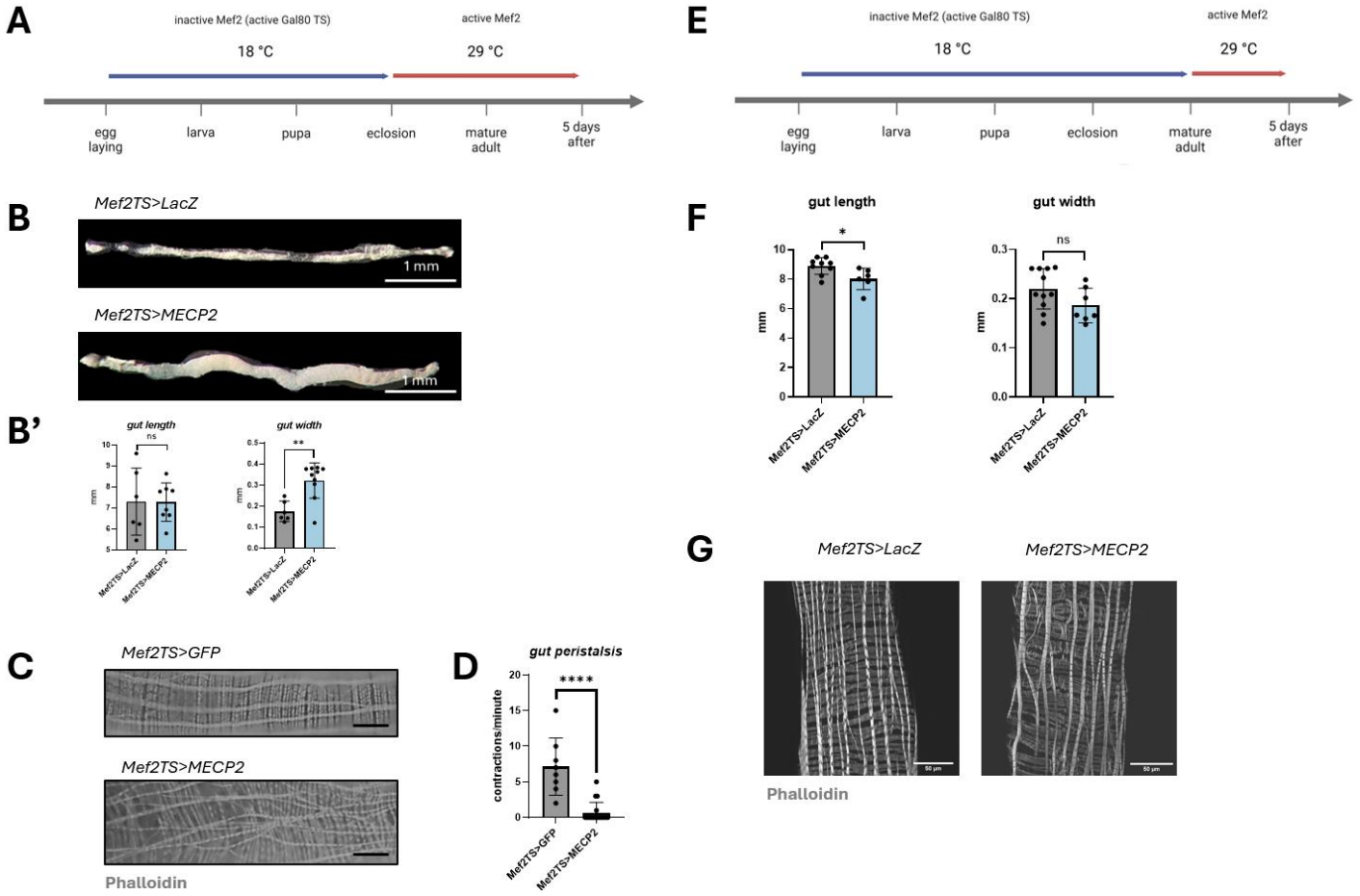

Fig. 7 Temporal requirement of *MECP2* expression for gut–muscle phenotypes (A) Schematic representation of the TARGET system used to temporally control *MECP2* expression under the *Mef2*-GAL4 driver. The temperature-sensitive GAL80^ts repressor blocks GAL4 activity at 18 °C and allows *MECP2* expression at 29 °C. **(B)** Brightfield images of

dissected guts from adult flies with MECP2 induced immediately after eclosion (early induction). **(B')** Quantification of gut length and width under early induction (n ≈ 15). **(C)** Phalloidin stained visceral muscles under early *MECP2* induction. **(D)** Quantification of peristaltic contractions in the early induction condition (n ≈ 15). **(E)** Schematic illustrating the late induction paradigm, in which *MECP2* expression is activated five days after eclosion, once visceral muscle development is complete. **(F)** Quantification of gut length and width in flies with late *MECP2* induction (N ≈ 15). **(G)** Representative confocal images of phalloidin-stained guts under late induction (N ≈ 15).

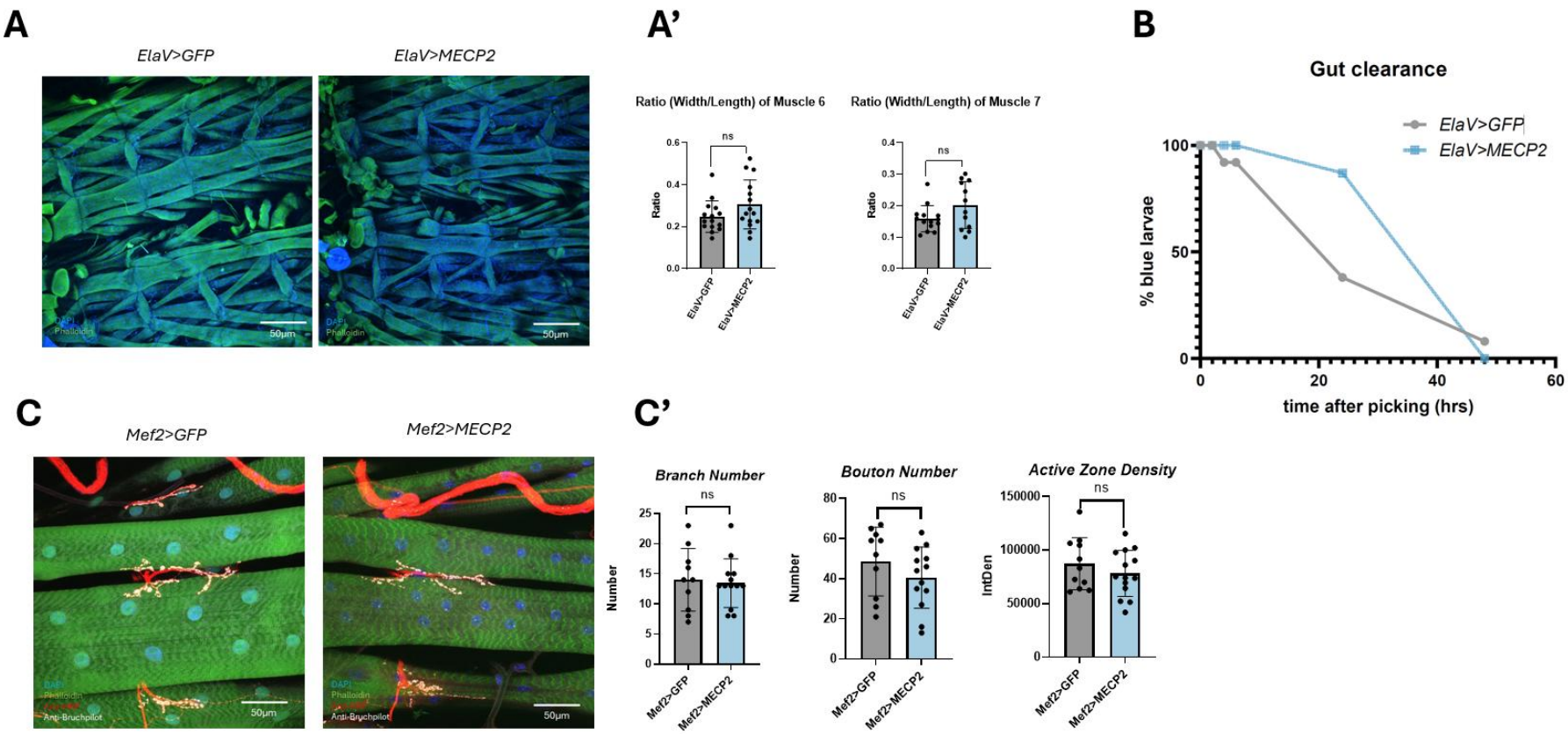

Fig. 8 The fly muscle defects associated with *MECP2* misexpression is neurologically independent. (A) Confocal images of larval body wall muscles (L3 stage) stained with Phalloidin (green) and DAPI (blue). Scale bar, 50 µm. **(A'**) Quantification of muscle thickness (width/length ratio) in muscles 6 and 7 across abdominal segments A1–A3. **(B)** Gut clearance assay in control and MECP2-expressing larvae. N=30 larvae per genotype are analysed. **(C)** Confocal images of larval neuromuscular junctions stained for Phalloidin (green), DAPI (blue), neuronal marker (red), and active zones (white). Scale bar, 50 µm. **(C')** Quantification of neuromuscular junction (NMJ) branching, bouton number, and active zone density.

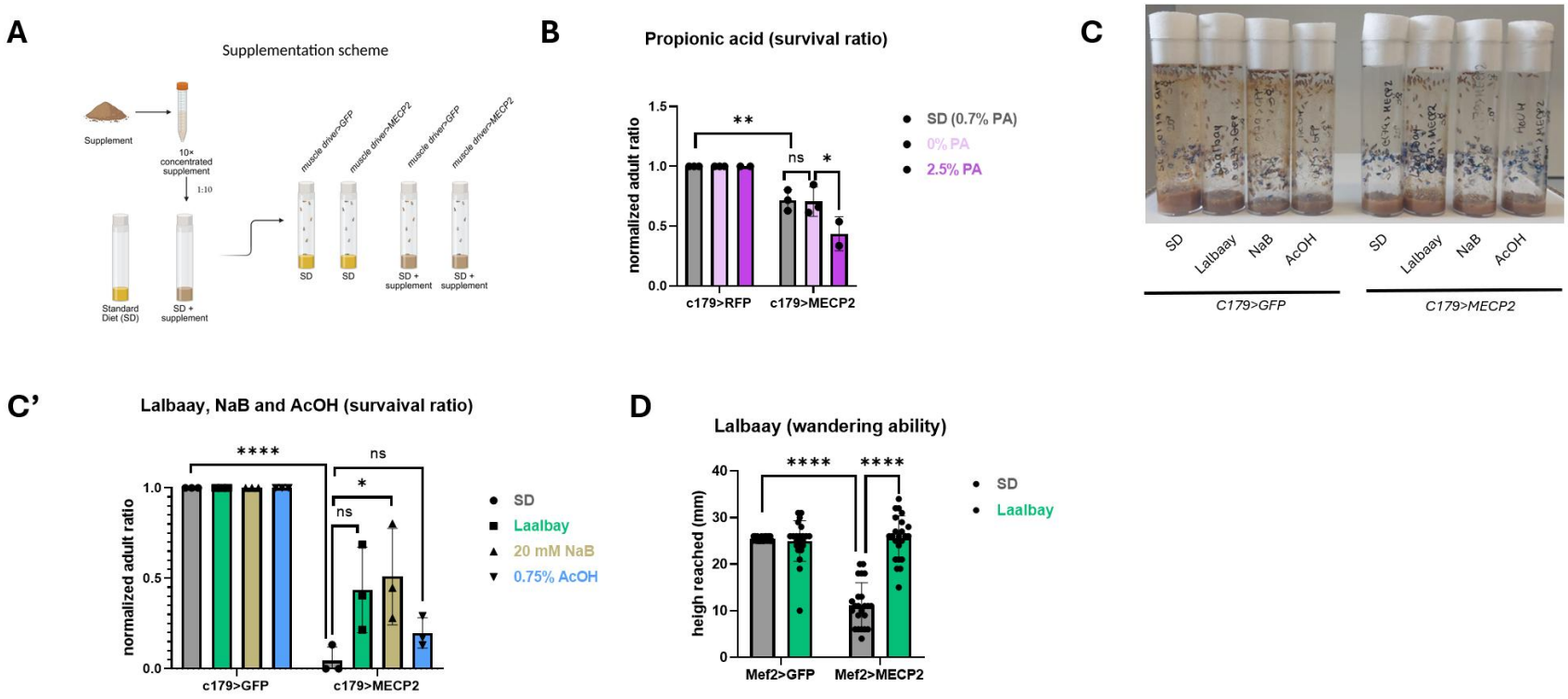

Fig. 9 SCFA supplementations: beneficial effects of butyrate in *MECP2*-overexpressing flies (A) Schematic of the dietary supplementation protocol, indicating the concentrations used and the genotypes analyzed. **(B)** Scatter plot showing the survival ratio for the progeny of the cross *c179>MECP2* (experimental) versus *c179>RFP* (control), under standard diet (SD 0.7% propionic acid) or propionic acid (PA) depleted diet (0% PA) or PA-supplemented (2.5% PA). The survival ratio was calculated as the observed vs. expected ratio of progeny for each genotype, based on Mendelian expectations due to the use of a balancer chromosome. For normalization, the average survival of the control (*c179 > RFP*) was set to 1 in each condition. Each dot represents one biological replicate (N ≈ 80 animals per replicate). **(C)** Representative images of *Drosophila* vials at 12 days after egg laying. Crosses were performed with synchronized egg laying, same number of parental flies, and equal amounts of food. The images show the adult progeny resulting from each cross and dietary condition. **(C')** Quantification of survival ratios from three independent biological replicates under different dietary conditions (*N* ≈ 80 animals per replicate): butyrate-supplemented diet (20mM NaB), equimolar Lalbaay treatment (containing the same NaB concentration), and acetate at 0.75% (0.75% AcOH). Data are normalized as in panel A. **(D)** Scatter plot showing pupal height (in

mm) as a readout of locomotor ability in animals expressing *MECP2* under the control of the muscle-specific *Mef2-GAL4* driver (*Mef2 > MECP2*) compared to control (*Mef2 > GFP*). Each dot represents a single pupa; data from three independent crosses are pooled.

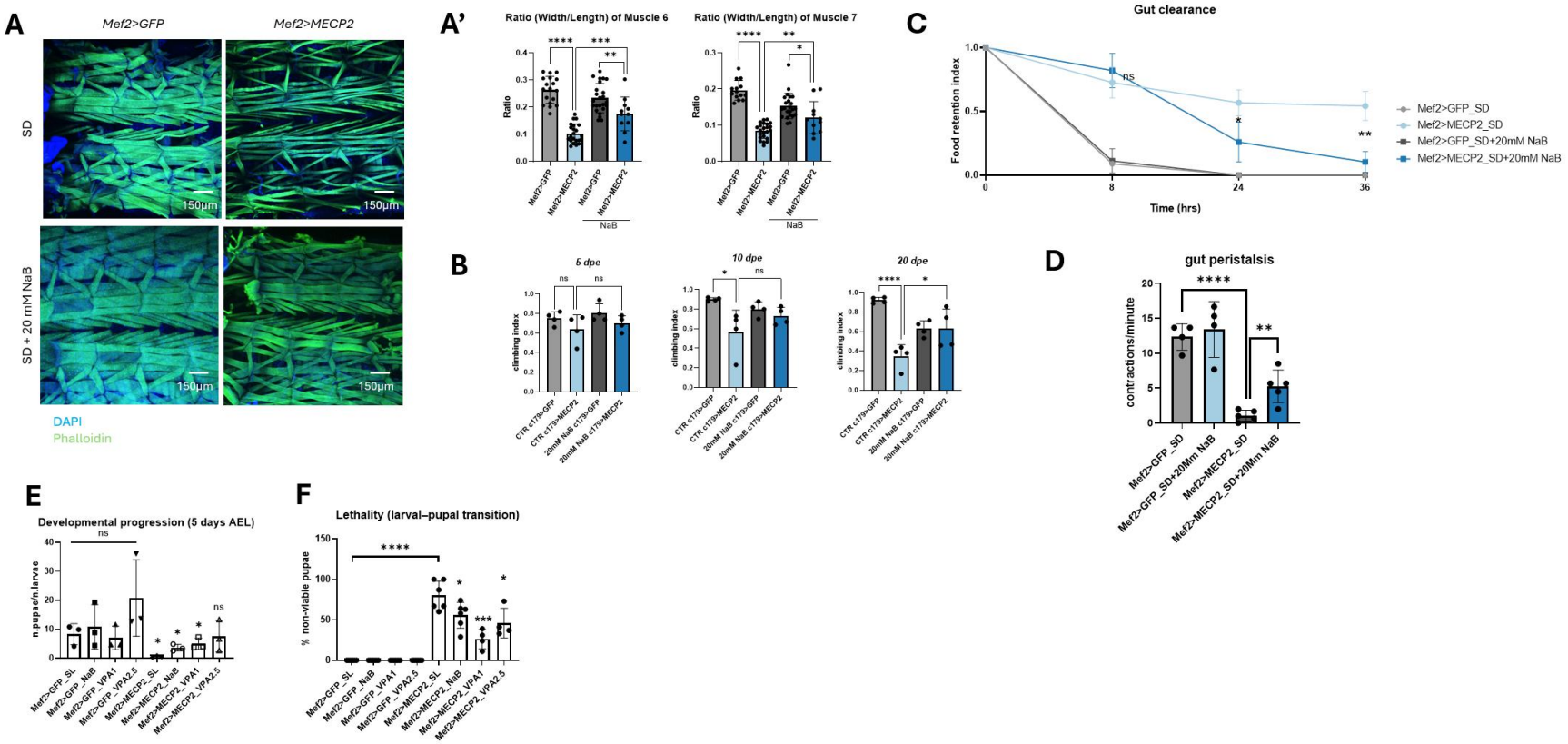

Fig. 10 Butyrate rescues morphological and functional muscle and gut defects involving epigenetic mechanisms. (A) Confocal images of larval body wall muscles (muscles 6 and 7) stained with Phalloidin (green) and DAPI (blue). Scale bar: 150 µm. **(A')** Quantification of muscle aspect ratio (width/length) in the indicated genotypes. **(B)** Climbing assay in adult flies after NaB supplementation. Performance was assessed at 5, 10, 20, and 30 days post-eclosion (dpe). Left: schematic of the assay design. **(C)** Gut clearance assay in NaB-fed larvae. Mean and SEM are plotted for five independent biological replicates. A significant improvement is observed in *MECP2*-overexpressing animals treated with NaB compared to standard diet (**, $p < 0.01$). **(D)** Quantification of peristaltic waves per minute in larvae of the indicated genotypes. The average of three animals per biological replicate (n = 5) was used. **(E)** Effect of NaB and valproic acid (VPA) supplementation on larval developmental progression. Pupation rate was calculated as the percentage of pupae over total larvae 5 days after

egg laying (AEL) from three independent replicates. **(F)** Viability is expressed as the percentage of pupae reaching adulthood. Each dot represent the average lethality calculated on animals from a single independent vial.

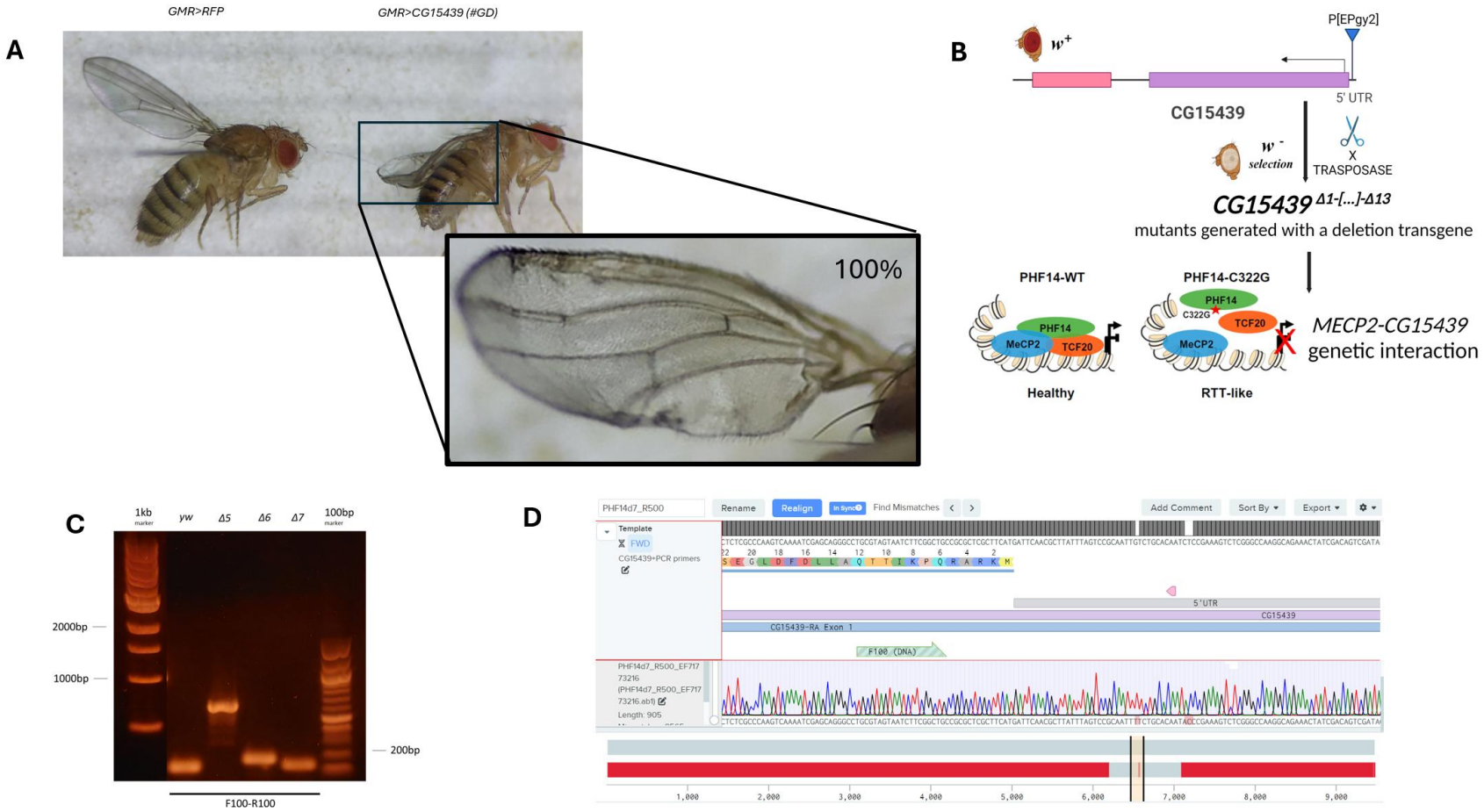

Fig. 11 . Exploring a MeCP2 Interactor: Preliminary Characterization of PHF14/CG15439. (A) Representative images of adult *Drosophila* wings from *GMR > RFP* control (left) and *GMR>CG15439-RNAi (GD9021)* animals (right). An inset shows a magnified view of the disrupted wing phenotype observed upon CG15439 knockdown. Approximately 30 animals were analyzed, all displaying wing abnormalities of variable severity. **(B)** Schematic representation of the strategy used for generation of CG15439 mutants by imprecise excision of a P-element insertion. The cartoon also illustrates the intended application of the generated lines for future genetic interaction studies with MeCP2. **(C)** PCR analysis of genomic DNA extracted from larvae of four genotypes – yw, Δ5, Δ6, and Δ7 - selected based on the absence of eye pigmentation. Primers were designed ~100 bp upstream and downstream of the P-

element insertion site. The gel shows that line Δ5 retains a larger band suggestive of a partial P-element fragment, whereas Δ6 and Δ7 display shorter products indicative of more complete excision events. **(D)** Example of sequencing analysis of line Δ7, visualized using Benchling software. Mismatches highlighted in red mark sequence alterations at the excision site, supporting the successful generation of a CG15439 putative mutant alleles.

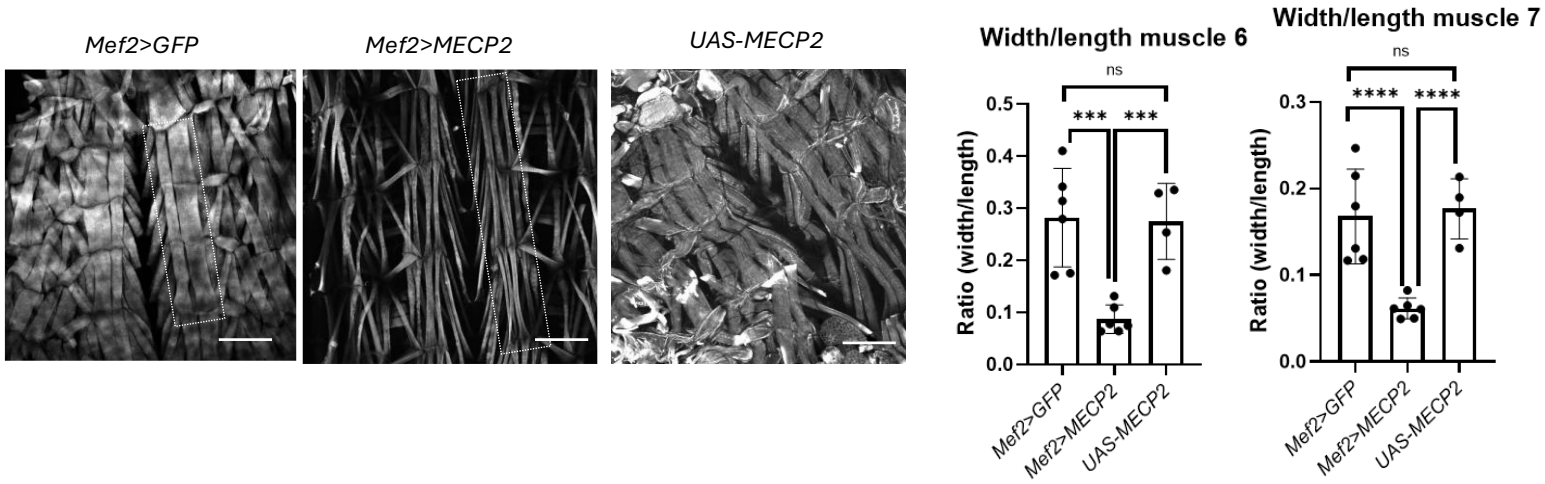

Fig S1. The UAS-MECP2 line does not display a leaky effect. (A) Confocal images of body wall muscles comparing the negative control (*Mef2>GFP*), the overexpressing line (*Mef2>MECP2*), and the UAS responder alone (*UAS-MECP2*), all stained with phalloidin (grey). Scale bar: 150 μm. **(B)** Quantification of the width/length ratio of segments A1–A3 of reference muscles 6 and 7 across the indicated genotypes. Each point represents the average ratio of the measured segments within each sample.

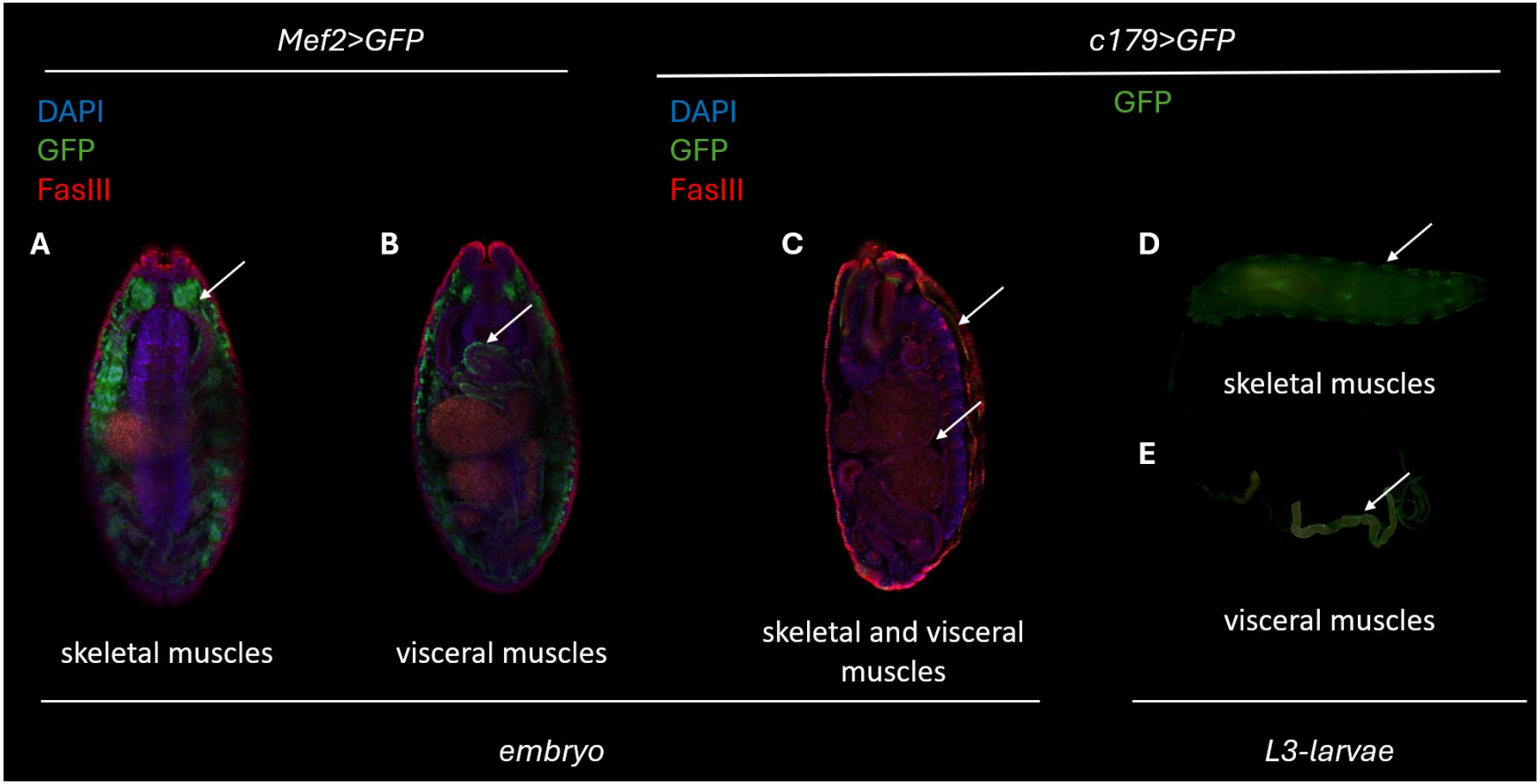

Fig. S2. Temporal expression of *c179>GFP* and *Mef2>GFP* in *Drosophila* embryos and larvae. Immunostaining of synchronized embryos with anti-GFP (green) to detect transgene expression, anti-FasIII (red) to label cell membranes, and DAPI (blue) to visualize nuclei.**(A)** Representative *Mef2>GFP* embryo, highlighting skeletal muscles (white arrow). **(B)** Same *Mef2>GFP* embryo as in (A), shown in a different focal plane to highlight visceral muscles (white arrow). N=50 **(C)** Representative *c179>GFP* embryo; no GFP signal is detectable at this embryonic stage, only FasIII marks skeletal and visceral muscles (white arrows). N=50 **(D, F)** Representative *c179>GFP* L3 larvae, showing endogenous GFP fluorescence in skeletal and muscles respectively, indicating that *c179* expression begins at the larval stage.

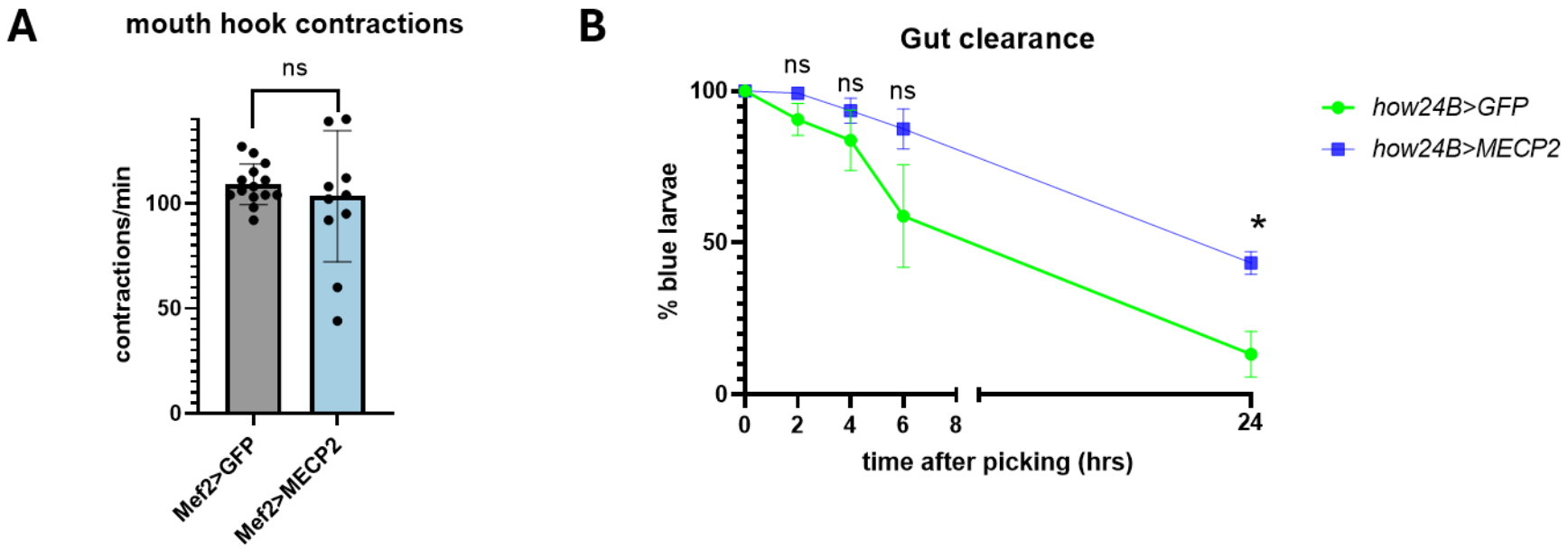

Fig. S3. (A) Mouth hook contractions in third-instar larvae. Each column represents the mean number of body-wall contractions per minute for five larvae of each replicate, with individual points representing single larvae of the indicated genotypes (N = 4 biological replicates per genotype). Data are presented as mean ± SEM. **(B) Gut clearance assay with *how24B-GAL4* driver.** Quantification of gut clearance over time. The percentage of larvae retaining blue dye was measured at several time points after picking. Control larvae (green line) progressively cleared the dye, reaching nearly 0% at 24 hours, whereas *MECP2*-overexpressing larvae (blue line) retained blue coloration (~50%). Data are expressed as mean ± SEM. Approximately 30 larvae were analyzed per experiment, across 4 independent experiments. Statistical analysis indicates no significant differences up to 6 hours post-picking, followed by significant differences at 24 hours.

Initium sapientiae timor Domini (Psalm 111:10)